

## Part IV

# **PV Systems**

217

Copyright Delft University of Technology, 2014

This copy is provided for free, for personal use only.



# 15

## Introduction to PV systems

### 15.1 Introduction

After we have discussed the fundamental scientific theories required for solar cells in Part II and have taken a look at modern PV technology in Part III, we now will use the gained knowledge to discuss complete PV systems. A PV system contains many different components besides the PV modules. For successfully planning a PV system it is crucial to understand the function of the different components and to know their major specifications. Further, it is important to know the effect on the location of the (expected) performance of a PV system.

### 15.2 Types of PV systems

PV systems can be very simple, consisting of just a PV module and load, as in the direct powering of a water pump motor, which only needs to operate when the sun shines. However, when for example a whole house should be powered, the system must be operational day and night. It also may have to feed both AC and DC loads, have reserve power and may even include a back-up generator. Depending on the system configuration, we can distinguish three main types of PV systems: stand-alone, grid-connected, and hybrid. The basic PV system principles and elements remain the same. Systems are adapted to meet particular requirements by varying the type and quantity of the basic elements. A

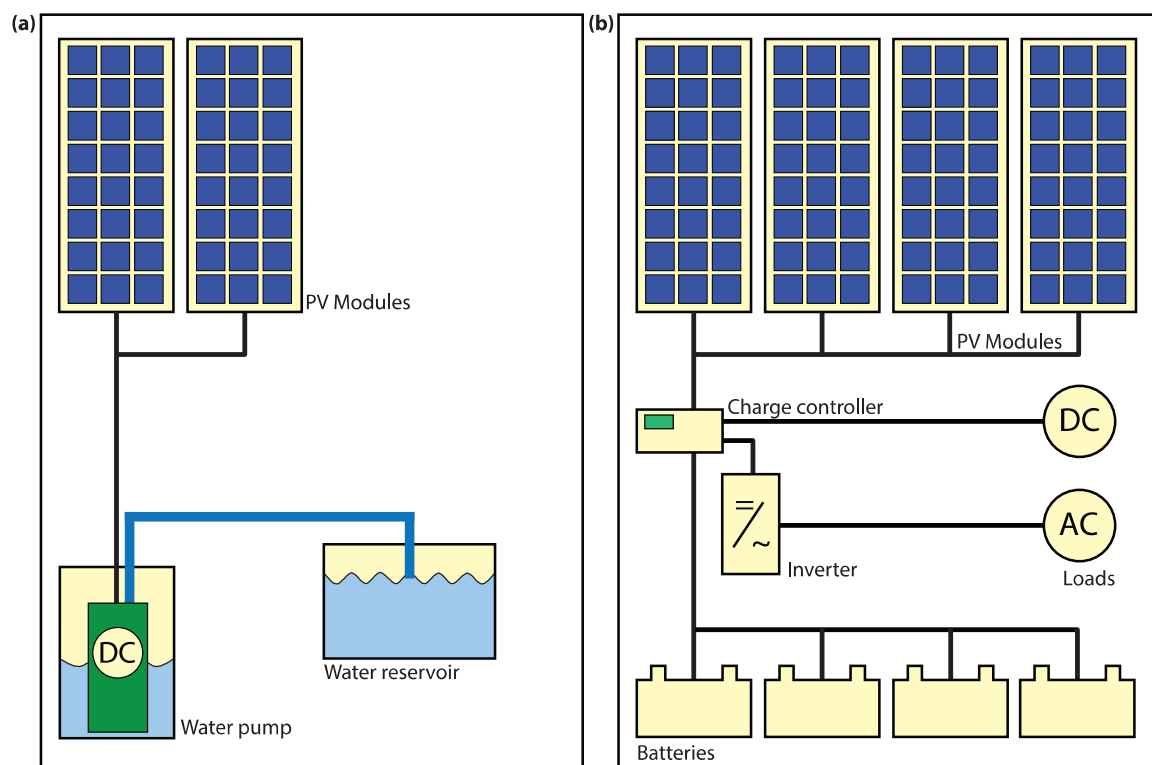


**Figure 15.1:** Schematic representation of (a) a simple DC PV system to power a water pump with no energy storage and (b) a complex PV system including batteries, power conditioners, and both DC and AC loads.

modular system design allows easy expansion, when power demands change.

### 15.2.1 Stand-alone systems

Stand-alone systems rely on solar power only. These systems can consist of the PV modules and a load only or they can include batteries for energy storage. When using batteries charge regulators are included, which switch off the PV modules when batteries are fully charged, and may switch off the load to prevent the batteries from being discharged below a certain limit. The batteries must have enough capacity to store the energy produced during the day to be used at night and during periods of poor weather. Figure 15.1 shows schematically examples of stand-alone systems; (a) a simple DC PV system without a battery and (b) a large PV system with both DC and AC loads.

### 15.2.2 Grid-connected systems

Grid-connected PV systems have become increasingly popular for building integrated applications. As illustrated in Fig. 15.2, they are connected to the grid via inverters, which convert the DC power into AC electricity. In small systems as they are installed in residential homes, the inverter is connected to the distribution

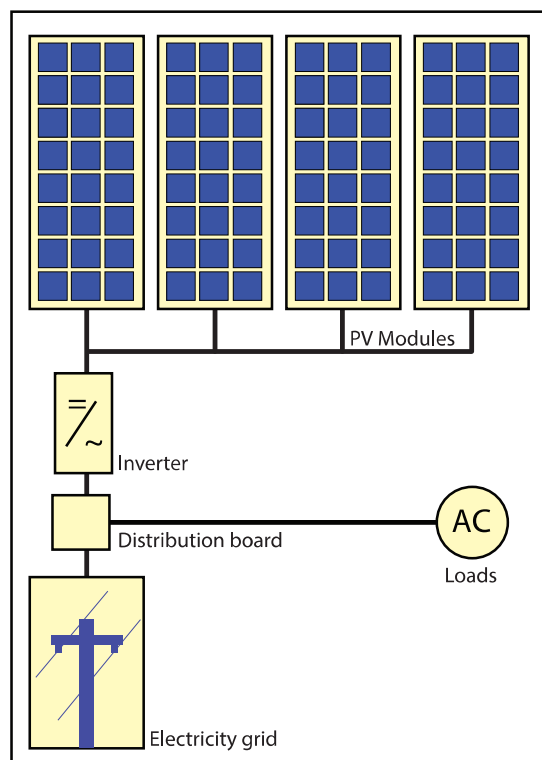


**Figure 15.2:** Schematic representation of a grid-connected PV system.

board, from where the PV-generated power is transferred into the electricity grid or to AC appliances in the house. These systems do not require batteries, since they are connected to the grid, which acts as a buffer into that an oversupply of PV electricity is transported while the grid also supplies the house with electricity in times of insufficient PV power generation.

Large PV fields act as power stations from that all the generated PV electricity is directly transported to the electricity grid. They can reach peak powers of up to several hundreds of  $MW_p$ . Figure 15.3 shows a 25.7  $MW_p$  system installed in Germany.

### 15.2.3 Hybrid systems

Hybrid systems consist of combination of PV modules and a complementary method of electricity generation such as a diesel, gas or wind generator. A schematic of an hybrid system shown in Fig. 15.4. In order to optimise the different methods of electricity generation, hybrid systems typically require more sophisticated controls than stand-alone or grid-connected PV systems. For example, in the case of an PV/diesel system, the diesel engine must be started when the battery reaches a given discharge level and stopped again when battery reaches an adequate state of charge. The back-up generator can be used to recharge batteries only or to supply the load as well.



**Figure 15.3:** The 25.7  $MW_p$  Lauingen Energy Park in Bavarian Swabia, Germany [82].

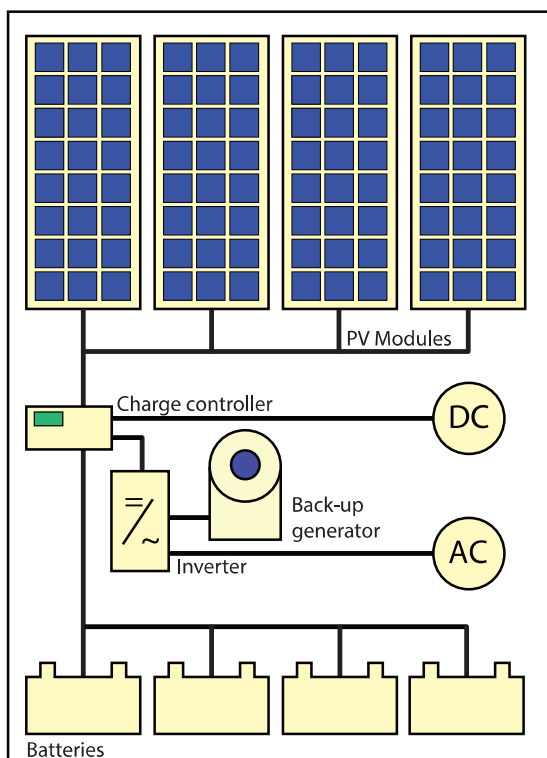


**Figure 15.4:** Schematic representation of a hybrid PV system that has a diesel generator as alternative electricity source..

### 15.3 Components of a PV system

As we have seen earlier in this book, a solar cell can convert the energy contained in the solar radiation into electrical energy. Due to the limited size of the solar cell it only delivers a limited amount of power under fixed current-voltage conditions that are not practical for most applications. In order to use solar electricity for practical devices, which require a particular voltage and/or current for their operation, a number of solar cells have to be connected together to form a *solar panel*, also called a *PV module*. For large-scale generation of solar electricity solar panels are connected together into a *solar array*.

Although, the solar panels are the heart of a *PV system*, many other components are required for a working system, that we already discussed very briefly above. Together, these components are called the *Balance of System* (BOS). Which components are required depends on whether the system is connected to the electricity grid or whether it is designed as a stand-alone system. The most important components belonging to the BOS are:

- A *mounting structure* is used to fix the modules and to direct them towards the sun.
- *Energy storage* is a vital part of stand-alone systems because it assures that the system can deliver electricity during the night and in periods of

bad weather. Usually, *batteries* are used as energy-storage units.

- *DC-DC converters* are used to convert the module output, which will have a variable voltage depending on the time of the day and the weather conditions, to a fixed voltage output that *e.g.* can be used to charge a battery or that is used as input for an inverter in a grid-connected system.
- *Inverters* or *DC-AC converters* are used in grid-connected systems to convert the DC electricity originating from the PV modules into AC electricity that can be fed into the electricity grid.
- *Cables* are used to connect the different components of the PV system with each other and to the electrical load. It is important to choose cables of sufficient thickness in order to minimise resistive losses.

Even though not a part of the PV system itself, the *electric load*, *i.e.* all the electric appliances that are connected to it have to be taken into account during the planning phase. Further, it has to be considered whether the loads are AC or DC loads.

The different components of a PV system are schematically presented in Fig. 15.5 and will be discussed in detail in Chapter 17.

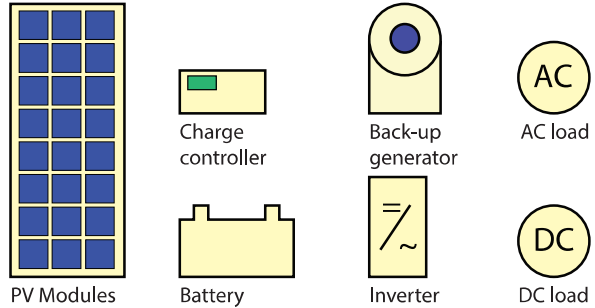


**Figure 15.5:** A schematic of the different components of a PV system.

# 16

## Location issues

In Chapter 5 we discussed solar radiation on earth and introduced the AM1.5 spectrum, normalised to a total irradiance of  $1000 \text{ W/m}^2$ . This spectrum is used to evaluate the performance of solar cells and modules in laboratories and industry. The AM1.5 spectrum represents the solar irradiance if the centre of the solar disc is at an angle of  $48.2^\circ$  off the zenith (or  $41.2^\circ$  above the horizon).

Of course, the sun not always is at this position, but the position is dependent on the time of the day and the year and of course it is dependent on the location on earth. In this section we will discuss how to calculate the position of the sun at every location on earth at an arbitrary time and date. Furthermore we will discuss scattering of sunlight when it traverses the at-

mosphere and how this influences the direct and diffuse spectrum. We also will discuss the influence of the mounting angle and position of a PV module on the irradiance at the module.

### 16.1 The position of the sun

For planning a PV system it is crucial to know the position of the sun in the sky at the location of the solar system at a given time. In this section we explain how this position can be calculated.

Since celestial objects like the sun, the moon and the stars are very far away from the earth it is convenient to describe their motion projected on a sphere with ar-

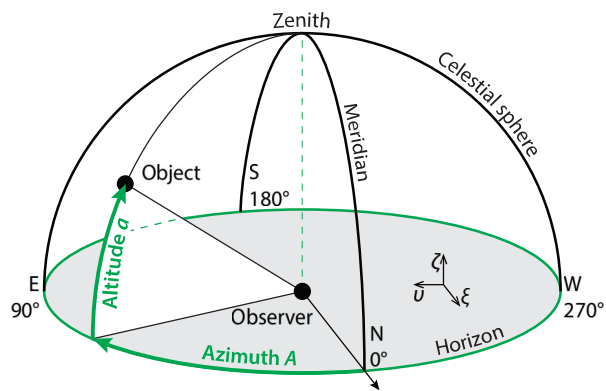


**Figure 16.1:** Illustrating the definition of the *altitude*  $a$  and the *azimuth*  $A$  in the horizontal coordinate system. Note that North is at the bottom of the figure.

bitrary radius and concentric to the earth. This sphere is called the *celestial sphere*. The position of every celestial object thus can be parameterised by two angles. For photovoltaic applications it is most convenient to use the *horizontal coordinate system*, where the horizon of the observer constitutes the *fundamental plane*. In this coordinate system, the position of the sun is expressed by two angles that are illustrated in Fig. 16.1: The *altitude*  $a$  that is the angular elevation of the centre of the solar disc above the horizontal plane. Its angular range is  $a \in [-90^\circ, 90^\circ]$ , where negative angles correspond to the object being below the horizon and thus not visible. The *azimuth*  $A$  that is the angle between the line of sight projected on the horizontal plane and due North. It is usually counted eastward, such that  $A = 0^\circ, 90^\circ, 180^\circ, 270^\circ$  correspond to due North, East, South and West, respectively. Its angular range is  $A \in [0^\circ, 360^\circ]$ . In a different convention also used by the PV community, due South corresponds to  $0^\circ$  and is counted westward, the angles then are in between  $-180^\circ$  and  $180^\circ$ . Figure 16.1 also shows the *meridian*, which is great circle on the celestial sphere passing through the celestial North and South poles as well as the zenith.

Instead of using the spherical coordinates  $a$  and  $A$ , we also could use Cartesian coordinates, that we here call  $\xi$  ( $x_i$ ),  $\upsilon$  ( $\text{upsilon}$ ) and  $\zeta$  ( $\text{zeta}$ ) and that are also depicted in Fig. 16.1. The principal direction is parallel to  $\xi$ . The Cartesian coordinates are connected to the spherical

coordinates via

$$\begin{pmatrix} \xi \\ v \\ \zeta \end{pmatrix} = \begin{pmatrix} \cos a \cos A \\ \cos a \sin A \\ \sin a \end{pmatrix}. \quad (16.1)$$

Note that  $\xi^2 + v^2 + \zeta^2 = 1$  for all points on the celestial sphere.

Earth orbits the sun in an elliptic orbit at an average distance of about 150 million kilometres. Due to the elliptic orbit the speed of Earth is not constant. This is because of Kepler's second law that states that "A line joining a planet and the Sun sweeps out equal areas during equal intervals of time." On the celestial sphere the sun seems to move on a circular path with one revolution per year. This path is called the *ecliptic* and illustrated in Fig. 16.2. For describing the apparent movement of the sun on the celestial sphere it is convenient to use coordinates in that the ecliptic lies in the fundamental plane. These coordinates are called the *ecliptic coordinates*. As principal direction, the position of the sun at the spring (*vernal equinox*) (thus around 21 March) is used, which is indicated by the sign of Aries,  $\gamma$ . As obvious from Fig. 16.2,  $\gamma$  lies both in the ecliptic plane as well as in the equatorial plane. The ecliptic coordinate system is sketched in Fig. 16.3 (a). The two angular coordinates are called the *ecliptic longitude*  $\lambda$  and the *ecliptic latitude*  $\beta$ . Note, that in this coordinate system the rotation of the earth around its axis is not taken into account.

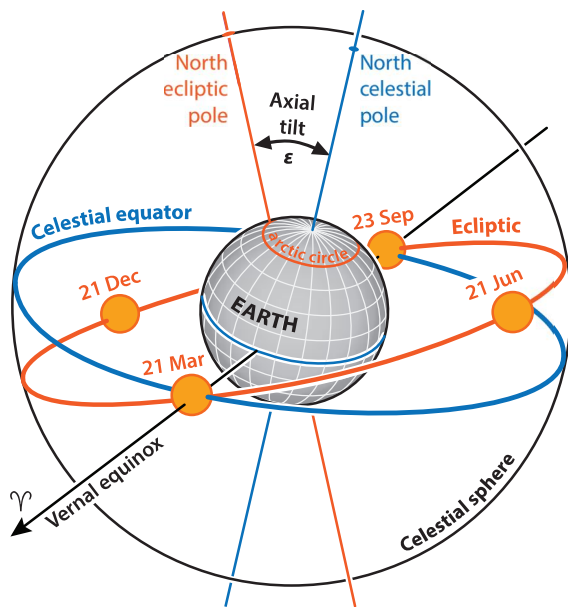


**Figure 16.2:** Illustrating the *ecliptic*, i.e. the apparent movement of the sun around earth. Further, the *celestial equator* and the direction of the *vernal equinox* are indicated. The sizes of Sun and Earth are not in scale.

In ecliptic coordinates approximate position the position of the sun can be expressed easily. The approximation presented here has an accuracy of about 1 arcminute within two centuries of 2000 and is published by the the *Astronomical Applications Department* of the *U.S. Naval Observatory*.

To express the position of the sun we first have to express the time  $D$  elapsed since Greenwich noon, Terrestrial Time, on 1 January 2000, in days. For astonomic purposes it may be convenient to relate  $D$  to the Julian date JD via

$$D = \text{JD} - 2451545.0. \quad (16.2)$$

The Julian Date<sup>1</sup> that is defined as the number of days since 1 January 4713 BC in a proleptic<sup>2</sup> Julian calendar or since 24 November 4717 BC in a proleptic Gregorian calendar.

Now, the *mean longitude* of the sun corrected to the aberration of the light is given by

$$q = 280.459^\circ + 0.98564736^\circ D \quad (16.3)$$

Because of the elliptic orbit of earth and hence a varying speed throughout the year, we have to correct with the so-called *mean anomaly* of the Sun,

$$g = 357.529^\circ + 0.98560028^\circ D. \quad (16.4)$$

<sup>1</sup>Calculating the Julian Date is implemented in MatLab.

<sup>2</sup>Proleptic means that a calendar is applied to dates before its introduction.

It may be convenient to normalise  $q$  and  $g$  to the range  $[0^\circ, 360^\circ]$  by adding or subtracting multiples of  $360^\circ$ .

Now the ecliptic longitude of the sun is given by

$$\lambda_S = q + 1.915^\circ \sin g + 0.020^\circ \sin 2g. \quad (16.5)$$

The ecliptic latitude can be approximated by

$$\beta_S = 0. \quad (16.6)$$

For estimating the radiation it might also be convenient to approximate the distance of the Sun from the Earth. In astronomical units (AU) this is given by

$$R = 1.00014 - 0.01671 \cos g - 0.00014 \cos 2g. \quad (16.7)$$

As stated above, for PV applications it is convenient to use horizontal coordinates. We therefore have to transform from ecliptic coordinates into the horizontal coordinates. This is done via *three rotations* that are to be performed after each other consecutively:

First, we have to transform from ecliptic coordinates into equatorial coordinates. As illustrated in Fig. 16.2, the fundamental plane of these coordinates is tilted to the ecliptic with an angle  $\epsilon$ ,

$$\epsilon = 23.429^\circ - 0.00000036^\circ D \quad (16.8)$$

The principal direction is again given by the vernal equinox  $\Upsilon$ . In Fig. 16.3 (b) the equatorial coordinate

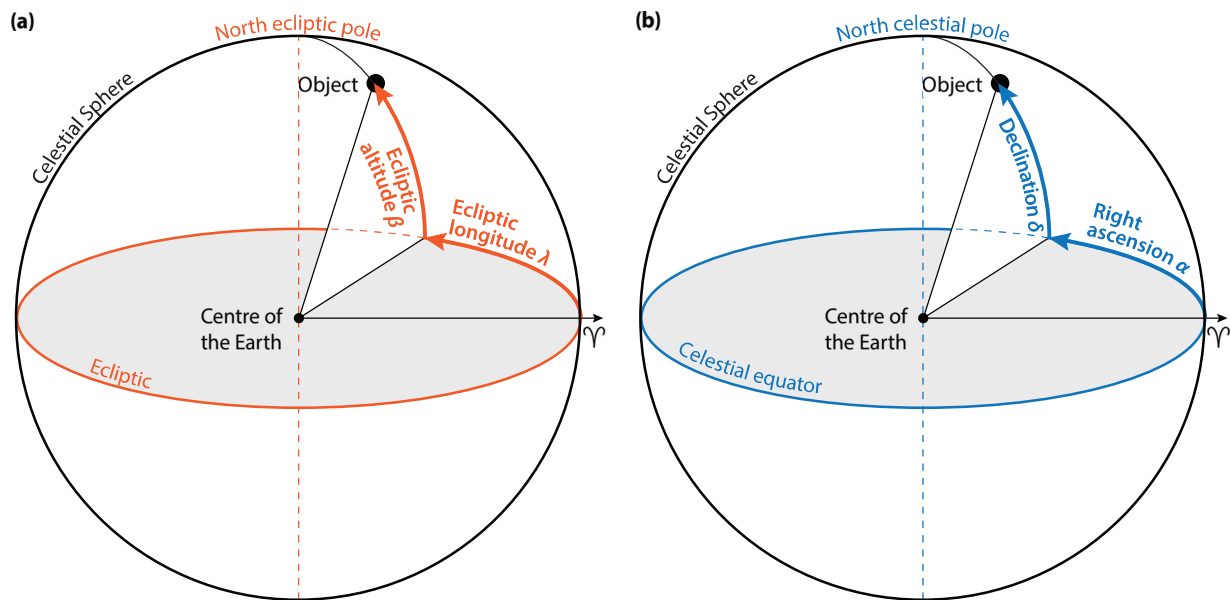


**Figure 16.3:** Illustrating (a) the *ecliptic coordinate system* and (b) the *equatorial coordinate system*.

system is sketched. The two coordinates are called the *right ascension*  $\alpha$  and the *declination*  $\delta$ . The transformation from ecliptic coordinates to equatorial coordinates is a rotation by the angle  $\epsilon$  about the vernal equinox as rotational axis. Mathematically this is expressed by

$$\begin{pmatrix} \cos \delta \cos \alpha \\ \cos \delta \sin \alpha \\ \sin \delta \end{pmatrix} = \begin{pmatrix} 1 & 0 & 0 \\ 0 & \cos \epsilon & -\sin \epsilon \\ 0 & \sin \epsilon & \cos \epsilon \end{pmatrix} \begin{pmatrix} \cos \beta \cos \lambda \\ \cos \beta \sin \lambda \\ \sin \beta \end{pmatrix}. \quad (16.9)$$

Secondly, we have to take the rotation of the earth around its axis into account. We do this by using the so-called *hour angle*  $h$  instead of the right ascension  $\alpha$ . Those two angles are connected to each other via

$$h = \theta_L - \alpha, \quad (16.10)$$

where  $\theta_L$  is the *local mean sidereal time*, i.e. the angle between the vernal equinox and the meridian. All these angles are illustrated in Fig. 16.4. A sidereal day is the duration between two passes of the vernal equinox through the meridian and it is slightly shorter than a solar day. We can understand this by realising that the earth has to rotate by  $360^\circ$  and approximately  $360^\circ/365.25$  between two passes through the meridian. The duration of *mean sidereal day* is approximately 23 h, 56 m and 4 s.

For calculating  $\theta_L$  we first have to determine the Greenwich Mean Sidereal Time (GMST), which is (approxim-

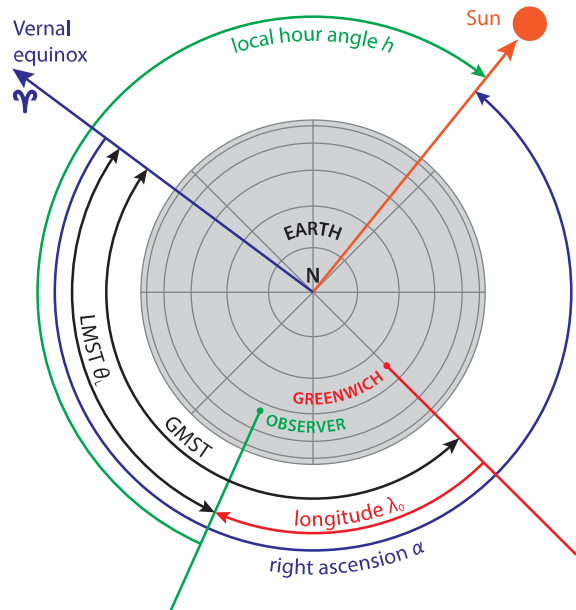


**Figure 16.4:** Illustrating the right ascension  $\alpha$ , the local hour angle  $h$ , the Greenwich Mean Sidereal Time GMST and the local mean sidereal time  $\theta_L$ .

ately) given by

$$\begin{aligned} \text{GMST} = & 18.697374558 \text{ h} \\ & + 24.06570982441908 \text{ h} \cdot D \\ & + 0.000026 \text{ h} \cdot T^2, \end{aligned} \quad (16.11)$$

where  $D$  is as defined above and  $T$  is the number of centuries past since Greenwich noon, Terrestrial Time, on 1 January 2000,

$$T = \frac{D}{36525}. \quad (16.12)$$

For many applications, the quadratic term may be omitted. GMST is given in hours and has to be normalised to the range [0 h, 24 h]. We then can obtain the *local* mean sidereal time in degrees with

$$\theta_L = \text{GMST} \frac{15^\circ}{\text{hour}} + \lambda_0, \quad (16.13)$$

where  $\lambda_0$  is the longitude of the observer.

We thus have to the following transform about the rotational axis of the earth,

$$\begin{pmatrix} \cos \delta \cos h \\ \cos \delta \sin h \\ \sin \delta \end{pmatrix} = \begin{pmatrix} \cos \theta_L & \sin \theta_L & 0 \\ \sin \theta_L & -\cos \theta_L & 0 \\ 0 & 0 & 1 \end{pmatrix} \begin{pmatrix} \cos \delta \cos \alpha \\ \cos \delta \sin \alpha \\ \sin \delta \end{pmatrix}. \quad (16.14)$$

Note that this transform is no rotation but a reflection at an angle of  $\theta_L/2$ . We thus now transformed the principal direction of the coordinate system from vernal equinox to the local mean sidereal time.

Thirdly we transform to the horizontal coordinate system by rotating with the latitude angle  $\phi_0$  of the observer. While the ecliptic and equatorial coordinate systems use the centre of the earth as origin, the horizontal coordinate system uses the actual position on the surface of Earth as origin. However, because of the distance of celestial objects in general and the Sun in particular being much larger than the radius of the Earth, we may neglect this translational shift of the origin of the coordinate systems.

The rotational axis of the third transform is the axis that is normal to both the principal direction  $\theta_L$  and the rotational axis of the earth ( $\delta = 90^\circ$ ).

$$\begin{pmatrix} \xi' \\ v' \\ \zeta \end{pmatrix} = \begin{pmatrix} \sin \phi_0 & 0 & -\cos \phi_0 \\ 0 & 1 & 0 \\ \cos \phi_0 & 0 & \sin \phi_0 \end{pmatrix} \begin{pmatrix} \cos \delta \cos h \\ \cos \delta \sin h \\ \sin \delta \end{pmatrix}. \quad (16.15)$$

However, here the directions  $\xi'$  and  $v'$  point to due South and West, respectively. We thus must apply  $\xi' \rightarrow -\xi$  and  $v' \rightarrow -v$  in order to get the directions such as they are defined in Fig. 16.1 ( $\xi$  and  $v$  pointing to due North and East, respectively). We do this with the matrix transform

$$\begin{pmatrix} \xi \\ v \\ \zeta \end{pmatrix} = \begin{pmatrix} -1 & 0 & 0 \\ 0 & -1 & 0 \\ 0 & 0 & 1 \end{pmatrix} \begin{pmatrix} \xi' \\ v' \\ \zeta \end{pmatrix}. \quad (16.16)$$

By combining Eqs. (16.9), (16.14)–(16.16) we directly can transform from ecliptic to horizontal coordinates,

$$\begin{pmatrix} \xi \\ v \\ \zeta \end{pmatrix} = \begin{pmatrix} -1 & 0 & 0 \\ 0 & -1 & 0 \\ 0 & 0 & 1 \end{pmatrix} \begin{pmatrix} \sin \phi_0 & 0 & -\cos \phi_0 \\ 0 & 1 & 0 \\ \cos \phi_0 & 0 & \sin \phi_0 \end{pmatrix} \begin{pmatrix} \cos \theta_L & \sin \theta_L & 0 \\ \sin \theta_L & -\cos \theta_L & 0 \\ 0 & 0 & 1 \end{pmatrix} \begin{pmatrix} 1 & 0 & 0 \\ 0 & \cos \epsilon & -\sin \epsilon \\ 0 & \sin \epsilon & \cos \epsilon \end{pmatrix} \begin{pmatrix} \cos \beta \cos \lambda \\ \cos \beta \sin \lambda \\ \sin \beta \end{pmatrix}. \quad (16.17)$$

Please note that matrix multiplications do not commute, *i.e.* the order in which the rotations are applied must not be altered. Now, we apply that the ecliptic latitude of the sun  $\beta_S = 0$ . By calculating Eq. (16.32) we find

$$\xi_S = \cos a_S \cos A_S = -\sin \phi_0 \cos \theta_L \cos \lambda_S - (\sin \phi_0 \sin \theta_L \cos \epsilon - \cos \phi_0 \sin \epsilon) \sin \lambda_S, \quad (16.18a)$$

$$v_S = \cos a_S \sin A_S = -\sin \theta_L \cos \lambda_S + \cos \theta_L \cos \epsilon \sin \lambda_S, \quad (16.18b)$$

$$\zeta_S = \sin a_S = \cos \phi_0 \cos \theta_L \cos \lambda_S + (\cos \phi_0 \sin \theta_L \cos \epsilon + \sin \phi_0 \sin \epsilon) \sin \lambda_S, \quad (16.18c)$$

where we also used the the relationship between Cartesian and spherical horizontal coordinates from Eq. (16.1). Dividing Eq. (16.18b) by Eq. (16.18a) and leaving Eq. (16.18c) unchanged leads to the final expressions for the solar position,

$$\tan A_S = \frac{v_S}{\xi_S} = \frac{-\sin \theta_L \cos \lambda_S + \cos \theta_L \cos \epsilon \sin \lambda_S}{-\sin \phi_0 \cos \theta_L \cos \lambda_S - (\sin \phi_0 \sin \theta_L \cos \epsilon - \cos \phi_0 \sin \epsilon) \sin \lambda_S}, \quad (16.19a)$$

$$\sin a_S = \zeta_S = \cos \phi_0 \cos \theta_L \cos \lambda_S + (\cos \phi_0 \sin \theta_L \cos \epsilon + \sin \phi_0 \sin \epsilon) \sin \lambda_S. \quad (16.19b)$$

$A_S$  and  $a_S$  now can be derived by applying inverse trigonometric functions. While  $\arcsin$  uniquely delivers an altitude in between  $-90^\circ$  and  $90^\circ$ , applying  $\arctan$  leads to ambiguities. For deriving an azimuth in between  $0^\circ$  and  $360^\circ$ , we have to look in which quadrant is lying. Therefore we use  $\xi$  and  $v$  from Eqs. (16.18a) and (16.18b), respectively. We find

$$\xi > 0 \wedge v > 0 \Rightarrow A_S = \arctan f(\dots), \quad (16.20a)$$

$$\xi < 0 \Rightarrow A_S = \arctan f(\dots) + 180^\circ, \quad (16.20b)$$

$$\xi > 0 \wedge v < 0 \Rightarrow A_S = \arctan f(\dots) + 360^\circ. \quad (16.20c)$$

$f(\dots)$  denotes the function at the right hand side of Eq. (16.19a). Note that an altitude  $a_S < 0^\circ$  corresponds to the sun being below the horizon. This means that the Sun is not visible and no solar energy can be harvested.

The approximations presented on the previous pages are accurate within arcminutes for 200 centuries of 2000. Several years ago, NREL presented a much more complicated model, the so-called Solar Position Algorithm (ASP), with uncertainties of only  $\pm 0.0003^\circ$  in the period from 2000 BC to 6000 AD [83].

### Example

As an example we will calculate the position of the Sun in Delft on 14 April 2014 at 11:00 local time.

For determining the solar position we need next to date and time (in UTC) the latitude and longitude. Since the time zone in Delft on 14 April is the CEST, the Central European Summer Time, the time difference with UTC is +2 hours, such that 11:00 CEST corresponds to 9:00 UTC. According to Google Maps, the latitude and longitude of the Markt in the centre of Delft are given by

$$\begin{aligned}\phi_0 &= 52.01^\circ \text{N} = +52.01^\circ, \\ \lambda_0 &= 4.36^\circ \text{E} = +4.36^\circ.\end{aligned}$$

For the calculation we first have to express date and time as the time elapsed since 1 January 2000 noon UTC.

$$D = 4 \cdot 366 + 10 \cdot 365 + 2 \cdot 31 + 28 + 13 - 0.5 + \frac{9}{24} = 5216.875.$$

Now we can calculate the mean longitude  $q$  and the mean anomaly  $g$  of the sun according to Eqs. (16.3) and (16.4),

$$\begin{aligned}q &= 280.459^\circ + 0.98564736^\circ D = 22.4580712^\circ, \\ g &= 357.529^\circ + 0.98560028^\circ D = 99.28246073^\circ,\end{aligned}$$

where the values were normalised to  $[0^\circ, 360^\circ]$ . From Eq. (16.5) we thus obtain for the latitude of the Sun in ecliptic coordinates

$$\lambda_S = q + 1.915^\circ \sin g + 0.020^\circ \sin 2g = 24.34162696^\circ.$$

For the axial tilt  $\epsilon$  of the Earth we obtain from Eq. (16.8)

$$\epsilon = 23.429^\circ - 0.00000036^\circ D = 23.42712193^\circ.$$

The Greenwich Mean Sidereal Time (GMST) is given by Eq. (16.11),

$$GMST = 18.697374558 \text{ h} + 24.06570982441908 \text{ h} \cdot D + 0.000026 \text{ h} \cdot T^2 = 22.49731535 \text{ h},$$

where we used  $T = D / 36525$  and normalised to  $[0 \text{ h}, 24 \text{ h}]$ . We then find for the local mean sidereal time  $\theta_L$

$$\theta_L = GMST \frac{15^\circ}{\text{hour}} + \lambda_0 = 341.8197303^\circ,$$

Now we have all variables required to calculate the solar position. From Eqs. (16.19) and (16.20) we thus find

$$\tan A_S = \frac{-\sin \theta_L \cos \lambda_S + \cos \theta_L \cos \epsilon \sin \lambda_S}{-\sin \phi_0 \cos \theta_L \cos \lambda_S - (\sin \phi_0 \sin \theta_L \cos \epsilon - \cos \phi_0 \sin \epsilon) \sin \lambda_S} = -1.318180633.$$

$$\sin a_S = \cos \phi_0 \cos \theta_L \cos \lambda_S + (\cos \phi_0 \sin \theta_L \cos \epsilon + \sin \phi_0 \sin \epsilon) \sin \lambda_S = 0.589415473,$$

which leads to the solar altitude  $a_S=36.1^\circ$  and the solar azimuth  $A_S=127.2^\circ$ .

## 16.2 The sun path at different locations

In this section we discuss the solar paths throughout the year at several locations around the earth. Figures 16.5-16.8 shows four examples: Delft, the Netherlands ( $\phi_0 = 52.01^\circ \text{ N}$ ), the North Cape, Norway ( $\phi_0 = 71.17^\circ \text{ N}$ ), Cali, Colombia ( $\phi_0 = 3.42^\circ \text{ N}$ ), and Sydney, Australia ( $\phi_0 = 33.86^\circ \text{ S}$ ). Note that all the times are given in the apparent solar time (AST). While in Delft and on the North Cape, the Sun at noon always is South of the zenith, in Sydney it is always North. In Cali, close to the equator, the Sun is either South or North, depending on the time of the year. Since the North Cape is north of the arctic circle, the Sun does not set around 21 June. This phenomenon is called the *midnight sun*. On the other hand, the sun always stays below the horizon around 21 December - this is called the *polar night*.

## 16.3 The equation of time

Figure 16.9 shows the position of the sun throughout the year in Delft at 8:30, 12:00 and 15:30 mean solar time (MST), *i.e.* UTC +  $\lambda_0$ , where the longitude  $\lambda_0$  is expressed in hours. We see that the Sun not only changes from altitude but also from azimuth in the course of a

year, such that it seems to run along the shape of an *Eight*. This closed curve is called the *analemma*.

The difference between the apparent solar time (AST), *i.e.* the timescale where the sun really is highest at noon every day, and mean solar time is described by the so-called equation of time, which is defined as

$$\text{EoT} = \text{AST} - \text{MST}. \quad (16.21)$$

The equation of time is given as the difference between the mean longitude  $q$ , as defined in Eq. (16.3), and the right ascendent  $\alpha_S$  of the sun in the equatorial coordinate system,

$$\text{EoT}(D) = [q(D) - \alpha_S(D)] \frac{1 \text{ hour}}{15 \text{ deg}}. \quad (16.22)$$

The right ascendent is connected to the ecliptic longitude of the sun  $\lambda_S$ , as given in Eq. (16.5) via

$$\tan \alpha_S = \cos \epsilon \tan \lambda_S, \quad (16.23)$$

and  $\epsilon$  is the axial tilt as given in Eq. (16.8).

The equation of time has two major contributors: the anomaly due to the elliptic orbit of the Earth around the Sun and the Axial tilt of the rotational axis of the Earth with respect to the ecliptic. Both effects are shown in Fig. 16.10. In this figure, also the total EoT is shown, which is nearly the sum of the two contributors (The maximal deviation is less than a minute).

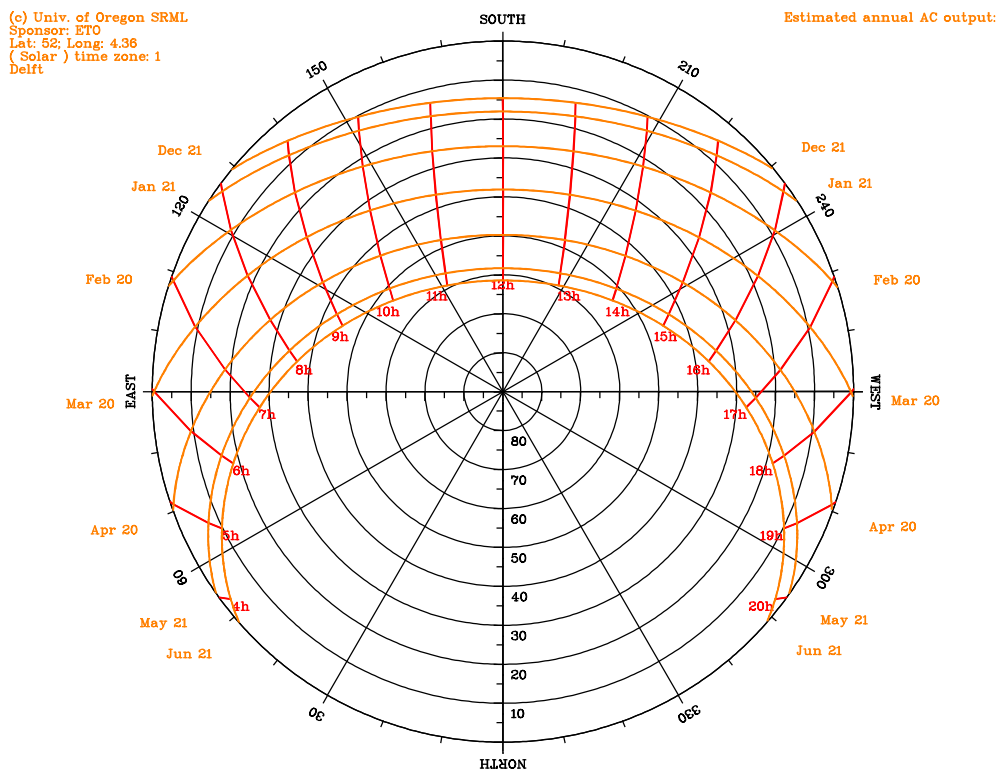


**Figure 16.5:** The sun path in apparent solar time in Delft, the Netherlands ( $\phi_0 = 52.01^\circ \text{ N}$ ). The sun path was calculated with the Sun path chart program by the *Solar Radiation Monitoring Lab.* of the *Univ. of Oregon* [84].

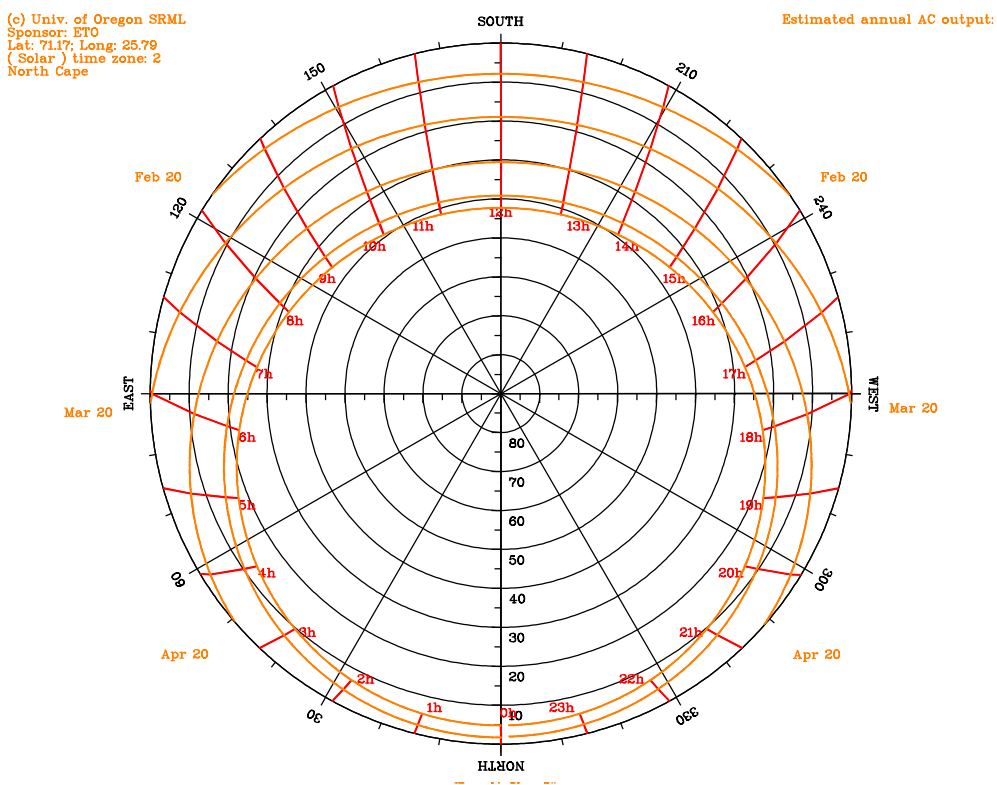


**Figure 16.6:** The sun path in apparent solar time on the North Cape, Norway ( $\phi_0 = 71.17^\circ \text{ N}$ ). The sun path was calculated with the Sun path chart program by the *Solar Radiation Monitoring Lab.* of the *Univ. of Oregon* [84].

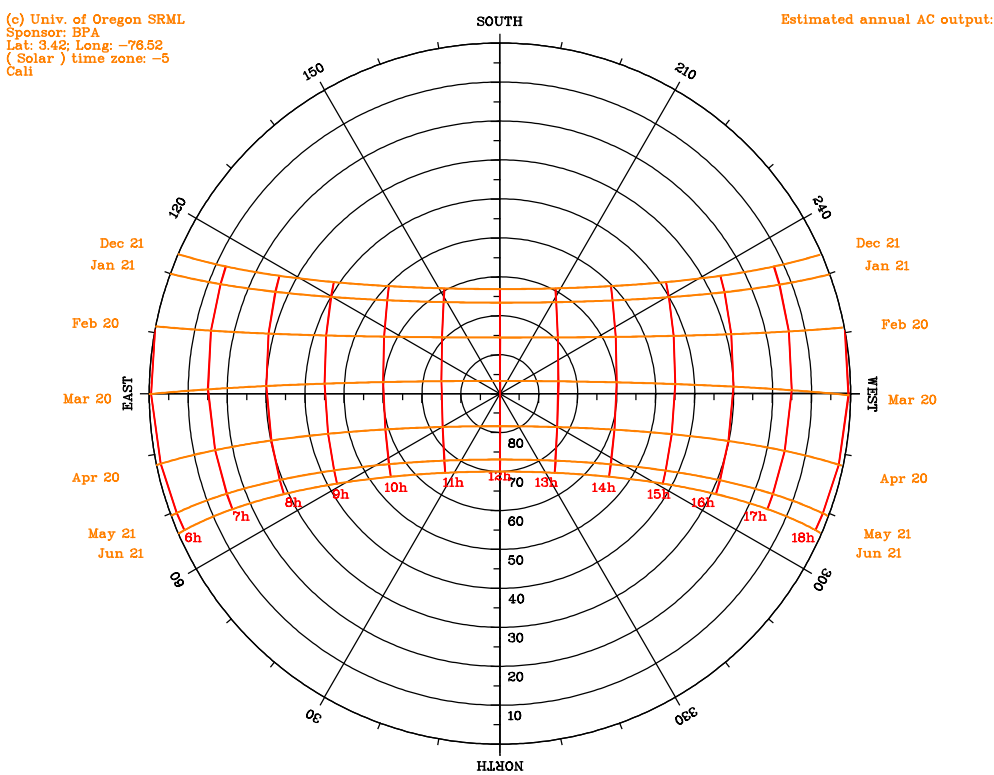


**Figure 16.7:** The sun path in apparent solar time in Cali, Colombia ( $\phi_0 = 3.42^\circ \text{ N}$ ). The sun path was calculated with the Sun path chart program by the *Solar Radiation Monitoring Lab.* of the *Univ. of Oregon* [84].

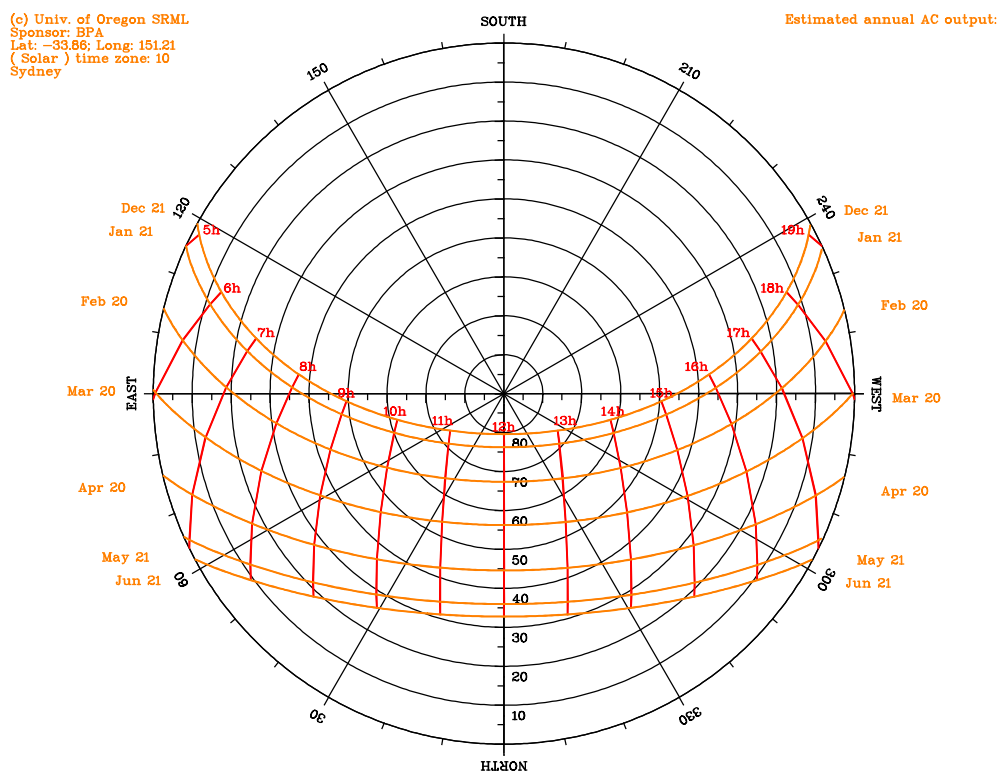


**Figure 16.8:** The sun path in apparent solar time in Sydney, Australia ( $\phi_0 = -33.86^\circ$  S). The sun path was calculated with the Sun path chart program by the *Solar Radiation Monitoring Lab.* of the *Univ. of Oregon* [84].

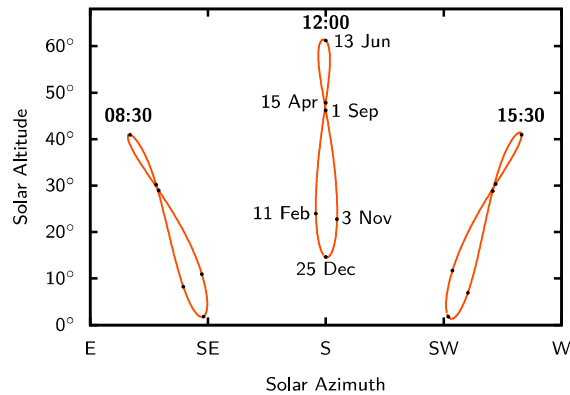


**Figure 16.9:** The analemma, *i.e.* the apparent curve of the sun throughout the year when observed at the same mean solar time every day. The analemma is shown for Delft ( $52^{\circ}$  N latitude) at three points in time during the day.

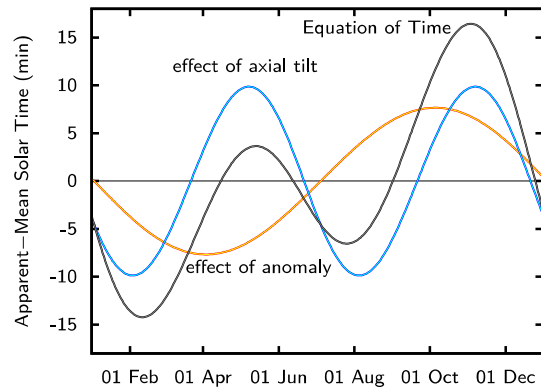


**Figure 16.10:** The effect of the anomaly of the terrestrial orbit and the axial tilt of the Earth rotation axis on the difference between apparent and mean solar time. The equation of time nearly is the sum of these two effects.

We see that the largest negative shift is on 11 February, where, the apparent noon is about 14 min 12 s prior to the mean solar noon. The largest positive shift is on 3 November, when the apparent solar noon is about 16 min 25 s past the mean solar noon. These points are also marked in Fig. 16.9. There, also the zeros of the EoT are shown, which are on 15 April, 13 June, 1 September, and 25 December.

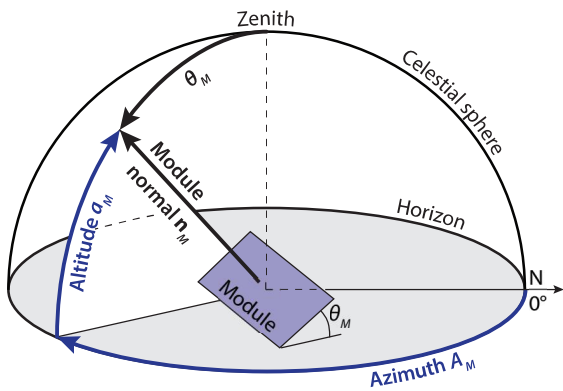


**Figure 16.11:** Illustrating the angles used to describe the orientation of a PV module installed on a horizontal plane.

## 16.4 Irradiance on a PV module

After having discussed how to calculate the position of the Sun everywhere on the Earth and having looked at several examples, it now is time to discuss the implications for the irradiance present on solar modules. For this discussion we assume that the solar module is mounted on a horizontal plane and that it is tilted under an angle  $\theta_M$ , as illustrated in Fig. 16.11. The angle between the projection of the normal of the module onto the horizontal plane and due north is  $A_M$ . We

then can describe the position of the module by the direction of the module normal in horizontal coordinates  $(A_M, a_M)$ , where the altitude is given by  $a_M = 90^\circ - \theta$ . Let now the sun be at the position  $(A_S, a_S)$ . Then the direct irradiance on the module  $G_M$  is given by the equation

$$G_M^{\text{dir}} = I_e^{\text{dir}} \cos \gamma, \quad (16.24)$$

where  $\gamma = \angle(A_M, a_M)(A_S, a_S)$  is the angle between the surface normal and the incident direction of the sunlight. Now we know that the scalar product of two unit vectors is equal to the cosine of the enclosed angle. Thus, we can write,

$$\cos \gamma = \mathbf{n}_M \cdot \mathbf{n}_S. \quad (16.25)$$

The normal vectors are given by

$$\mathbf{n}_M = \begin{pmatrix} \xi_M \\ v_M \\ \zeta_M \end{pmatrix} = \begin{pmatrix} \cos a_M \cos A_M \\ \cos a_M \sin A_M \\ \sin a_M \end{pmatrix}, \quad (16.26)$$

$$\mathbf{n}_S = \begin{pmatrix} \xi_S \\ v_S \\ \zeta_S \end{pmatrix} = \begin{pmatrix} \cos a_S \cos A_S \\ \cos a_S \sin A_S \\ \sin a_S \end{pmatrix}. \quad (16.27)$$

where we used the relationship between Cartesian and spherical horizontal coordinates given in Eq. (16.1).

Hence, we find

$$\begin{aligned}
 \cos \gamma &= \mathbf{n}_M \cdot \mathbf{n}_S \\
 &= \cos a_M \cos A_M \cos a_S \cos A_S \\
 &\quad + \cos a_M \sin A_M \cos a_S \sin A_S + \sin a_M \sin a_S \\
 &= \cos a_M \cos a_S (\cos A_M \cos A_S + \sin A_M \sin A_S) \\
 &\quad + \sin a_M \sin a_S \\
 &= \cos a_M \cos a_S \cos (A_M - A_S) + \sin a_M \sin a_S.
 \end{aligned} \tag{16.28}$$

Thus we obtain for the irradiance

$$\begin{aligned}
 G_M^{\text{dir}} &= I_e^{\text{dir}} [\cos a_M \cos a_S \cos (A_M - A_S) + \sin a_M \sin a_S] \\
 &= I_e^{\text{dir}} [\sin \theta \cos a_S \cos (A_M - A_S) + \cos \theta \sin a_S].
 \end{aligned} \tag{16.29}$$

Note that this equation only holds when the sun is above the horizon ( $a_S > 0$ ) and the azimuth of the sun is within  $\pm 90^\circ$  of  $A_M$ ,  $A_S \in [A_S - 90^\circ, A_S + 90^\circ]$ . Otherwise,  $G_M^{\text{dir}} = 0$ .

If the azimuth of the solar position is the same as the azimuth of the module normal  $A_M = A_S$ , Eq. (16.29) becomes

$$\begin{aligned}
 G_M^{\text{dir}} &= I_e^{\text{dir}} [\cos a_M \cos a_S + \sin a_M \sin a_S] \\
 &= I_e^{\text{dir}} \cos (a_M - a_S).
 \end{aligned} \tag{16.30}$$

When using the tilt angle  $\theta = 90^\circ - a_M$  we find

$$G_M^{\text{dir}} = I_e^{\text{dir}} \sin (\theta + a_S). \tag{16.31}$$

## Modules mounted on a tilted roof

When a module is mounted on a horizontal plane, it is easy to determine its normal  $\mathbf{n}_M$ . However, when a module is to be mounted on an arbitrarily tilted roof things become more complicated. We thus will derive how to calculate the normal of the module in horizontal coordinates when the coordinates with respect to the roof are given. In fact, we thus have to transform the module normal from the *roof coordinate system* to the horizontal coordinate system.

As illustrated in Fig. 16.12 (a), the orientation of the roof in horizontal coordinates is characterised by the azimuth  $A_R$  and the altitude  $a_R$  of its normal  $\mathbf{n}_R$ . The module is installed on the roof, and its orientation with respect to the roof is best described in the roof coordinate system, where the fundamental plane is parallel to the roof and the principal direction is along the gradient of the roof, as illustrated in Fig. 16.12 (b). In this system, the module normal is given by the azimuth  $\phi_M$  and the altitude is given by  $\delta_M$ . The coordinate transform itself is transformed by combining two rotations:

First, we rotate with the angle  $90^\circ - a_R$  around the axis that is perpendicular to both  $\mathbf{n}_R$  and the gradient direction of the roof. Secondly, we rotate with the angle  $A_R + 180^\circ$  along the zenith. We thus obtain

$$\begin{pmatrix} \xi_M \\ v_M \\ \zeta_M \end{pmatrix} = \begin{pmatrix} \cos a_M \cos A_M \\ \cos a_M \sin A_M \\ \sin a_M \end{pmatrix} = \begin{pmatrix} -\cos A_R & \sin A_R & 0 \\ -\sin A_R & -\cos A_R & 0 \\ 0 & 0 & 1 \end{pmatrix} \begin{pmatrix} \sin a_R & 0 & -\cos a_R \\ 0 & 1 & 0 \\ \cos a_R & 0 & \sin a_R \end{pmatrix} \begin{pmatrix} \cos \delta_M \cos \phi_M \\ \cos \delta_M \sin \phi_M \\ \sin \delta_M \end{pmatrix}. \quad (16.32)$$

The coordinates of the module in the horizontal coordinate system then are given by

$$\xi_M = \cos a_M \cos A_M = -\cos A_R \sin a_R \cos \delta_M \cos \phi_M + \sin A_R \cos \delta_M \sin \phi_M + \cos A_R \cos a_R \sin \delta_M, \quad (16.33a)$$

$$v_M = \cos a_M \sin A_M = -\sin A_R \sin a_R \cos \delta_M \cos \phi_M - \cos A_R \cos \delta_M \sin \phi_M + \sin A_R \cos a_R \sin \delta_M, \quad (16.33b)$$

$$\zeta_M = \sin a_M = \cos a_R \cos \delta_M \cos \phi_M + \sin a_R \sin \delta_M. \quad (16.33c)$$

Dividing Eq. (16.33b) by Eq. (16.33a) and leaving Eq. (16.33c) unchanged leads to the final expressions for the module orientation in horizontal coordinates,

$$\tan A_M = \frac{-\sin A_R \sin a_R \cos \delta_M \cos \phi_M - \cos A_R \cos \delta_M \sin \phi_M + \sin A_R \cos a_R \sin \delta_M}{-\cos A_R \sin a_R \cos \delta_M \cos \phi_M + \sin A_R \cos \delta_M \sin \phi_M + \cos A_R \cos a_R \sin \delta_M}, \quad (16.34a)$$

$$\sin a_M = \cos a_R \cos \delta_M \cos \phi_M + \sin a_R \sin \delta_M. \quad (16.34b)$$

Finally, the cosine of the angle between the module orientation and the solar position is given by

$$\begin{aligned} \cos \gamma = \mathbf{n}_M \cdot \mathbf{n}_S &= \cos a_S \cos(A_R - A_S) (\cos a_R \sin \delta_M - \sin a_R \cos \delta_M \cos \phi_M) \\ &\quad + \cos a_S \sin(A_R - A_S) \cos \delta_M \sin \phi_M + \sin a_S (\cos a_R \cos \delta_M \cos \phi_M + \sin a_R \sin \delta_M). \end{aligned} \quad (16.35)$$

We will try to understand these results by discussing easy examples:

First, we look at a roof that faces eastward and has a tilt angle  $\theta_R$ . Then,  $a_R = 90^\circ - \theta_R$  and  $A_R = 90^\circ$ . On this roof a solar module is installed under a tilting angle  $\theta_M$  with respect to the roof. The modules are mounted parallel to the gradient of the roof. We thus have  $\delta_M = 90^\circ - \theta_M$  and  $\phi_M = 270^\circ$ . From Eqs. (16.34) we thus obtain

$$\begin{aligned}\sin a_M &= \cos a_R \cos \delta_M \cdot 0 + \sin a_R \sin \delta_M. \\ &= \sin a_R \sin \delta_M\end{aligned}\quad (16.36a)$$

$$\begin{aligned}\tan A_M &= \frac{-0 - 0 + 1 \cdot \cos a_R \sin \delta_M}{0 + \sin A_R \cos \delta_M \sin 1 + 0} \\ &= \cos a_R \tan \delta_M.\end{aligned}\quad (16.36b)$$

In the second example, the roof is facing southwards and tilted under an angle  $\theta_R$ . We thus have  $a_R = 90^\circ - \theta_R$  and  $A_R = 180^\circ$ . Now the module tilted under an angle  $\theta_M$  with respect to the roof and mounted perpendicular to the gradient of the roof. Hence,  $\delta_M = 90^\circ - \theta_M$  and  $\phi_M = 180^\circ$ . Using Eqs. (16.34) we find

$$\begin{aligned}\sin a_M &= \cos a_R \cos \delta_M \cdot (-1) + \sin a_R \sin \delta_M. \\ &= \cos(a_R + \eta_M) = \sin(a_R - \theta_M).\end{aligned}\quad (16.37a)$$

$$\tan A_M = \frac{-0 - 0 + 0}{-\sin a_R \cos \delta_M + 0 + \cos A_R \sin \delta_M} = 0. \quad (16.37b)$$

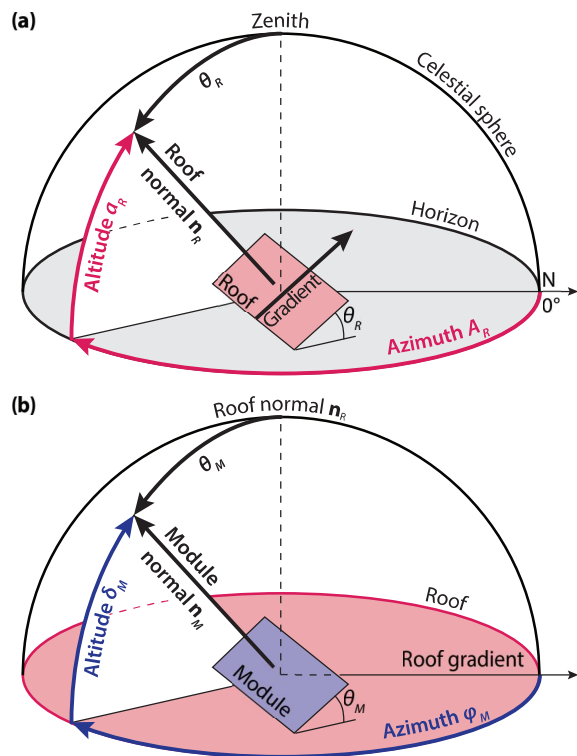


**Figure 16.12:** Illustrating the angles used to describe (a) the orientation of a roof on a horizontal plane and (b) the orientation of a module mounted on a roof.

## 16.5 Direct and diffuse irradiance

As sunlight traverses the atmosphere, it is partially scattered, leading to an attenuation of the *direct beam* component. On the other hand, the scattered light also partially will arrive at on the earth's surface as *diffuse light*. For PV applications it is important to be able to estimate the strength of the direct and diffuse components.

First, we discuss a simple model that allows to estimate the irradiance on a *cloudless sky* in dependence of the *air mass* and hence the altitude of the sun. As we have seen in section 5.5, the air mass is defined as

$$\text{AM} = \frac{1}{\cos \theta} = \frac{1}{\sin a_s}, \quad (16.38)$$

where we used that the angle between the sun and the zenith  $\theta$  is connected to the solar altitude via  $\theta = 90^\circ - a_s$ . This equation, however, does not take the curvature of the earth into account. If the curvature is taken into account, we find [85]

$$\text{AM}(a_s) = \frac{1}{\sin a_s + 0.50572(6.07995 + a_s)^{-1.6364}}. \quad (16.39)$$

To estimate the direct irradiance at a certain solar altitude  $a_s$  and altitude of the observer  $h$ , we can use the following empirical equation [86]

$$I_e^{\text{dir}} = I_e^0 \left[ (1 - ch) \cdot 0.7^{(\text{AM}^{0.678})} + ch \right], \quad (16.40)$$

with the constant  $c = 0.14$ . The solar constant is given as  $I_e^0 = 1361 \text{ W m}^{-2}$ . In a first approximation, the diffuse irradiance is about 10% of the direct irradiance. For the global irradiance we hence obtain [87]

$$I_e^{\text{global}} \approx 1.1 \cdot I_e^{\text{dir}}. \quad (16.41)$$

A more accurate model was developed in the framework of the *European Solar Radiation Atlas* [88]. In that model the direct irradiance for clear sky is given by

$$I_e^{\text{dir}} = I_0^0 \varepsilon \exp [-0.8662 T_L(\text{AM2}) m \delta_R(m)]. \quad (16.42)$$

$I_0$  is the *solar constant* that takes a value of  $1361 \text{ W m}^{-2}$ . The factor  $\varepsilon$  allows to correct for deviations of the sun-earth distance from its mean value.  $a_s$  is the solar altitude angle.  $T_L(\text{AM2})$  is the *Linke turbidity factor* with that the haziness of the atmosphere is taken into account. In this equation its value at an Air Mass 2 is used.  $m$  is the relative optical air mass, and finally  $\delta_R(m)$  is the integral Rayleigh optical thickness. The different components can be evaluated as follows:

The *correction factor*  $\varepsilon$  is given by

$$\varepsilon = \frac{I_e(R)}{I_e^0} = \frac{R^2}{\text{AU}^2}. \quad (16.43)$$

The distance between earth and sun as a multiple of astronomic units (AU) is given in Eq. (16.7). We thus

obtain

$$\varepsilon = (1.00014 - 0.01671 \cos g - 0.00014 \cos 2g)^2, \quad (16.44)$$

which leads to annual variations of about  $\pm 3.3\%$ .

The *Linke Turbidity factor* approximates absorption and scattering in the atmosphere and takes both absorption by water vapour and scattering by aerosol particles into account. It is a unit-less number and typically takes values between 2 for very clear skies and 7 for heavily polluted skies.

The relative optical air mass  $m$  expresses the ratio of the optical path length of the solar beam through the atmosphere to the optical path through a standard atmosphere at sea level with the Sun at zenith. It can be approximated as a function of the solar altitude  $a_S$  by

$$m(a_S) = \frac{\exp(-z/z_h)}{\sin a_S + 0.50572(a_S + 6.07995)^{-1.6364}}. \quad (16.45)$$

Here,  $z$  is the site elevation and  $z_h$  is the scale height of the Rayleigh atmosphere near the Earth surface, given by 8434.5 m.

Finally, the Rayleigh optical thickness  $\delta_R(m)$  is given by

$$\begin{aligned} \frac{1}{\delta_R(m)} = & 6.62960 + 1.75130 m - 0.12020 m^2 \\ & + 0.00650 m^3 - 0.00013 m^4. \end{aligned} \quad (16.46)$$

In their paper, Rigollier *et al.* also take the effect of refraction at very low altitudes into account [88]. This, however is not relevant for our application.

They also present an expression for the diffuse irradiance of the light, which is given by

$$I_e^{\text{dif}} = I_e^0 \varepsilon T_{rd}[T_L(\text{AM2})] F_d[a_S, T_L(\text{AM2})], \quad (16.47)$$

where  $T_{rd}$  is the diffuse transmission function at zenith, which is a second-order polynomial of  $T_L(\text{AM2})$ .  $T_{rd}$  has typical values in between 0.05 for very clear skies and 0.22 for a very turbid atmosphere.  $F_d$  is a diffuse angular function, given as a second-order polynomial of  $\sin a_S$ . For more details we refer to the paper [88].

## 16.6 Shadowing

*Shadowing* had to be kept in mind when planning a PV system that consists of several rows of PV modules, which are placed behind each other. In this section we will determine how far behind the module the shadow reaches in dependence of the solar position, the module orientation and the length  $l$  of the module. Figure 16.13 shows the important notions that we use in this derivation.

For the determination we look at a module that is tilted at an angle  $\theta_M$ . Its normal angle has an azimuth  $A_M$ .

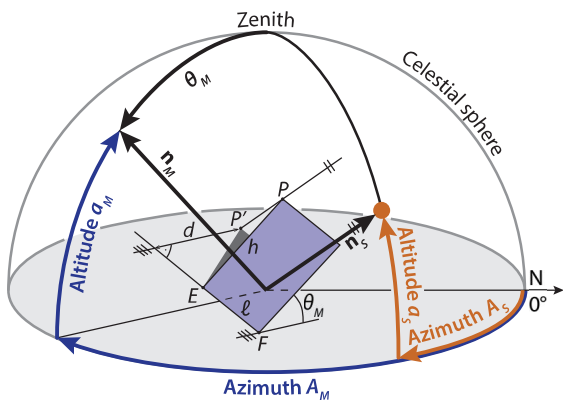


**Figure 16.13:** Derivation of the length  $d$  of a shadow behind a PV module with ground length  $l$  and height  $h$ . The module has the normal  $\mathbf{n}_M$  while the position of the sun is given by the direction  $\mathbf{n}_S$ . The length of the shadow  $d$  is given as the distance between the line connecting the lower module corners  $E$  and  $F$  and the projection of the upper corner  $P$  on the ground ( $P'$ ).

This module touches the ground at two corner points that we call  $E$  and  $F$ . Without loss of generality, we may assume that  $E$  is at the origin of our horizontal coordinate system,  $E = (0, 0, 0)$ . Further,  $P$  is the corner point of top the module lying above  $E$ . The length of the module, i.e. the distance between  $E$  and  $P$  is  $l$ ,  $\overline{EP} = l$ . The shadow of this point on the horizontal plane, we denote by  $P'$ . Then, the length of the shadow  $d$  is defined as the shortest distance between  $P'$  and the line  $g$ , which connects  $E$  with  $F$ .

For the determination of  $d$  we first must derive  $P$ , and then  $P'$ . The normal of the module  $\mathbf{n}_M$  is given by

$$\mathbf{n}_M = \begin{pmatrix} \cos \alpha_M \cos A_M \\ \cos \alpha_M \sin A_M \\ \sin \alpha_M \end{pmatrix} = \begin{pmatrix} \sin \theta_M \cos A_M \\ \sin \theta_M \sin A_M \\ \cos \theta_M \end{pmatrix}. \quad (16.48)$$

The direction vector  $\mathbf{r}$  of the line  $g$  connecting  $E$  with  $F$  is then given as

$$\mathbf{r} = \begin{pmatrix} \sin A_M \\ -\cos A_M \\ 0 \end{pmatrix}. \quad (16.49)$$

Then, we can calculate the direction vector  $\mathbf{h}$  of the line

that connects  $E$  with  $P$  with the vector product

$$\begin{aligned}\mathbf{h} &= -\mathbf{n}_M \times \mathbf{r} \\ &= -\begin{pmatrix} \sin \theta_M \cos A_M \\ \sin \theta_M \sin A_M \\ \cos \theta_M \end{pmatrix} \times \begin{pmatrix} \sin A_M \\ -\cos A_M \\ 0 \end{pmatrix} \\ &= \begin{pmatrix} -\cos \theta_M \cos A_M \\ -\cos \theta_M \sin A_M \\ \sin \theta_M \end{pmatrix},\end{aligned}\quad (16.50)$$

where the  $-$  sign is because of the fact that the horizontal coordinate system is left-hand. Since  $\mathbf{h}$  has length 1, i.e. it is a unit vector, we easily can derive the position of the point  $P$  with

$$P = E + l \cdot \mathbf{h} = l \begin{pmatrix} -\cos \theta_M \cos A_M \\ -\cos \theta_M \sin A_M \\ \sin \theta_M \end{pmatrix}. \quad (16.51)$$

For calculating the position of  $P'$  we define the line  $s$ , which goes through  $P$  and points towards the sun,

$$s(t) = P + t \cdot \mathbf{n}_S. \quad (16.52)$$

When the position of the sun is described by its altitude  $a_S$  and azimuth  $A_S$ , we find

$$s(t) = l \begin{pmatrix} -\cos \theta_M \cos A_M \\ -\cos \theta_M \sin A_M \\ \sin \theta_M \end{pmatrix} + t \begin{pmatrix} \cos a_S \cos A_S \\ \cos a_S \sin A_S \\ \sin a_S \end{pmatrix} \quad (16.53)$$

We find the shadow  $P'$  of the point  $P$  as the intersection of the line  $s$  with the horizontal plane,  $z = 0$ ,

$$l \sin \theta_M + t \sin a_S = 0. \quad (16.54)$$

Hence,

$$t = -l \frac{\sin \theta_M}{\sin a_S}. \quad (16.55)$$

The coordinates of  $P' = (P'_x, P'_y, 0)$  then are given as

$$P'_x = -l (\cos \theta_M \cos A_M + \sin \theta_M \cot a_S \cos A_S), \quad (16.56a)$$

$$P'_y = -l (\cos \theta_M \sin A_M + \sin \theta_M \cot a_S \sin A_S). \quad (16.56b)$$

As stated already earlier, the length of the shadow  $d$  is given as the shortest distance between  $P'$  and the line  $g$  connecting  $E$  and  $F$ . Let  $g'$  be the line through  $P'$  that is perpendicular to  $g$ ,  $g \perp g'$ . Since  $E = (0, 0, 0)$  we find for  $g$  and  $g'$

$$g(u) = u \cdot \mathbf{r}, \quad (16.57a)$$

$$g'(v) = P' + v \cdot \mathbf{r}', \quad (16.57b)$$

where the direction vector  $\mathbf{r}'$  is given as

$$\mathbf{r}' = \begin{pmatrix} \cos A_M \\ \sin A_M \\ 0 \end{pmatrix}. \quad (16.58)$$

$d$  is the distance between  $P'$  and the intersection of  $g$

with  $g'$ . At this intersection we have

$$\begin{aligned} g(u) &= g'(v), \\ u \begin{pmatrix} \sin A_M \\ -\cos A_M \\ 0 \end{pmatrix} &= P' + v \begin{pmatrix} \cos A_M \\ \sin A_M \\ 0 \end{pmatrix} \\ \hline u \sin A_M &= P'_x + v \cos A_M \\ -u \cos A_M &= P'_y + v \sin A_M \\ \hline u \sin A_M \cos A_M &= P'_x \cos A_M + v \cos^2 A_M \\ -u \cos A_M \sin A_M &= P'_y \sin A_M + v \sin^2 A_M \end{aligned}$$

By adding the last two equations we find

$$P'_x \cos A_M + v \cos^2 A_M + P'_y \sin A_M + v \sin^2 A_M = 0, \quad (16.59)$$

and hence

$$v = -P'_x \cos A_M - P'_y \sin A_M. \quad (16.60)$$

Using Eqs. (16.56), we derive

$$\begin{aligned} v &= l[(\cos \theta_M \cos A_M + \sin \theta_M \cot a_S \cos A_S) \cos A_M \\ &\quad + (\cos \theta_M \sin A_M + \sin \theta_M \cot a_S \sin A_S) \sin A_M] \\ &= l(\cos \theta_M \cos^2 A_M + \sin \theta_M \cot a_S \cos A_S \cos A_M \\ &\quad + \cos \theta_M \sin^2 A_M + \sin \theta_M \cot a_S \sin A_S \sin A_M). \end{aligned} \quad (16.61)$$

Because the direction vector  $\mathbf{r}'$  of the line  $g'$  is a unit vector, the length of the shadow  $d$  is equal to  $v$ . Therefore we obtain from Eq. (16.61) with some trigonometric

operations

$$d = l [\cos \theta_M + \sin \theta_M \cot a_S \cos(A_M - A_S)]. \quad (16.62)$$

As a rule of thumb,  $d$  should be at least three times  $l$ ,  $d > 3l$ .

### Example

A PV system should be installed on a flat roof in Naples (Italy). The area of the roof that can be utilized for installing the PV system is  $10 \times 10 \text{ m}^2$ . The roof is oriented such that the sides are parallel to the East-West and North-South directions, respectively.

The owner of the roof decides to use Yingli PANDA 60 modules with dimensions of  $1650 \times 990 \times 40 \text{ mm}^3$ . The modules are installed facing south with a tilt of  $30^\circ$ .

He wants to install as many modules as possible under the condition that on the shortest day of the year no mutual shading must occur for the duration of 6 hours.

Should the modules be mounted with the long or short side touching the ground? How many modules can be mounted in this case?

**Answer:** The shortest day of course is 21 December. The solar position on this day at 9:00 and 15:00 is

Time	Altitude ( $^\circ$ )	Azimuth ( $^\circ$ )
9:00	13.59	138.55
15:00	13.13	222.17

Because of the Equation of Time, the sun is not at its highest point at exactly 12:00 noon. We see, that the solar altitude at 15:00 is just slightly lower than at 9:00. Thus, when using 9:00 for calculating the length of the shadow, the duration without mutual shading will be slightly shorter than 6 hours. Thus, we use the position at 15:00 for the calculation.

The length of the shadow can be calculated with equation (16.62)

$$d = l [\cos \theta_M + \sin \theta_M \cot a_S \cos(A_M - A_S)].$$

We have  $\theta_M=30^\circ$ ,  $A_M=180^\circ$ ,  $a_S=13.13^\circ$ , and  $A_S=222.17^\circ$ .

If the module is mounted to the ground on the short side, we have  $l=1650$  mm. Hence, we find  $d=4050$  mm. The area directly beneath the module at the last row is

$$d' = l \cos \theta_M = 1429 \text{ mm}.$$

Thus, we can mount **three rows** behind each other, because

$$2d + d' = 2 \cdot 4050 + 1429 = 9529 \text{ mm}, \quad (16.63)$$

which is less than 10 m. In one row fit 10 modules because  $10 \cdot 990 = 9900$  mm. Thus, we can place 30 modules.

If the module is mounted to the ground on the long side, we have  $l=990$  mm. Hence, we find  $d=2430$  mm. The area directly beneath the module at the last row is

$$d' = l \cos \theta_M = 857 \text{ mm}.$$

Thus, we can mount **four rows** behind each other, because

$$3d + d' = 3 \cdot 2430 + 857 = 8147 \text{ mm},$$

which is lower than 10 m. In one row fit 6 modules because  $6 \cdot 1650 = 9900$  mm. Thus, we can place 24 modules.

# 17

## Components of PV Systems

### 17.1 PV modules

In this section we will discuss *PV modules* (or solar modules), their fabrication and how to determine their performance.

Before we start with the actual treatment of PV modules, we briefly want to introduce different terms. Figure 17.1 (a) shows a crystalline *solar cell*, which we discussed in Chapter 12. For the moment we will consider only modules that are made from this type of solar cells. A *PV module*, is a larger device in which many solar cells are connected, as illustrated in Fig. 17.1 (b). The names PV module and solar module are often used interchangeably. A *solar panel*, as illustrated in Fig. 17.1

(c), consists of several PV modules that are electrically connected and mounted on a supporting structure. Finally, a *PV array* consists of several solar panels. An example of such an array is shown in Fig. 17.1 (d). This array consists of two strings of two solar panels each, where *string* means that these panels are connected *in series*.

#### 17.1.1 Series and parallel connections in PV modules

If we make a solar module out of an ensemble of solar cells, we can connect the solar cells in different ways: first, we can connect them in a *series connec-*

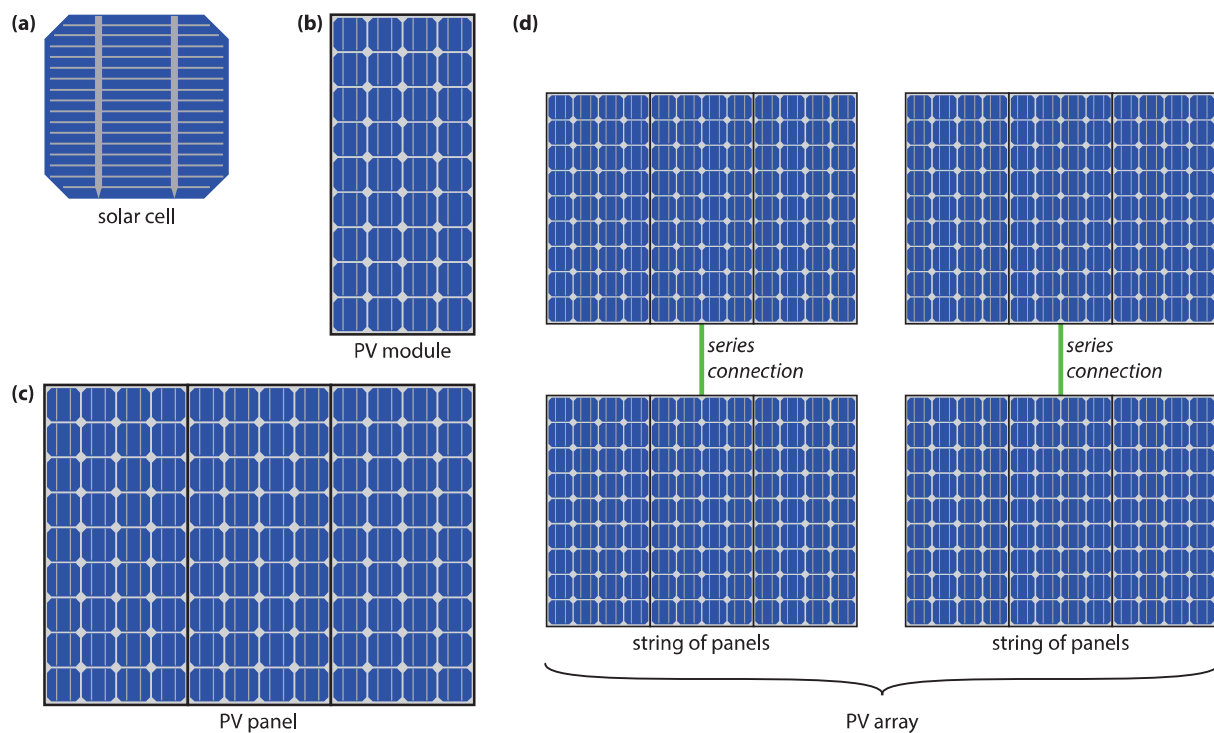


**Figure 17.1:** Illustrating (a) a solar cell, (b) a PV module, (c) a solar panel, and (d) a PV array.

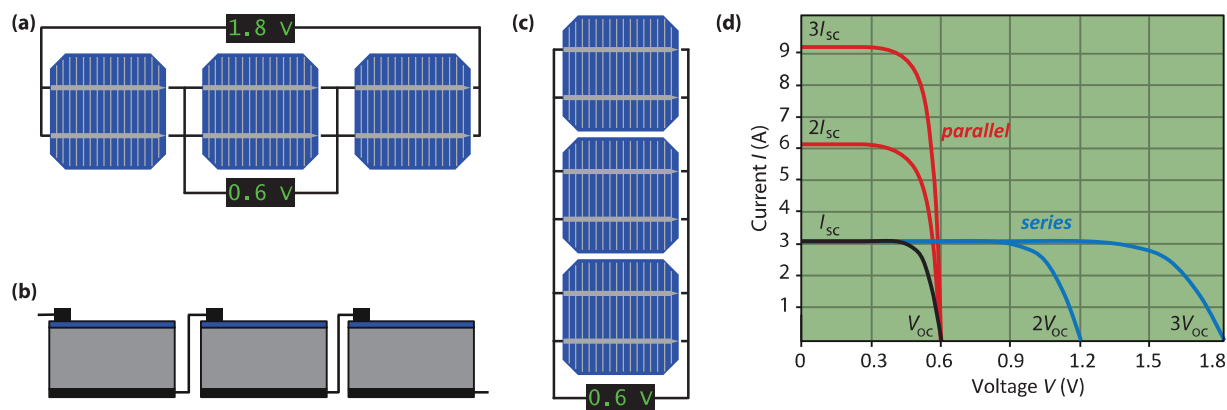


**Figure 17.2:** Illustrating (a) a series connection of three solar cells and (b) realisation of such a series connection for cells with a classical front metal grid. (c) Illustrating a parallel connection of three solar cells. (d)  $I$ - $V$  curves of solar cells connected in series and parallel.

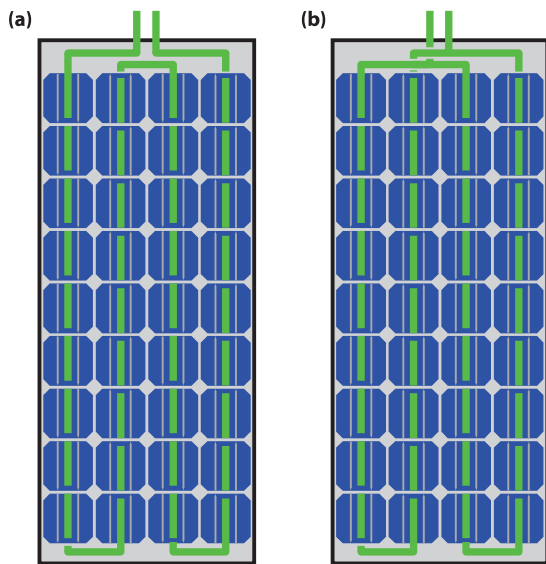
tion as shown in Fig. 17.2 (a). In a series connection the voltages add up. For example, if the open circuit voltage of one cell is equal to 0.6 V, a string of three cells will deliver an open circuit voltage of 1.8 V. For solar cells with a classical front metal grid, a series connection can be established by connecting the bus bars at the front side with the back contact of the neighbouring cell, as illustrated in Fig. 17.2 (b). For series connected cells, the current does not add up but is determined by the photocurrent in each solar cell. Hence, the total current in a string of solar cells is equal to the current generated by one single solar cell.

Figure Fig. 17.2 (d) shows the *I-V* curve of solar cells connected in series. If we connect two solar cells in series, the voltages add up while the current stays the same. The resulting open circuit voltage is two times that of the single cell. If we connect three solar cells in series, the open circuit voltage becomes three times as large, whereas the current still is that of one single solar cell.

Secondly, we can connect solar cells in *parallel* as illustrated in Fig. 17.2 (c), which shows three solar cells connected in parallel. If cells are connected in parallel, the voltage is the same over all solar cells, while the currents of the solar cells add up. If we connect *e.g.* three cells in parallel, the current becomes three times as large, while the voltage is the same as for a single cell, as illustrated in Fig. 17.2 (d).

The reader may have noticed that we used *I-V* curves, *i.e.* the *current-voltage* characteristics, in the previous paragraphs. This is different to Parts II and III, where we used *I-V* curves instead, *i.e.* the *current density - voltage* characteristics. The reason for this switch from *J* to *I* is that on module level, the total current that the module can generate is of higher interest than the current density. As the area of a module is a constant, the shapes of the *I-V* and *J-V* curves of a module are similar.

For a total module, therefore the voltage and current output can be partially tuned via the arrangements of the solar cell connections. Figure 17.3 (a) shows a typical PV module that contains 36 solar cells connected in series. If a single junction solar cell would have a short circuit current of 5 A, and an open circuit voltage of 0.6 V, the total module would have an output of  $V_{oc} = 36 \cdot 0.6 \text{ V} = 21.6 \text{ V}$  and  $I_{sc} = 5 \text{ A}$ . However, if two strings of 18 series-connected cells are connected in parallel, as illustrated in Fig. 17.3 (b), the output of the module will be  $V_{oc} = 18 \cdot 0.6 \text{ V} = 10.8 \text{ V}$  and  $I_{sc} = 2 \times 5 \text{ A} = 10 \text{ A}$ . In general, for the *I-V* characteristics of a module consisting of  $m$  identical cells in series and  $n$  identical cells in parallel the voltage multiplies by a factor  $m$  while the current multiplies by a factor  $n$ . Modern PV modules often contain 60 ( $10 \times 6$ ), 72 ( $9 \times 8$ ) or 96 ( $12 \times 8$ ) solar cells that are usually all connected in series in order to minimise resistive losses.



**Figure 17.3:** Illustrating a PV module consisting (a) of a string of 36 solar cells connected in series and (b) of two strings of 18 solar cells each that are connected in parallel.

### 17.1.2 PV module parameters

In a nutshell, for a PV module a set of parameters can be defined, similar than for solar cells. The most common parameters are the *open circuit voltage*  $V_{oc}$ , the *short circuit current*  $I_{sc}$  and the *module fill factor*  $FF_M$ . On module level, we have to distinguish between the *aperture area efficiency* and the *module efficiency*. The aperture area is defined as the area of the PV-active parts only. The total module area is given as the aperture area plus the dead area consisting of the interconnections and the edges of the module. Clearly, the aperture area efficiency is larger than the module efficiency.

Determining the efficiency and the fill factor of a PV module is less straight-forward than determining voltage and current. In an ideal world with perfectly matched solar cells and no losses, one would expect that the efficiency and fill factor at both the module and cell levels to be the same. This is not the case in real life. As mentioned above. The cells are connected with each other using interconnects that induce resistive losses. Further, there might be small mismatches in the interconnected cells. For example, if  $m \times n$  cells are interconnected, the cell with the lowest current in a string of  $m$  cells in series determines the module current. Similarly, the string with the lowest voltage in the  $n$  strings that are connected in parallel dictates the module voltage. The reason for mismatch between individual cells are inhomogeneities that occur during

the production process. Hence, in practice PV module perform a little less than what one would expect from ideally matched and interconnected solar cells. This loss in performance translates to a lower fill factor and efficiency at module level. If the illumination across the module is not constant or if the module is heats up non-uniformly, the module performance reduces even further.

Often, differences between cell and module performance are mentioned in datasheets that are provided by the module manufacturers. For example, the datasheet of a Sanyo HIT-N240SE10 module gives a cell level efficiency of 21.6%, but a module level efficiency of only 19%. Despite all the technological advancements being made at solar cell level for improving the efficiency, still a lot must be done at the PV systems level to ensure a healthy PV yield. For the performance of a PV system, not only the module performance is important, but also the yield of the PV system.

### 17.1.3 Partial shading and bypass diodes

PV modules have so-called *bypass diodes* integrated. To understand the reason for using such diodes, we have to consider modules in real-life conditions, where they can be *partially shaded*, as illustrated in Fig. 17.4 (a). The shade can be from an object nearby, like a tree, a chimney or a neighbouring building. It also can be caused

by a leaf that has fallen from a tree. Partial shading can have significant consequences for the output of the solar module. To understand this, we consider the situation in which one solar cell in the module shaded for a large part shaded. For simplicity, we assume that all six cells are connected in series. This means that the current generated in the shaded cell is significantly reduced. In a series connection the current is limited by the cell that generates the lowest current, this cell thus dictates the maximum current flowing through the module.

In Fig. 17.4 (b) the theoretical *I-V* curve of the five unshaded solar cells and the shaded solar cell is shown. If the cells are connected to a constant load  $R$ , the voltage across the module is dropping due to the lower current generated. However, since the five unshaded solar cells are forced to produce high voltages, they act like a reverse bias source on the shaded solar cell. The dashed line in Fig. 17.4 (b) represents the reverse bias load put on the shaded cell, which is the *I-V* curve of the five cells, reflected across the vertical axis equal to 0 V. Hence, the shaded solar cell does not generate energy, but starts to dissipate energy and heats up. The temperature can increase to such a critical level, that the encapsulation material cracks, or other materials wear out. Further, high temperatures generally lead to a decrease of the PV output as well.

These problems occurring from partial shading can be

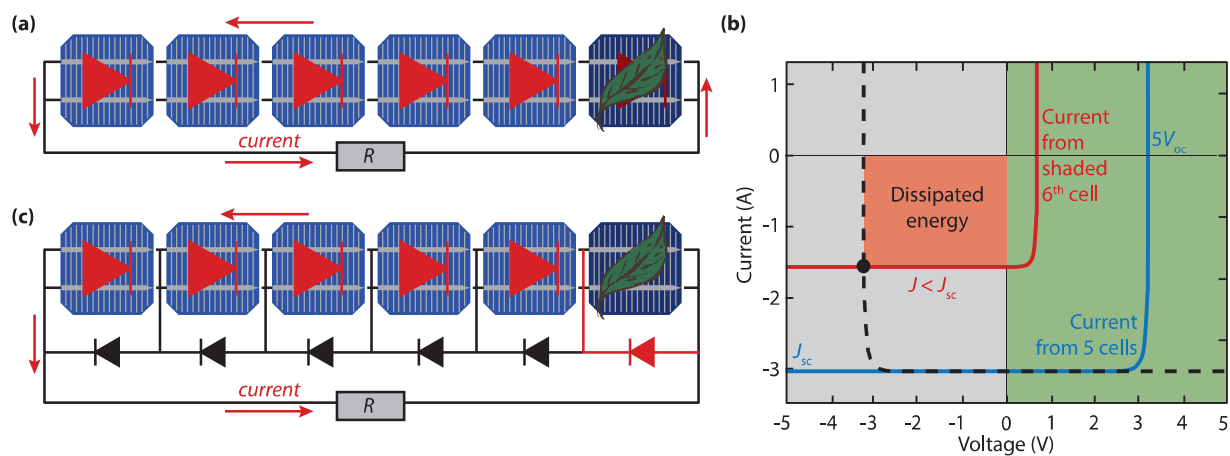


**Figure 17.4:** Illustrating (a) string of six solar cells of which one is partially shaded, which (b) has dramatic effects on the  $I$ - $V$  curve of this string. (c) Bypass diodes can solve the problem of partial shading.

prevented by including bypass diodes in the module, as illustrated in 17.4 (c). As discussed in Chapter 8, a diode blocks the current when it is under negative voltage, but conducts a current when it is under positive voltage. If no cell is shaded, no current is flowing through the bypass diodes. However, if one cell is (partially) shaded, the bypass diode starts to pass current through because of the biasing from the other cells. As a result current can flow around the shaded cell and the module can still produce the current equal to that of a unshaded single solar cell.

For cells that are connected in parallel, partial shading is less of a problem, because the currents generated in the others cells do not need to travel through the shaded cell. However, a module consisting of 36 cells in parallel have very high currents (above 100 A) combined with a very low voltage (approx. 0.6 V). This combination would lead to very high resistive losses in the cables; further an inverter that has only 0.6 V as input will not be very efficient, as we will see in Section 17.3. Therefore, combining the cells in series and using bypass diodes is much better an option to do.

#### 17.1.4 Fabrication of PV modules

As discussed in the subsection 17.1.5, a PV module must withstand various influences in order to survive a lifetime of 25 years or even longer. In order to ensure

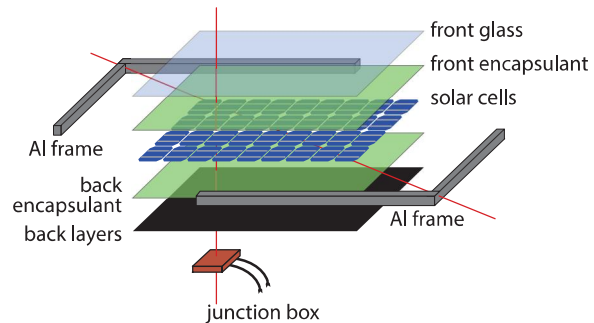


**Figure 17.5:** The components of a typical c-Si PV module.

a long lifetime, the components of that a PV module is built must be well chosen. Fig. 17.5 shows the typical components of a usual crystalline silicon PV module. Of course, the layer stack may consist of different materials dependent on the manufacturer. The major components are [89]:

- *Soda-lime* glass with a thickness of several millimetres, which provides mechanical stability while being transparent for the incident light. It is important the glass has a low iron content because iron leads to absorption of light in the glass which can lead to losses. Further, the glass must be *tempered* in order to increase its resistance to impacts.

- The solar cells are sandwiched in between two layers of *encapsulants*. The most common material is *ethylene-vinyl-acetate* (EVA), which is a thermoplastic polymer (plastic). This means that it goes into shape when it is heated but that these changes are reversible.
- The *back layer* acts as a barrier against humidity and other stresses. Depending on the manufacturer, it can be another glass plate or a composite polymer sheet. A material combination that is often used is PVF-polyester-PVF, where PVF stands for *polyvinyl fluoride*, which is often known by its brand name *Tedlar*<sup>®</sup>. PVF has a low permeability for vapours and is very resistive against weathering. A typical polyester is *polyethylene terephthalate* (PET)
- A *frame* usually made from aluminium is put around the whole module in order to enhance the mechanical stability.
- A *junction box* usually is placed at the back of the module. In it the electrical connections to the solar cell are connected with the wires that are used to connect the module to the other components of the PV system.

One of the most important steps during module production is *laminating*, which we briefly will explain for the case that EVA is used as encapsulant [89]. For lamination, the whole stack consisting of front glass, the

encapsulants, the interconnected solar cells, and the back layer are brought together in a laminator, which is heated above the melting point of EVA, which is around 120°C. This process is performed *in vacuo* in order to ensure that air, moisture and other gasses are removed from within the module stack. After some minutes, when the EVA is molten, pressure is applied and the temperature is increased to about 150°C. Now the *curing* process starts, *i.e.* a curing agent, which is present in the EVA layer, starts to cross-link the EVA chains, which means that transverse bonds between the EVA molecules are formed. As a result, EVA has elastomeric, rubberlike properties.

The choice of the layers that light traverses before entering the solar cell is also very important from an optical point of view. If these layers have an increasing refractive index, they act as antireflective coating and thus can enhance the amount of light that is in-coupled in the solar cell and finally absorbed, which increases the current produced by the solar cell.

### 17.1.5 Lifetime testing of PV Modules

The typical lifetime of PV systems is about 25 years. In these as little maintenance as possible should be required on the system components, especially the PV modules are required to be maintenance free. Furthermore, degradation in the different components of that

the module is made should be little: manufacturers typically guarantee a power between 80% and 90% of the initial power after 25 years. During the lifetime of 25 years or more, PV modules are exposed to various external stress from various sources [90]:

- *temperature* changes between night and day as well as between winter and summer,
- *mechanical stress* for example from wind, snow and hail,
- stress by agents transported via the *atmosphere* such as dust, sand, salty mist and other agents,
- *moisture* originating from rain, dew and frost,
- *humidity* originating from the atmosphere,
- *irradiance* consisting of direct and indirect irradiance from the sun; mainly the highly-energetic UV radiation is challenging for many materials.

Before PV modules are brought to the market, they are usually tested extensively in order to assure their stability against these various stresses. The required tests are extensively defined in the standards *IEC 61215* for modules based on crystalline silicon solar cells and in *IEC 61646* for thin-film modules. Since the modules cannot be tested during a period of 25 years, *accelerated stress testing* must be performed. The required tests are [91]:

- *Thermal cycles* for studying whether thermal stress

leads to broken interconnects, broken cells, electrical bond failure, adhesion of the junction box, ...

- *Damp heat* testing to see whether the modules suffer from corrosion, delamination, loss of adhesion and elasticity of the encapsulant, adhesion of the junction box, ...
- *Humidity freeze* testing in order to test delamination, adhesion of the junction box, ...
- *UV testing*, because UV light can lead to delamination, loss of adhesion and elasticity of the encapsulant, ground fault due to backsheet degradation. Mainly, UV light can lead to a discoloration of the encapsulant and back sheet, which means that they get yellow. This can lead to losses in the amount of light that reaches the solar cells.
- *Static mechanical loads* in order to test whether strong winds or heavy snow loads lead to structural failures, broken glass, broken interconnect ribbons or broken cells.
- *Dynamic mechanical load*, which can lead to broken glass, broken interconnect ribbons or broken cells.
- *Hot spot* testing in order to see whether hot spots due to shunts in cells or inadequate bypass diode protection are present.
- *Hail testing* to see whether the module can handle the mechanical stress induced by hail.

- *Bypass diode thermal testing* to study whether overheating of these diodes causes degradation of the encapsulant, backsheet or the junction box.
- *Salt spray testing* to see whether salt that is present in salty mist or that is used in salty water for snow and ice removal leads to corrosion of PV module components.

How these tests are to be performed is defined in other standards, for example IEC 61345 for UV testing and IV 61701 for salt-mist corrosion testing. Usually these tests are carried out by organisations like TÜV Rheinland. Refining the test requirements and understanding which accelerated tests are required to guarantee a lifetime of 25 years and more is subject to ongoing research and development.

### 17.1.6 Thin-film modules

Making thin-film modules is very different from making modules from c-Si solar cells. While for c-Si technology producing solar cells and producing PV modules are two distinct steps, in thin-film technology producing cells and modules cannot be separated from each other. To illustrate this we look at a PV module where the thin-films are deposited in *superstrate configuration* on glass, as illustrated in Fig. 17.6. For making such a module, a transparent front contact, a stack of

(photo)active layers that also contain one or more semiconductor junctions, and a metallic back contact are deposited onto each other. In industrial production, the glass plates on that these layers are deposited can be very large, with sizes significantly exceeding  $1 \times 1 \text{ m}^2$ .

Such a stack of layers deposited onto a large glass plate in principle forms one very large solar cell that will produce a very high current. Since all the current would have to be transported across the front and back contacts, which are very thin, resistive losses in the module is even a bigger problem than for c-Si modules. Therefore, the module is produced such that it consists of many very narrow cells of about 1 cm width and the length being equal to the module length. These cells then are connected in series across the width of the module. On the very left and right of the module metallic busbars collect the current and conduct it to the bottom of the module where they are connected with external cables.

The series connection is established with *laser scribing*. In total, *three* laser scribes are required for separating two cells from each other and establishing a series connection between them. The first laser scribe, called P1, is performed after the transparent front contact is deposited, as shown in Fig. 17.6 (a). The wavelength of the laser is such that the laser light is absorbed in the front contact and the material is evaporated, leaving a “gap” in the front contact, as shown in Fig. 17.6 (b).

Then the photoactive layers are deposited onto the front contact and also fill the gaps. Then, the second laser scribe, called P2, is performed, as illustrated in Fig. 17.6 (c). The laser wavelength has to be chosen such that it is not absorbed in the transparent front contact but in the absorber layer. For example, if the absorber consists of amorphous silicon, green laser light can be used. The P2 scribe leaves a gap in the absorber layer, as illustrated in Fig. 17.6 (d). The next step is the deposition of the metallic back contact that also fills the P2 gap. Finally, the third laser scribe (P3) is performed as illustrated in Fig. 17.6 (e). The wavelength for this scribe has to be chosen such that it is neither absorbed in the front contact nor in the absorber stack, so it is, for example, infrared. The P3 scribe shoots a gap into the back contact, as shown in Fig. 17.6 (f).

To understand the action of the laser scribes, we take a look at Fig. 17.6 (f): the P1 scribe filled with absorber material forms a barrier, since the absorber is orders of magnitudes less conductive than the transparent front contact. Similar, the P3 scribes forms an insulating gap in the metallic back contact. However, the P2 scribe that also is filled with metal forms a highly conducting connection between the front and back contacts – here the actual series connection is performed.

For example, for making CIGS solar cells, first the molybdenum back contact is deposited on top of the glass substrate and the cell areas are defined by P1 laser

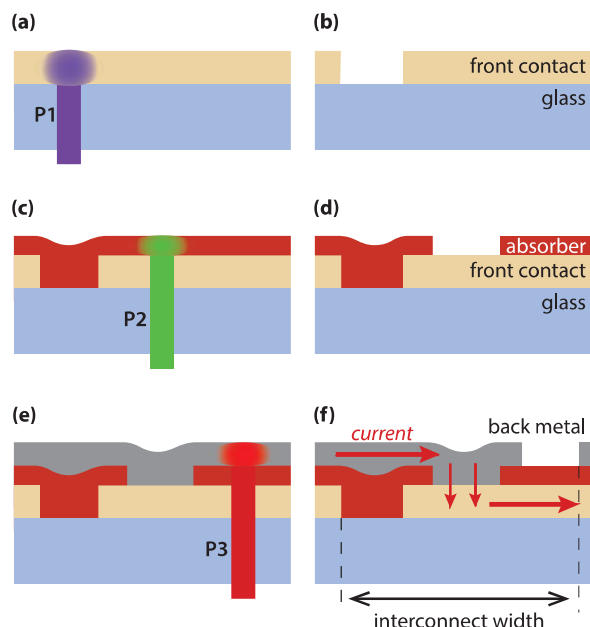


**Figure 17.6:** Schematic of creating an interconnect in thin-film module. (Explanation given in the text).

scribes. Then the CIGS  $p$  layer and the CdS  $n$  layer are deposited including a P2 laser scribe step. Finally the intrinsic and  $n$ -doped zinc oxide is deposited, followed by a final P3 laser scribe step. Now the front TCO electrode is connected with the Molybdenum back contact of the next solar cell.

The performance of such an interconnect established via laser scribes and hence the total module performance is determined by several things. First, the P2 scribe has to be highly conductive, This means that it has to be wide enough and that there must be no barrier at the interface between the front contact and the metal of the P2 scribe. Further, the P1 and P3 scribes must perform good barriers to effectively separate the cells from each other. Thirdly, the region between the P1 and P3 scribes does not contribute to the the current generated by the module. Therefore, the ratio between this width and the total cell width (including the scribes) has to be as small as possible. Another issue is the fact that the three laser scribes are performed in different steps of production and thus often in different machines. Further, the distance between the scribes might be different at the different processes when they are performed at different temperatures. This, aligning the glass plates in all the production steps is extremely important for manufacturing high-quality thin-film modules.

The production steps and also the exact processing of the laser scribes is of course dependent on which thin-

film technology is used and even on the manufacturer itself. However, the basic principles and the action behind these processes is valid in general.

One advantage of thin-film PV technology is that they can be deposited onto flexible substrates. For example, the Dutch company HyET Solar developed a technology, where thin-film silicon layers are deposited onto a temporary aluminium substrate [92]. After the solar cell layers are encapsulated on the back side, the temporary substrate is etched away, and the front side is encapsulated. This results in a very low weight flexible substrate, which can be integrated for example in curved roof top elements. A very big advantage is that such very light modules can be installed on simple roof top constructions that only can handle little ballast. On such roofs, heave PV panels with glass cannot be installed. Further, if such flexible modules are directly integrated into roofing elements, installation costs can be reduces significantly. Often, installation costs are the largest contributor to the non-modular costs of a PV system. Currently, only thin-film silicon technologies have demonstrated flexible modules with reasonable efficiencies.

### 17.1.7 Some examples

Table 17.1 shows some parameters of PV modules using different PV technologies:

**Table 17.1:** Specifications of different PV modules.

	<b>SunPower X21-345</b>	<b>Avancis PowerMax140</b>	<b>Kaneka U-EA120</b>	<b>First Solar FS-392</b>
Technology	c-Si	CIS	a-Si/nc-Si	CdTe
Rated power $P_{\text{mpp}}$	(W <sub>p</sub> )	345	140	92.5
Rated current $I_{\text{mpp}}$	(A)	6.02	2.98	1.94
Rated voltage $V_{\text{mpp}}$	(V)	57.3	47	55
Short circuit current $I_{\text{sc}}$	(A)	6.39	3.31	2.6
Open circuit voltage $V_{\text{oc}}$	(V)	68.2	61.5	71
Dimensions	(m × m)	1.56 × 1.05	1.6 × 0.67	1.2 × 1.00
Max warranty on $P_{\text{mpp}}$	(years)	25	25	25

- A SunPower module made based on monocrystalline silicon solar cells,
- an Avancis module based on copper indium diselenide (CIS) technology,
- a Kaneka amorphous silicon /nanocrystalline silicon tandem (a-Si:H/nc-Si:H) module, and
- a module of First Solar based on cadmium telluride (CdTe) technology.

## 17.2 Maximum power point tracking

In this section we discuss the concept of *Maximum power point tracking* (MPPT). This concept is very unique to the field of PV Systems, and hence brings a very special application of power electronics to the field of photovoltaics. The concepts discussed in this section are equally valid for cells, modules, and arrays, although MPPT usually is employed at PV module/array level.

As discussed earlier, the behaviour of an illuminated solar cell can be characterised by an *I-V* curve. Interconnecting several solar cells in series or in parallel merely increases the overall voltage and/or current, but

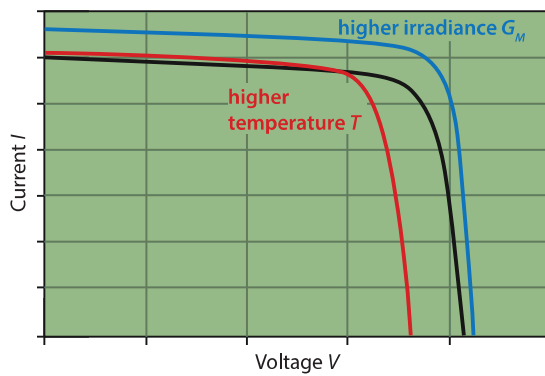


**Figure 17.7:** Effect of increased temperature  $T$  or irradiance  $G_M$  on the  $I$ - $V$  curve.

does not change the shape of the  $I$ - $V$  curve. Therefore, for understanding the concept of MPPT, it is sufficient to consider the  $I$ - $V$  curve of a solar cell. The  $I$ - $V$  curve is dependent on the module temperature on the irradiance, as we will discuss in detail in Section 18.3. For example, an increasing irradiance leads to an increased current and slightly increased voltage, as illustrated in Fig. 17.7. The same figure shows that an increasing temperature has a detrimental effect on the voltage.

Now we take a look at the concept of the *operating point*, which is defined as the particular voltage and

current, at that the PV module operates at any given point in time. For a given irradiance and temperature, the operating point corresponds to a unique  $(I, V)$  pair which lies onto the  $I$ - $V$  curve. The power output at this operating point is given by

$$P = I \cdot V. \quad (17.1)$$

The operating point  $(I, V)$  corresponds to a point on the power-voltage ( $P$ - $V$ ) curve, shown in Fig. 17.8. For generating the highest power output at a given irradiance and temperature, the operating point should such correspond to the maximum of the ( $P$ - $V$ ) curve, which is called the *maximum power point* (MPP).

If a PV module (or array) is directly connected to an electrical load, the operating point is dictated by that load. For getting the maximal power out of the module, it thus is imperative to force the module to operate at the maximum power point. The simplest way of forcing the module to operate at the MPP, is either to force the voltage of the PV module to be that at the MPP (called  $V_{\text{mpp}}$ ) or to regulate the current to be that of the MPP (called  $I_{\text{mpp}}$ ).

However, the MPP is dependent on the ambient conditions. If the irradiance or temperature change, the  $I$ - $V$  and the  $P$ - $V$  characteristics will change as well and hence the position of the MPP will shift. Therefore, changes in the  $I$ - $V$  curve have to be tracked continuously such that the operating point can be adjusted to

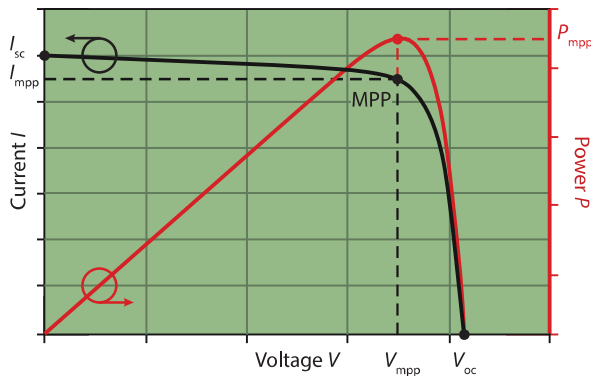


**Figure 17.8:** A generic  $I$ - $V$  curve and the associated  $P$ - $V$  curve. The maximum power point (MPP) is indicated.

be at the MPP after changes of the ambient conditions.

This process is called *Maximum Power Point Tracking* or MPPT. The devices that perform this process are called *MPP trackers*. We can distinguish between two categories of MPP tracking:

- *Indirect* MPP tracking, for example performed with the *Fractional Open Circuit Voltage* method.
- *Direct* MPP tracking, for example performed with the *Perturb and Observe* method or the the *Incremental Conductance* method.

All the MPPT algorithms that we discuss in this section are based on finding the and tuning the voltage until  $V_{MPP}$  is found. Other algorithms, which are not discussed in this section, work with the power instead and aim to find  $I_{MPP}$ .

### 17.2.1 Indirect MPPT

First, we discuss *indirect* MPP Tracking, where simple assumptions are made for estimating the MPP based on a few measurements.

#### Fixed voltage method

For example, in the *fixed voltage* method (also called *constant voltage* method), the operating voltage of the

solar module is adjusted only on a seasonal basis. This model is based on the assumption that for the same level of irradiance higher MPP voltages are expected during winter than during summer. It is obvious that this method is not very accurate. It works best at locations with minimal irradiance fluctuations between different days.

### Fractional open circuit voltage method

One of the most common *indirect* MPPT techniques is the *fractional open circuit voltage* method. This method exploits the fact that – in a very good approximation – the  $V_{\text{mpp}}$  is given by

$$V_{\text{mpp}} = k \cdot V_{\text{oc}}, \quad (17.2)$$

where  $k$  is a constant. For crystalline silicon,  $k$  usually takes values in between 0.7 and 0.8. In general,  $k$  of course is dependent on the type of solar cells. As changes in the open circuit voltage can be easily tracked, changes in the  $V_{\text{mpp}}$  can be easily estimated just by multiplying with  $k$ . This method thus can be implemented easily. However, there are also certain drawbacks.

First, using a constant factor  $k$  only allows to roughly estimate the position of the MPP. Therefore, the operating point usually will not be exactly on the MPP but in its proximity, with is called the *MPP region*. Secondly,

every time the system needs to respond to a change in illumination conditions, the  $V_{\text{oc}}$  must be measured. For this measurement, the PV module needs to be disconnected from the load for a short while, which will lead to a reduced total output of the PV system. The more often the  $V_{\text{oc}}$  is determined, the larger the loss in output will be. This drawback can be overcome by slightly modifying the method. For this modification a pilot PV cell is required, which is highly matched with the rest of the cells in the module. The pilot cell receives the same irradiance as the rest of the PV module, and a measurement of the pilot PV cell's  $V_{\text{oc}}$  also gives an accurate representation of that of the PV module, hence it can be used for estimating  $V_{\text{mpp}}$ . Therefore, the operating point of the module can be adjusted without needing to disconnect the PV module.

### 17.2.2 Direct MPPT

Now we discuss *direct* MPP tracking, which is more involved than indirect MPPT, because current, voltage or power measurements are required. Further, the system must respond more accurately and faster than in indirect MPPT. We shall look at a couple of the most popular kind of algorithms.

**Table 17.2:** A summary of the possible options in the P&O algorithm.

Prior Perturbation	Change in Power	Next Perturbation
Positive	Positive	Positive
Positive	Negative	Negative
Negative	Positive	Negative
Negative	Negative	Positive

### Perturb and observe (P&O) algorithm

The first algorithm that we discuss is the *Perturb and Observe* (P&O) algorithm, which also is known as "hill climbing" algorithm. In this algorithm, a perturbation is provided to the voltage at that the module is currently driven. This perturbation in voltage will lead to a change in the power output. If an increasing voltage leads to an increasing in power, the operating point is at a lower voltage than the MPP, and hence further voltage perturbation towards higher voltages is required to reach the MPP. In contrast, if an increasing voltage leads to a decreasing power, further perturbation towards lower voltages is required in order to reach the MPP. Hence, the algorithm will converge towards the MPP over several perturbations. This principle is summarised in Table 17.2.

A problem with this algorithm is that the operat-

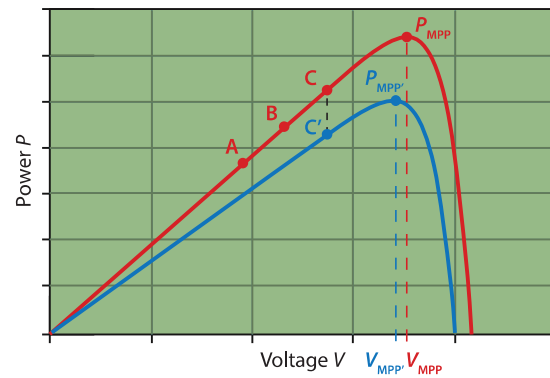


**Figure 17.9:** The *perturb&observe* algorithm struggles from rapidly changing illumination conditions.

ing point is never steady at the MPP but meandering around the MPP. If very small perturbation steps are used around the MPP, this meandering, however, can be minimised. Additionally, the P&O algorithm struggles from rapidly changing illuminations. For example, if the illumination (and hence the irradiance) changes in between two sampling instants in the process of convergence, then the algorithm essentially fails in its convergence efforts, as illustrated in Fig. 17.9. In the latest perturbation, the algorithm has determined that the MPP lies to the right at a higher voltage than of point B, and hence the next step is a perturbation to converge towards the MPP accordingly. If the illumination was constant, it would end up at C and the algorithm would conclude that the MPP is at still higher voltages, which is correct. However, as the illumination changes rapidly before the next perturbation, the next perturbation shifts the operating point to C' instead to C, such that

$$P_{C'} < P_B \quad (17.3)$$

While the MPP still lies to the right of C', the P&O algorithm thinks that it is on the left of C'. This wrong assumption is detrimental to the speed of convergence of the P&O algorithm, which is one of the critical figures of merit for MPPT techniques. Thus, drastic changes in weather conditions severely affect the efficacy of the P&O algorithm's.

### Incremental conductance method

Next, we look at the *Incremental Conductance Method*. The *conductance*  $G^1$  of an electrical component is defined as

$$G = \frac{I}{V} \quad (17.4)$$

At the MPP, the slope of the *P-V* curve is zero, hence

$$\frac{dP}{dV} = 0. \quad (17.5)$$

We can write

$$\frac{dP}{dV} = \frac{d(IV)}{dV} = I + V \frac{dI}{dV}. \quad (17.6)$$

If the sampling steps are small enough, the approximation

$$\frac{dI}{dV} \approx \frac{\Delta I}{\Delta V} \quad (17.7)$$

can be used. We call  $\Delta I / \Delta V$  the *incremental conductance* and  $I/V$  the *constantaneous conductance*. Hence, we have

$$\frac{\Delta I}{\Delta V} = -\frac{I}{V} \quad \text{if} \quad V = V_{\text{mpp}}, \quad (17.8a)$$

$$\frac{\Delta I}{\Delta V} > -\frac{I}{V} \quad \text{if} \quad V < V_{\text{mpp}}, \quad (17.8b)$$

$$\frac{\Delta I}{\Delta V} < -\frac{I}{V} \quad \text{if} \quad V > V_{\text{mpp}}. \quad (17.8c)$$

<sup>1</sup>The electrical conductance  $G$  must not be confused with the irradiance incident on the module  $G_M$ .

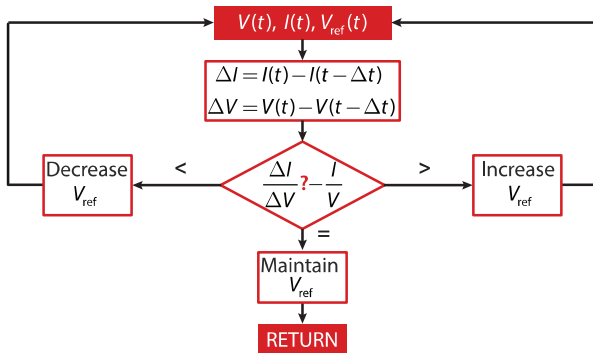


**Figure 17.10:** A conceptual flowchart of the *incremental conductance* algorithm.

These relationships are exploited by the incremental conductance algorithm.

Figure 17.10 shows a conceptual flowchart. Note that this flowchart is not exhaustive. While both, the instantaneous voltage and current are the observable parameters, the instantaneous voltage is also the controllable parameter.  $V_{\text{ref}}$  is the voltage value forced on the PV module by the MPPT device. It is the latest approximation of the  $V_{\text{mpp}}$ . For any change of the operating point, the algorithm compares the instantaneous with the incremental conductance values. If the incremental conductance is larger than the negative of the instantan-

eous conductance, the current operating point is to the left of the MPP; consequently,  $V_{\text{ref}}$  must be incremented. In contrast, if the incremental conductance is lower than the negative of the instantaneous conductance, the current operating point is to the left of the MPP and the is consequently decremented. This process is iterated until the incremental conductance is the same as the negative instantaneous conductance, in which case  $V_{\text{ref}} = V_{\text{mpp}}$ .

The incremental conductance algorithm can be more efficient than the P&O algorithm as it does not meander around the MPP under steady state conditions. Further, small sampling intervals make it less susceptible to changing illumination conditions. However, under conditions that are strongly varying and under partial shading, the incremental conductance method might also become less efficient. The major drawback of this algorithm is the complexity of its hardware implementation. Not only currents *and* voltages must be measured, but also the instantaneous and incremental conductances must be calculated and compared. How such a hardware design can look like however is beyond the scope of this book.

### 17.2.3 Some remarks

While a MPPT is used to find the MPP by changing the voltage, it does not perform changes of the operating voltage. This is usually done by a DC-DC converter

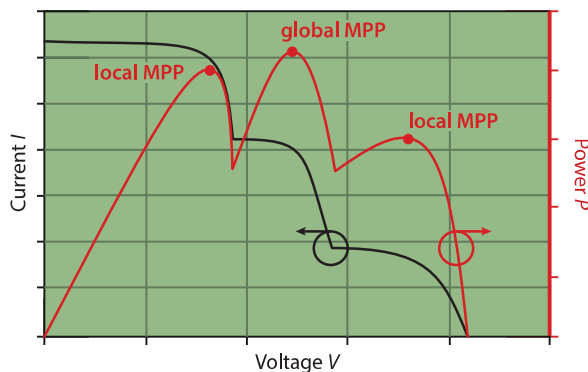


**Figure 17.11:** The  $P$ - $V$  curve of partially shaded system that exhibits several local maxima.

that will be discussed in section 17.3.2.

In modern PV systems, the MPPT is often implemented within other system components like the inverters or charge controllers. The list of techniques presented in this section not exhaustive, we just discussed the most common ones. The development of more advanced MPPT techniques is going on rapidly and many scientific papers as well as patents are published in this area. Furthermore, manufacturers usually use proprietary techniques.

Up to now we only looked at situations the total  $I$ - $V$

curve is similar to that of a single cell. Let us now consider a system that is partially shaded, as illustrated in Fig. 17.11. Then, the  $P$ - $V$  curve will have different local maxima. Depending on the used MPPT algorithm, it is not sure at all that the algorithm finds the global maximum. Different companies use proprietary solutions to tackle this issue. Alternatively, each string can be connected to a separate MPPT. There are inverters that have connections for several strings (usually two).

## 17.3 Photovoltaic Converters

A core technology associated with PV systems is the power electronic converter. An ideal PV converter should draw the maximum power from the PV panel and supply it to the load side. In case of grid connected systems, this should be done with the minimum harmonic content in the current and at a power factor close to unity. For stand-alone systems the output voltage should also be regulated to the desired value. In this section a short review of different topologies often associated with PV systems is given. The semiconductor switches in the following are assumed to be ideal.

### 17.3.1 System configurations

Before digging into details about different converter topologies used for power conversion in PV systems, a general overview of different system architecture will be presented. The system architecture determines how PV modules are interconnected and how the interface with the grid is established. Which of these system architectures will be employed in a particular PV plant depends on many factors such as environment of the plant (whether the plant is situated in an urban environment or at an open area), scalability, costs etc. Figure 17.12 an overview of different system architectures is given. The main advantages and disadvantages of the different architectures are discussed below.

In general solar inverters should have the following characteristics [93]:

- Inverters should be highly efficient because the owner of the solar system requires the absolute maximum possible generated energy to be delivered to the grid/load.
- Special demands regarding the potential between solar generator and earth (depending on the solar module type).
- Special safety features like active islanding detection capability.
- Low limits for harmonics of the line currents. This

requirement is enforced by law in most countries since the harmonic limits of both sources and loads connected to the grid are regulated.

- Special demands on *electromagnetic interference* (EMI), which are regulated by law in most countries. The goal of these minimise the unwanted influence of EMI on other equipment in the vicinity or connected to the same supply. Think for example of the influence of a mobile phone on an old radio.
- In many instances the solar system is to be installed outdoors and inverters should adhere to certain specification regarding temperature and humidity conditions, e.g. IP 54.
- Design for high ambient temperatures.
- Designed for 20 years operation under harsh environmental conditions.
- Silent operation (no audible noise).

We have to distinguish between *single-phase* and *three-phase inverters*. For low powers, as they are common in small residential PV systems, single-phase inverters are used. They are connected to one phase of the grid. For higher powers, three-phase inverters are used that are connected to all phases of the grid. If a high power would be delivered to one phase, the currents flowing across the three phases would become very asymmetric

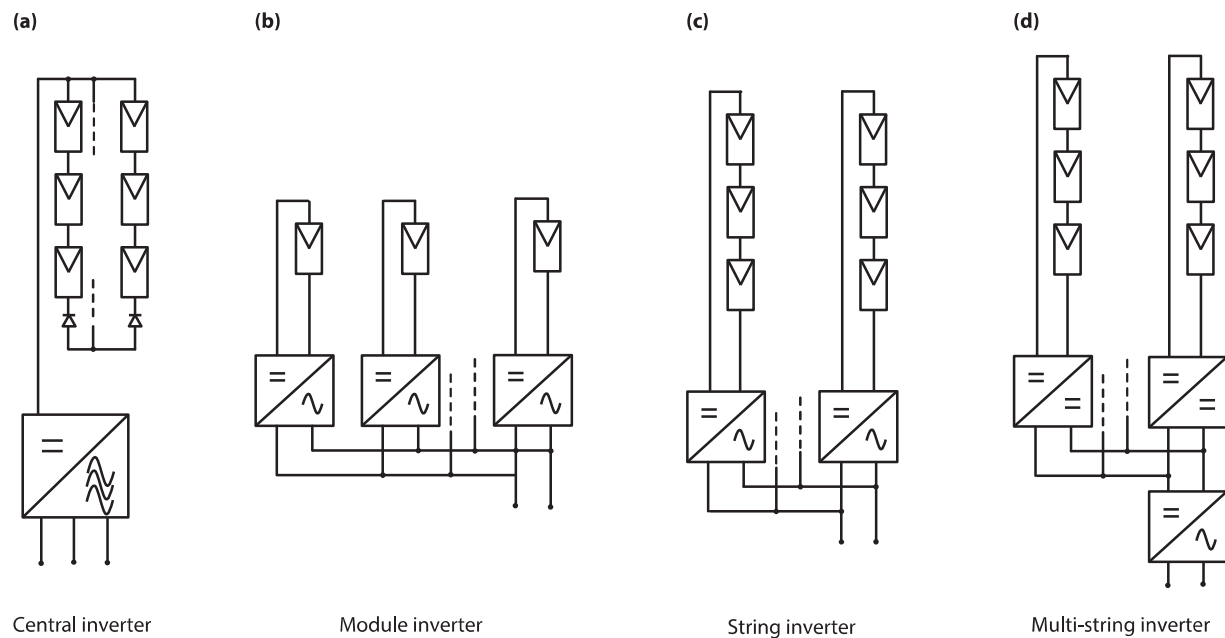


**Figure 17.12:** Different system architectures employed in PV systems.

leading to several problems in the electricity grid.

Note that the term *inverter* is often used for two different things: First, it is used for the actual inverter, which is the electronic building block that performs the DC-to-AC conversion, as described in section 17.3.3. Secondly, the term inverter also is used for the total unit produced by manufacturers, that nowadays usually contains, an MPP tracker, a DC-DC converter, an DC-AC converter and possibly also a charge controller of also a battery is connected.

### Central inverters

This is the simplest architecture employed in PV systems. Here, PV modules are connected in strings leading to an increased system voltage. Many strings are then connected in parallel forming a PV array, which is connected to one central inverter. The inverter performs maximum power point tracking and power conversion as shown in Fig. 17.12 (a), where a three-phase inverter is depicted. This configuration is mostly employed in very-large scale PV production, with central inverter usually being DC to three phase [94].

Many different inverter topologies are utilised as a three phase inverter. Sometimes they are organised as a single DC to three phase unit but sometimes as a three separate DC-to-AC single phase units working with a phase displacement of 120 degrees each. Having

all the PV modes connected in a single array in such a centralised configuration offers the lowest specific cost (cost per  $kW_{p_p}$  of installed power). Since central inverters only use a few components, they are very reliable what makes them the preferred option in large scale PV power plants.

In spite of their simplicity and low specific cost, central inverters suffer from the following disadvantages:

1. Due to the layout of the system, a large amount of power is carried over considerable distances using DC wiring. This can cause safety issues because fault DC currents are difficult to interrupt. Special precaution measures must be taken such as thicker insulation on the DC cabling and special circuit breakers, which can increase the costs.
2. All strings operate at the same maximum power point, which leads to mismatch losses in the modules. This is significant disadvantage. Mismatch losses increase even more with ageing and with partial shading of sections of the array. Mismatch between the different strings may significantly reduce the overall system output.
3. Low flexibility and expandability of the system. Due to the high ratings a system is normally designed as a unit and hence difficult to extend. In other words the system design is not very flexible.
4. Power losses in the string diodes, which are put in

series with each string to prevent current circulation inside strings.

### Module Integrated or module oriented inverters

A very different architecture is that of the *module integrated inverters*, as shown in 17.12 (b). These inverters operate directly at one or several PV modules and have power ratings of several hundreds of watts. Because of the low voltage rating of the PV module, these inverters require often require a two stage power conversion. In a first stage boosts the DC voltage is boosted to the required value while it is inverted to AC in the second stage. Often, a high frequency transformer is incorporated providing full galvanic isolation, which enhances the system flexibility even further. As their name suggests, these inverters are usually integrated with PV panel (so called 'AC PV panels'). In this way the highest flexibility and the expandability of system is obtained. One of the most distinguishing features of this system is the "plug and play" characteristic, which allows to build a complete (and readily expandable) PV system at a low investment cost. Another advantage of these inverters, is minimisation of the mismatch losses that can occur because of non-optimal MPPT.

All these advantages come at certain expenses. Because these inverters are mounted on a PV module, they must operate in harsh environment such as high tem-

perature and large daily and seasonal temperature variations. Also, the specific are the highest of all the inverter topologies. Many topologies for module integrated inverters have been proposed, with some of them being already implemented in commercially available inverters.

### String Inverters

*String inverter*, as illustrated in 17.12 (c), combine the advantages of central and module integrated inverter concepts with little tradeoffs. A number of PV modules that are connected in series form a PV string with a power rating of up to 5 kW<sub>p</sub> and with the open circuit voltage of up to 1 kV. Now, a number of smaller inverters can be used to connect the PV system to the grid.

One disadvantage of the topology is the fact that the high DC voltage requires special consideration, similarly as this already was the case for the central inverter architecture. Here, this issue is even more important because string inverters are usually being installed in households or on office buildings, without designated support structure or increased safety requirements. In general a qualified electrician is needed to perform the interconnections between the modules and the inverter. The protection of the system also requires special consideration, with emphasis on proper DC cabling.

Although partial shading of the string will influence the overall efficiency of the system, each string can independently be operated at its MPP. Also, because no strings are connected in parallel, there is no need for series diodes as in the case of PV arrays with many parallel strings. This reduces losses associated with these diodes. However, it still is a risk that within a string hot-spot occurs because of unequal current and power sharing inside the string.

### Multi String Inverters

The Multi String inverter concept, illustrated in Fig. 17.12 (d), has been developed to combine the advantage of the higher energy yield of a string inverter with the lower costs of a central inverter [95]. Lower power DC-DC converters are connected to individual PV strings each having its own MPP tracking, which independently optimises the energy output from each PV string. To expand the system within a certain power range only a new string with a DC-DC converter has to be included. All DC-DC converters are connected via a DC bus through a central inverter to the grid.

### Team Concept

Aside of the four system architecture already described, many other concepts are also present in literature.

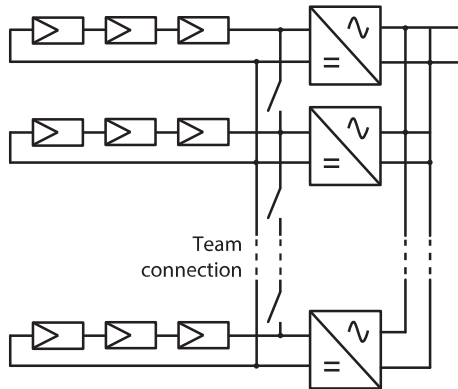


**Figure 17.13:** The team concept of inverters.

However, these concepts are less widely utilised than the ones already presented. One of the alternative concepts is so called team concept, which combines the string technology with the master-slave concept. A combination of several string inverters working with the team concept is shown in Figure 17.13. At very low irradiation the complete PV array is connected to a single inverter. This reduces the overall losses as any power electronic converter is designed such that it has maximum efficiency near full load. With increasing solar radiation more inverters are being connected dividing the PV array into smaller units until every string inverter operates close to its rated power. In this mode every string operates independently with its own MPP tracker. At low solar radiation the inverters are controlled in a master-slave fashion.

In literature many other concepts are discussed. For further reading on this subject, we refer for example to Ref. [96].

### 17.3.2 DC-DC converters

DC-DC converters fulfil multiple purposes. In an inverter, DC power is transformed into AC power. The DC input voltage of the inverter often is constant while the output voltage of the modules at MPP is not. Therefore a DC-DC converter is used to transform the variable voltage from the panels into stable voltage used

by the DC-AC inverter. Additionally, as already stated in section 17.2, the MPP Tracker controls the operating point of the modules, but it cannot set it. This also is done by the DC-DC converter. Further, in a stand-alone system the MPP voltage of the modules might differ from that required by the batteries and the load. Also here, a DC-DC converter is useful. Three topologies are used for DC-DC converters: *buck*, *boost*, and *buck-boost* converters. They are described below.

#### Step-Down (Buck) Converter

Figure 17.14 (a) illustrates the simplest version of a buck DC-DC converter. The unfiltered output voltage waveform of such a converter operated with pulse-width-modulation (PWM) is shown in Fig. 17.14 (b). If the switch is *on*, the input voltage  $V_d$  is applied to the load. When the switch is *off*, the voltage across the load is zero. From the figure we see that the average DC output voltage is denoted as  $V_o$ . From the unfiltered voltage, the average output voltage is given as

$$V_o = \frac{1}{T_s} \int_0^{T_s} v_o(t) dt = \frac{1}{T_s} (t_{\text{on}} V_d + t_{\text{off}} \cdot 0) = \frac{t_{\text{on}}}{T_s} V_d. \quad (17.9)$$

The different variables are defined in Fig. 17.14 (b). To simplify the discussion we define a new term, the duty

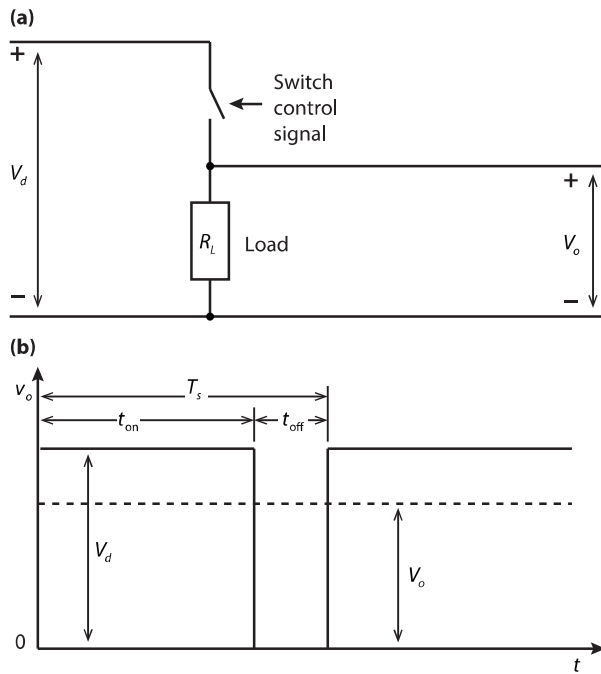


**Figure 17.14:** (a) A basic buck converter without any filters and (b) the unfiltered switched waveform generated by this converter.

cycle  $D$ , as

$$D := \frac{t_{on}}{T_s} \quad (17.10)$$

and hence

$$V_o = D \cdot V_d. \quad (17.11)$$

In general the output voltage with such a high harmonic content is undesirable, and some filtering is required. Figure 17.15 (a) shows a more complex model of a step-down converter that has output filters included and supplies a purely resistive load. As filter elements an inductor  $L$  and a capacitor  $C$  are used. The relation between the input and the output voltages, as given in Equ. 17.11, is valid in continuous conduction mode, i.e. when the current through the inductor never reaches zero value but flows continuously. We can change the ratio between the voltages on the input and output side by changing the duty cycle  $D$ . A detailed discussion about different modes of operation of a buck converter can be found in Reference [97].

In *steady-state operation* the time integral of the voltage across the inductor  $v_L$  taken during one switching cycle is equal to zero. If this is not the case, the circuit is not in steady state. Thus, in steady state, we obtain the following *inductor volt-second balance*:

$$\int_0^{T_s} v_L dt = \int_0^{t_{on}} v_L dt + \int_{t_{on}}^{T_s} v_L dt = 0. \quad (17.12)$$

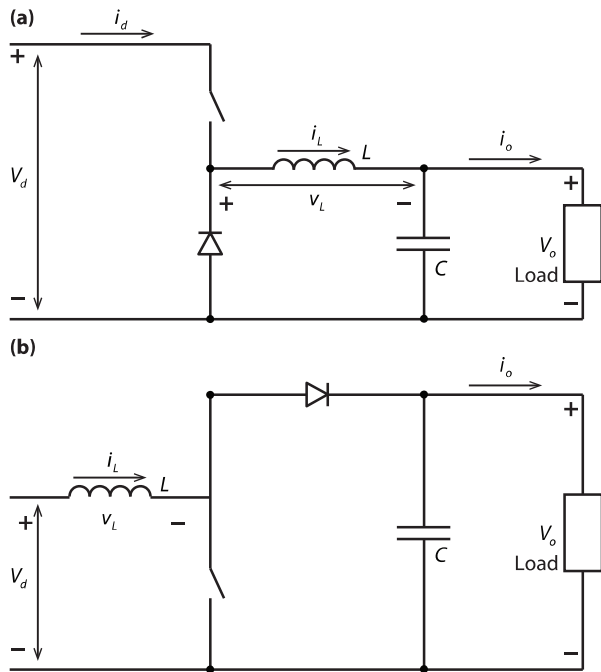


**Figure 17.15:** (a) A buck converter with filters and (b) a boost converter.

Solving this equation leads to

$$V_o = DV_d, \quad (17.13)$$

which is the same result as in Eq. 17.11.

### Step-Up (Boost) Converter

In a boost converter, illustrated in Fig. 17.15 (b), an input DC voltage \$V\_d\$ is boosted to a higher DC voltage \$V\_o\$. By applying the inductor volt-second balance across the inductor as explained in Eq. 17.12, we find

$$V_d t_{\text{on}} + (V_d - V_o) t_{\text{off}} = 0. \quad (17.14)$$

Using the definition for the duty cycle we find

$$\frac{V_o}{V_d} = \frac{1}{1 - D}. \quad (17.15)$$

The above relation is valid in the continuous conduction mode. The principle of operation is that energy stored in the inductor (during the switch is *on*) is later released against higher voltage \$V\_o\$. In this way the energy is transferred from lower voltage (solar cell voltage) to the higher voltage (load voltage).

### Buck-Boost Converter

In a *buck-boost converter* the output voltage can be both higher or lower than the input voltage. The simpli-

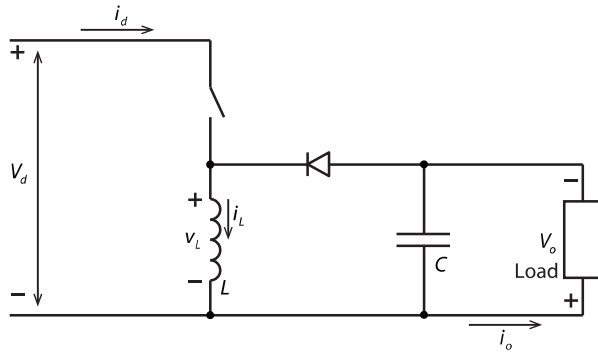


**Figure 17.16:** A buck-boost converter.

fied schematic of a buck-boost converter is depicted in Fig. 17.16. Using inductor volt second balance as in Eq. 17.12, we find

$$V_d t_{\text{on}} + (-V_o) t_{\text{off}} = 0 \quad (17.16)$$

and hence

$$\frac{V_o}{V_d} = \frac{D}{1-D} \quad (17.17)$$

in the continuous conduction mode.

The above described topologies are only the most basic DC-DC converter topologies. The interested reader can find more in-depth information in Reference [97].

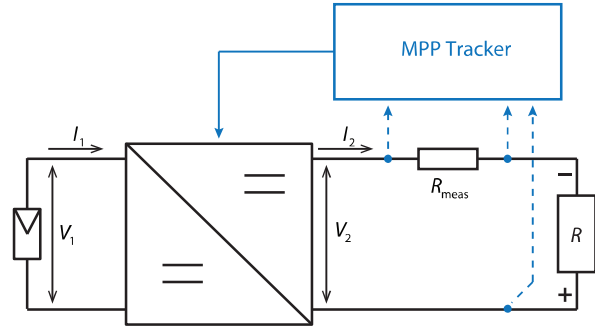


**Figure 17.17:** A combination of a unit performing an MPPT algorithm and a DC-DC converter (adapted from [98]).

### MPP Tracking

In section 17.2 we extensively discussed Maximum Power Point Tracking. Or – more specific we discussed different algorithms that are used for performing MPPT. In these algorithms, usually the operating point of the module is set such that its power output becomes maximal. However, the MPPT algorithm itself cannot actually adjust the voltage or current of the operating point. For this purpose a DC-DC converter is needed. Figure 17.17 shows such a combination of the unit performing the MPPT and DC-DC converter. As illustrated in the figure, this MPPT unit measures the voltage or the cur-

rent on the load side and can vary those by adapting the duty cycle of the DC-DC converter. In this illustration, current and voltage on the load side are measured, but they also can be measured on the PV side.

### Example

Assume a PV module has its MPP at  $V_{PV} = 17\text{ V}$  and  $I_{PV} = 6\text{ A}$  at a given level of solar irradiance. The module has to power a load with a resistance  $R_L = 10\Omega$ . Calculate the duty cycle of the DC-DC converter, if a buck-boost converter is used.

The maximum power from the module is  $P_{MPP} = V_{MPP} \cdot I_{MPP} = 102\text{ W}$ . If this power should be dissipated at the resistor, we have to use the relation

$$P_R = U_R^2 / R$$

and hence find for the voltage at the resistor

$$V_R = \sqrt{P_{MPP}R_L} = 31.94\text{ V}$$

Using Eq. (17.17),

$$\frac{V_o}{V_d} = \frac{D}{1-D}$$

with  $V_o = V_R$  and  $V_d = V_{PV}$  we find  $D = 0.65$ .

### 17.3.3 DC-AC converters (inverters)

Earlier in this section we have discussed different architectures that are used for the power conversion in PV systems. Further, we looked at DC-DC converters that are mainly used in combination with MPPTs in order to push the variable output from the PV modules to a level of constant voltage.

As nowadays most appliances are designed for the standard AC grids, for most PV systems a DC-AC converter is required. As already stated earlier, the term inverter is used both for the DC-AC converter and the combination of all the components that form the actual power converter.

#### The H-bridge inverter

Figure 17.18 shows a very simple example of a so called H-bridge or full-bridge inverter. On the left, the DC input is situated. The load (or in our case the AC output) is situated in between four switches. During usual operation we can distinguish between three situations:

**A All four switches open:** No current flows across the load.

**B S<sub>1</sub> and S<sub>4</sub> closed, S<sub>2</sub> and S<sub>3</sub> open:** Now a current is flowing to through the load, where + is connected

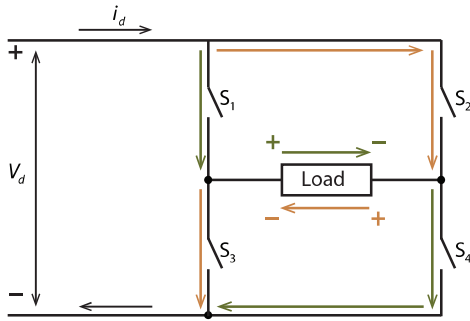


**Figure 17.18:** A simple representation of an H-bridge.

to the left- and – is connected to the right-hand side of the load.

**C S<sub>1</sub> and S<sub>4</sub> open, S<sub>2</sub> and S<sub>3</sub> closed:** Now a current is flowing to through the load, where – is connected to the left- and + is connected to the right-hand side of the load.

**WARNING** It must be assured that S<sub>1</sub> and S<sub>2</sub> never are open at the same time because this would lead to short-circuiting. The same is true for S<sub>3</sub> and S<sub>4</sub>.

From this list we see that the H-bridge configuration allows to put the load on three different levels, which are +V<sub>d</sub>, 0, and –V<sub>d</sub>. Continuously switching between

positive and negative voltages is exactly what is happening in AC. In the easiest operation mode, the H-bridge switches between situations B and C continuously, which will provide a square wave. Note that there will always be a *dead time* in the order of  $\mu\text{s}$  in order to prevent short-circuiting. While such a square wave might be useful for some applications, it is not suited at all for grid-connected installations. The reason for this are harmonic distortions. To understand this we look at a Fourier transform of a square wave, which is given as

$$V_{\text{square}}(t) = \frac{4}{\pi} \left[ \sin(2\pi\nu t) + \frac{1}{3} \sin(6\pi\nu t) + \frac{1}{5} \sin(10\pi\nu t) + \dots \right]. \quad (17.18)$$

Thus, such a square wave contains not only the principal sine function with frequency  $\nu$ , but also all the higher harmonics with frequencies  $3\nu$ ,  $5\nu$ , and so on. These higher harmonics can lead to distortions of the electricity grid and thus must be reduced as much as possible. One principle how to do this is *pulse-width modulation* (PWM) that we already discussed in the section on DC-DC conversion (17.3.2). In this configuration, each leg (the one via S<sub>1</sub> and S<sub>4</sub> and the one via S<sub>2</sub> and S<sub>3</sub>) in fact acts as a buck converter.

If a low-pass filter consisting of capacitors and inductors is used, as in Fig. 17.19, the high frequency components are filtered out and hence a very smooth sine

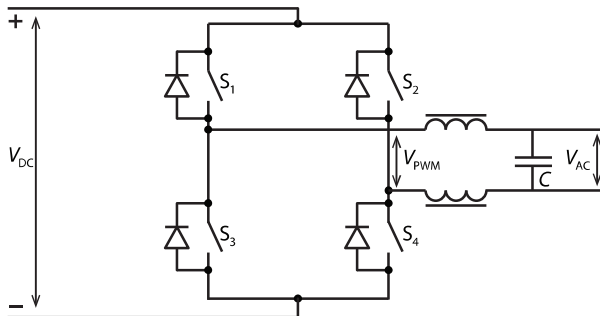


**Figure 17.19:** Illustration of an H-bridge containing a low-pass filter for removing the high-frequency components of the signal.

curve can be obtained that complies to the regulations for grid-connected systems. Figure 17.20 shows the unfiltered PWM output and the filtered sine output.

Note that in Fig. 17.19 diodes are connected in parallel to the switches. The reason for placing these diodes is the following: If the switch goes from closed to open very fast, no current can flow through the inductor anymore, meaning that the change of current flowing through the inductor is very high. This induces a voltage given by

$$V_{\text{induced}} = -L \frac{dI}{dt}, \quad (17.19)$$

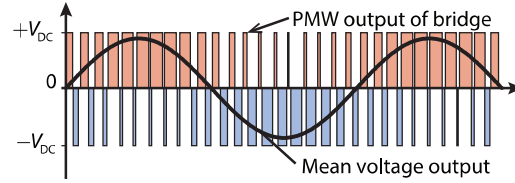


**Figure 17.20:** The unfiltered PWM signal and the sine signal that is obtained with a low-pass filter.

which is the higher the faster the current changes. As high induced voltages will damage the electric circuitry, they must be prevented. The diode ensures that current also can flow after the switch opens. Hence current is flowing always and no high induced voltages appear.

Since this configuration is grid-connected, we easily can determine the required DC input voltage, which must be minimal the peak voltage of the AC voltage. For an effective AC voltage of 240 V, as used in large parts of the world, the peak voltage is  $V_{\text{peak}} = 1.1\sqrt{2} \cdot 240 \text{ V} = 373 \text{ V}$ , where we also took a 10% tolerance into account.

If the PV array delivers a lower voltage, thus a boost converter would be required prior in addition to the inverter. Alternatively, a transformer can be used that transforms a lower-voltage AC signal to the 240 V AC signal. Such a system is sketched in Fig. 17.23. This system has the advantage of galvanic separation with all the advantages discussed below, but on the other hand

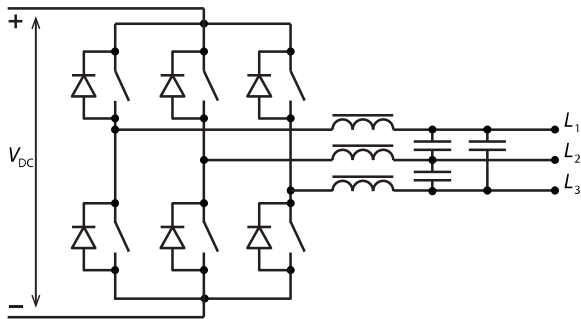


**Figure 17.21:** Illustrating a three-phase inverter.

the transformer reduces the overall efficiency.

Figure 17.21 shows a three-phase inverter. As it can be seen, it is very similar to the single-phase inverter discussed above, just it contains three legs of that each creates a sine-wave output with a phase shift of  $120^\circ$  between them.

### Half-bridge inverters

A simpler inverter topology, the so-called half-bridge inverter, is shown in Fig. 17.22. In contrast to the H-bridge configuration, here, two switches are replaced by capacitors and the midpoint in-between the two ca-

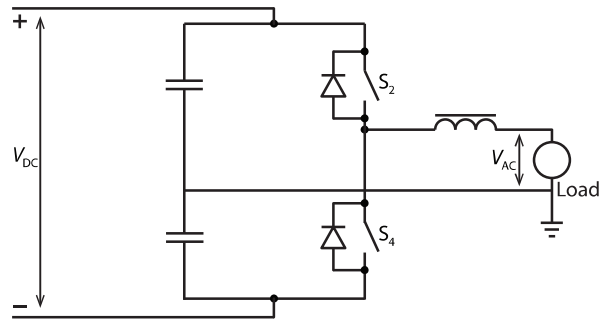


**Figure 17.22:** Illustrating a half-bridge inverter.

pacitors is directly connected to the ground. The half-bridge configuration is much simpler than the H-bridge configuration, but it has some drawbacks.

The main drawback is requirement for a high DC link voltage, which needs to be two times higher than that of a full bridge inverter. For a effective AC voltage of 240 V this would be 746 V. Because the topology provides two-levels in the output voltage (in difference to three levels for the full bridge configuration, a higher current ripple is present in the output filter inductor. Hence, larger value of the output filters are required.

### 17.3.4 Some remarks

#### Switches

All the DC-DC transformers and DC-AC transformers discussed above contain switches. Traditionally, in *line-commutated* inverters, *thyristors* are used as switches. A thyristor is a electronic component consistent of pnpn layers. It thus contains 3 p-n junctions. One disadvantage is that thyristors cannot be turned off, but only turned on. Thus, one has to wait for the next zero pass of the grid signal [98]. The current flow thus is rectangular which leads to a very high harmonic content requiring additional filters in order to make the output compatible with the electricity grid. Nowadays, thyristors only are used for inverters with a power of 100 kW and higher.

All other inverters are *self-commutated* inverters that generate an output with very little harmonic content as described above and in Fig. 17.20. The switches there are fully-controllable such that pulse-width modulation becomes possible. As switches, GTOs (gate turn-off thyristors), IGBTs (insulated-gate bipolar transistors) or MOSFETs (metal-oxide-semiconductor field-effect transistors) are used. More information can be found for example in Reference [20].

#### Overall configuration

Figure 17.23 shows an example of a transformer-less absorber as it could be sold for household systems. Besides the actual DC-AC converter, which is realised as an H-bridge, it also contains a DC-DC boost converter and an MPPT that uses the voltage and current measured on the PV side as input. The system sketched also contains several electronic components for increased safety: a residual current measurement to detect leakage currents above a certain threshold and to shut-down the inverter if these currents appear. Further, a grid-monitoring unit to prevent islanding (see below) [98].

#### Potential induced degradation (PID)

As mentioned earlier, in PV systems that have a transformer-less inverter, no galvanic separation between the DC- and the AC-parts of the system is given. Because of this lack of galvanic isolation, a potential of -500 V or more between the PV modules and the ground can occur, which can lead to potential induced degradation (PID). Many thin-film contain a TCO front contact that is deposited in superstrate configuration on the glass top plate. Positively charged sodium ions than can travel into the TCO because of this potential. This leads to corrosion and consequently to performance loss of the module. Also, for crystalline mod-

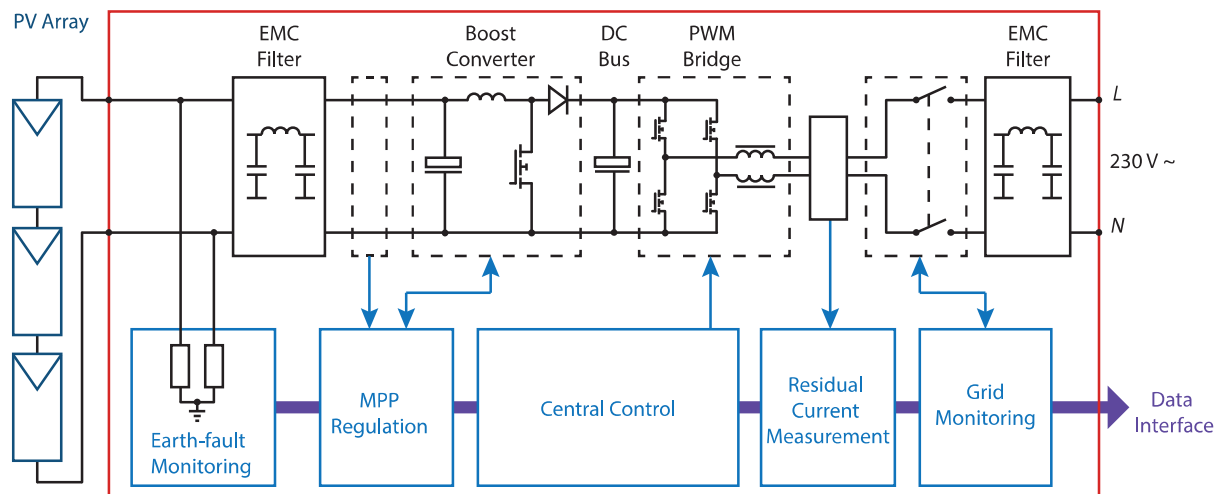


**Figure 17.23:** Illustrating an example of a transformer-less inverter unit as it is sold for residential PV systems. As switches, MOSFETs are used. (Adapted from [98]).

ules, PID can be a problem [98]. Therefore, for systems containing thin-film modules the inverter must have a transformer.

### Islanding

A potential danger of grid-connected systems is *islanding*. Imagine that a potential PV system is installed in a street where the electricity grid is shut-down in order to do maintenance work on the electricity cables. If it is a sunny day, the PV system will produce power and – without protection – would deliver the power to the grid. The electricity worker thus can be in danger. This phenomenon is called islanding and due to its danger it must be prevented.

The inverter therefore must be able to detect, when the electricity grid is shut-down. If this is the case, also the inverter must stop delivering power to the grid.

### Efficiency of power converters

For planning a PV system it is very important to know the efficiency of the power converters. This efficiency of DC-DC and DC-AC converters is defined as

$$\eta = \frac{P_o}{P_o + P_d}, \quad (17.20)$$

i.e. the fraction of the output power  $P_o$  to the sum of  $P_o$  with the dissipated power  $P_d$ . For estimating the efficiency we thus must estimate the dissipated (lost) power, which can be seen as a sum of several components,

$$P_d = P_L + P_{\text{switch}} + \text{other losses}, \quad (17.21)$$

i.e. the power lost in the inductor  $P_L$  and the power lost in the switch.  $P_L$  is given as

$$P_L = I_{L, \text{rms}}^2 R_L, \quad (17.22)$$

where  $I_{L, \text{rms}}$  is the mean current flowing through the inductor. The losses in the switch strongly depend on the type of switch that is used. Other losses are for example resistive losses in the circuitry in-between the switches.

For a complete inverter unit it is convenient to define the efficiency as

$$\eta_{\text{inv}} = \frac{P_{\text{AC}}}{P_{\text{DC}}}, \quad (17.23)$$

which is the ratio of the output AC power to the DC input power. Figure 17.24 shows the efficiency of a commercially available inverter for different input voltages. As we can see, in general the lower the output power, the less efficient the inverter. This efficiency characteristic must be taken into account when planning a PV system. Further, the efficiency is lower if the input voltage deviates from the nominal value.

## 17.4 Batteries

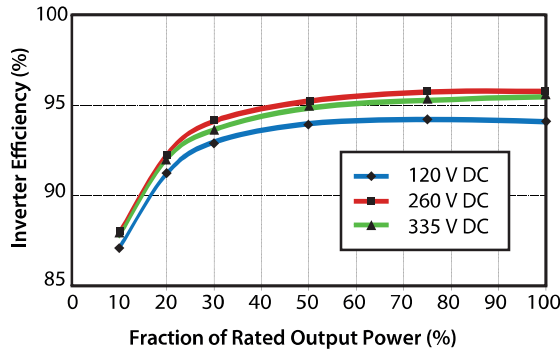


**Figure 17.24:** The power-dependent efficiency for several input voltages of a *Fronius Galvo 1.5-1 208-240* inverter at 240 V AC. The nominal input voltage is 260 V DC. (Data taken from Ref. [99]).

In this section we discuss a vital component not only of PV systems but of renewable energy systems in general. *Energy storage* is very important at both small and large scales in order to tackle the intermittency of renewable energy sources. In the case of PV systems, the intermittency of the electricity generation is of two kinds: first, *diurnal* fluctuations, *i.e.* the difference of irradiance during the 24 hour period. Secondly, the *seasonal* fluctuations, *i.e.* the difference of irradiance between the summer and winter months. There are several technological options for realising storage of energy. Therefore it is important to make an optimal choice.

Fig. 17.25 shows a *Ragone chart*, where the *specific energy* is plotted against the *peak power density*. Because it uses a double-logarithmic chart storage technologies with very different storage properties can be compared in one plot. Solar energy application require a high energy density and – depending on the application – also a reasonably high power density. For example, we cannot use capacitors because of their very poor energy density. For short term to medium term storage, the most common storage technology of course is the *battery*. Batteries have both the right energy density and power density to meet the daily storage demand in small and medium-size PV systems. However, the seasonal storage problem at large scales is yet to be solved.

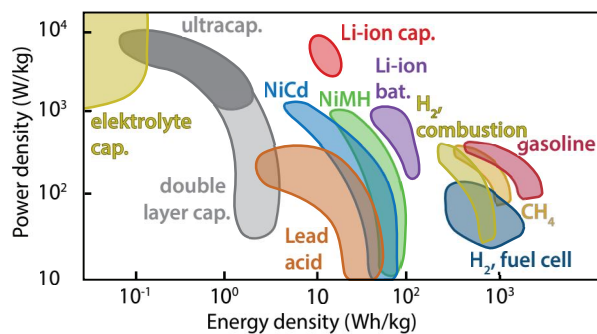


**Figure 17.25:** A Ragone chart of different energy storage methods. Capacitors are indicated with “cap”.

The ease of implementation and efficiency of the batteries is still superior to that of other technologies, like pumping water to higher levels, compressed air energy storage, conversion to hydrogen, flywheels, and others. Therefore we will focus on battery technology as a viable storage option for PV systems.

Batteries are electrochemical devices that convert chemical energy into electrical energy. We can distinguish between primary or secondary batteries. Primary batteries convert chemical energy to electrical energy *irreversibly*. For example, *zinc carbon* and *alkaline* batteries are primary batteries.

Secondary batteries or *rechargeable batteries*, as they are more commonly called, convert chemical energy to electrical energy *reversibly*. This means that they can be recharged when an over-potential is used. In other words, excess electrical energy is stored in these secondary batteries in the form of chemical energy. Typical examples for rechargeable batteries are *lead acid* or *lithium ion* batteries. For PV systems only secondary batteries are of interest.

### 17.4.1 Types of batteries

*Lead-acid* batteries are the oldest and most mature technology available. They will be discussed in detail later in this section.

Other examples are *nickel-metal hydride* (NiMH) and *nickel cadmium* (NiCd) batteries. NiMH batteries have a high energy density, which is comparable to that of lithium-ion batteries (discussed below). However, NiMH batteries suffer from a high rate of self discharge. On the other hand, NiCd batteries have much lower energy density than lithium ion batteries. Furthermore, because of the toxicity of cadmium, NiCd batteries are widely banned in the European Union for consumer use. Additionally, NiCd batteries suffer from what is called the *memory effect*: the batteries lose their usable energy capacity if they are repeatedly charged after only being partially discharged. These disadvant-

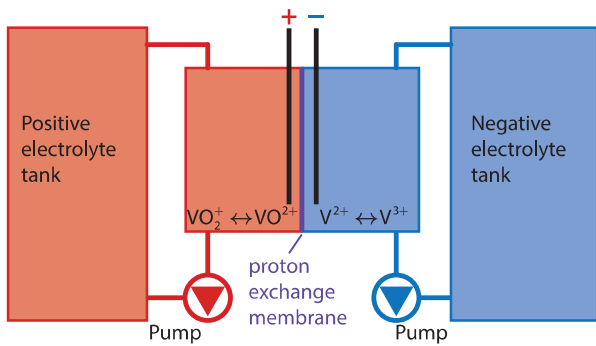


**Figure 17.26:** Schematic on a vanadium redox-flow battery that employs vanadium ions.

ages make NiMH and NiCD batteries unsuitable candidates for PV storage systems.

*Lithium ion batteries* (LIB) and *lithium-ion polymer* batteries, which are often referred to as lithium polymer (LiPo) batteries, have been heavily investigated in recent years. Their high energy density already has made them the favourite technology for light-weight storage applications for example in mobile telephones. However, these technologies still suffer from high costs and low maturity.

The last and the most recent category of batteries that we will discuss in this treatise are *redox-flow* batteries.

Lead-acid batteries and LIB, the two main storage options for PV systems, are similar in the sense that their electrodes undergo chemical conversion during charging and discharging, which makes their electrodes to degenerate with time, leading to inevitable “ageing” of the battery. In contrast, redox flow batteries combine properties of both batteries and fuel cells, as illustrated in Fig. 17.26. Two liquids, a *positive electrolyte* and a *negative electrolyte* are brought together only separated by a membrane, which only is permeable for protons. The cell thus can be charged and discharged without the reactants being mixed, which in principle prevents the liquids from ageing. The chemical energy in a redox flow battery is stored in its 2 electrolytes, which are stored in two separate tanks. Since it is easy to make the tanks larger, the maximal energy that can be stored in such a battery thus is not restricted. Further, the maximal output power can easily be increased by increasing the area of the membrane, for example by using more cells at the same time. The major disadvantages is that such a battery system requires additional components such as pumps, which makes them more complicated than other types of batteries.

Figure 17.27 shows a Ragone plot as it is used to compare different battery technologies. In contrast to Fig. 17.25, here the the gravimetric energy density and volumetric energy density are plotted against each other. The *gravimetric energy density* is the amount of energy stored per mass of the battery; it typically is meas-

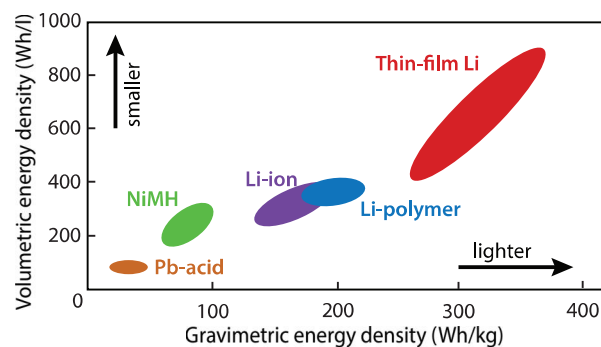


**Figure 17.27:** A Ragone chart for comparing different secondary battery technologies with each other.

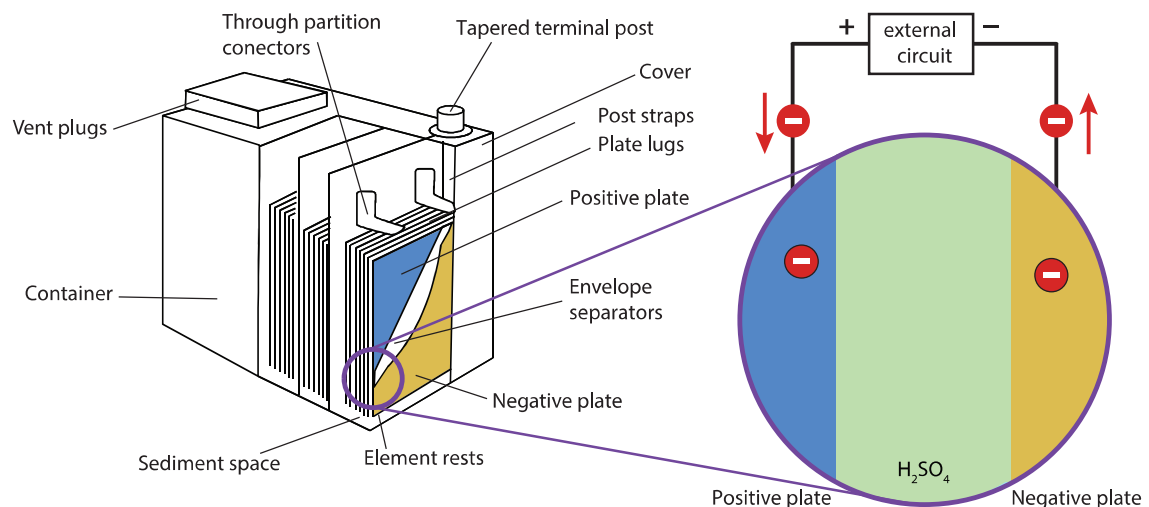
ured in Wh/kg. The volumetric energy density is the amount of energy stored per volume of battery; it is given in Wh/l. The higher the gravimetric energy density, the lighter the battery can be. The higher the volumetric energy density, the smaller the battery can be.

Figure 17.27 shows that lead acid batteries have both the lowest volumetric and gravimetric energy densities among the different battery technologies. Lithium ion batteries show ideal material properties for using them as storage devices. Redox-flow batteries are very promising. However, both LIB and redox-flow batteries are still in a development phase which makes these technolo-

gies still very expensive. Thus, because of the unequalled maturity and hence low cost of the lead-acid batteries, they are still the storage technology of choice for PV systems.

Figure 17.28 shows a sketch of a lead-acid battery. A typical battery is composed of several individual cells, of which each has a nominal cell voltage around 2 V. Different methods of assembly are used. In the *block assembly*, the individual cells share the housing and are interconnected internally. For example, to get the typical battery voltage of 12 V, six cells are connected in series. As the name suggests, lead acid batteries use an acidic electrolyte. More specifically they use diluted sulphuric acid  $H_2SO_4$ . Two plates of opposite polarity are inserted in the electrolyte solution, which act as the electrodes. The electrodes contain grid shaped lead carrier and porous active material. This porous active material has a sponge-like structure, which provides sufficient surface area for the electrochemical reaction. The active mass in the negative electrode is lead, while in the positive electrode lead dioxide ( $PbO_2$ ) is used.

When the battery is discharged, electrons flow from the negative to the positive electrode through the external circuit, causing a chemical reaction between the plates and the electrolyte. This forward reaction also depletes the electrolyte, affecting its *state of charge* (SoC). When the battery is recharged, the flow of electrons is reversed, as the external circuit does not have a load, but



**Figure 17.28:** Schematic of a lead-acid battery.

a source with a voltage higher than that of the battery enables the reverse reaction. In the PV systems, this source is nothing but the PV module or array providing clean solar power.

### 17.4.2 Battery parameters

Let us now discuss some parameters that are used to characterise batteries.

#### Voltage

First, we will discuss the *voltage* rating of the battery. The voltage at that the battery is rated is the *nominal voltage* at which the battery is supposed to operate. The so called *solar batteries* or lead acid grid plate batteries are usually rated at 12 V, 24 V or 48 V.

#### Capacity

When talking about batteries, the term *capacity* refers to the amount of charge that the battery can deliver at the rated voltage. The capacity is directly proportional to the amount of electrode material in the battery. This explains why a small cell has a lower capacity than a large cell that is based on the same chemistry, even though the open circuit voltage across the cell will

be the same for both the cells. Thus, the voltage of the cell is more chemistry based, while the capacity is more based on the quantity of the active materials used.

The capacity  $C_{\text{bat}}$  is measured in ampere-hours (Ah). Note that charge usually is measured in *coulomb* (C). As the electric current is defined as the rate of flow of electric charge, Ah is another unit of charge. Since  $1 \text{ C} = 1 \text{ As}$ ,  $1 \text{ Ah} = 3600 \text{ C}$ . For batteries, Ah is the more convenient unit, because in the field of electricity the amount of energy usually is measured in watt-hours (Wh). The energy capacity of a battery is simply given by multiplying the rated battery voltage measured in Volt by the battery capacity measured in Amp-hours,

$$E_{\text{bat}} = C_{\text{bat}} V, \quad (17.24)$$

which results in the battery energy capacity in Watt-hours.

#### C-rate

A brand new battery with 10 Ah capacity theoretically can deliver 1 A current for 10 hours at room temperature. Of course, in practice this is seldom the case due to several factors. Therefore, the *C-rate* is used, which is a measure of the rate of discharge of the battery relative to its capacity. It is defined as the multiple of the current over the discharge current that the battery can sustain over one hour. For example, a C-rate of 1 for a 10

Ah battery corresponds to a discharge current of 10 A over 1 hour. A C-rate of 2 for the same battery would correspond to a discharge current of 20 A over half an hour. Similarly, a C-rate of 0.5 implies a discharge current of 5 A over 2 hours. In general, it can be said that a C-rate of  $n$  corresponds to the battery getting fully discharged in  $1/n$  hours, irrespective of the battery capacity.

### Battery efficiency

For designing PV systems it is very important to know the *efficiency* of the storage system. For storage systems, usually the *round-trip efficiency* is used, which is given as the ratio of total storage system input to the total storage system output,

$$\eta_{\text{bat}} = \frac{E_{\text{out}}}{E_{\text{in}}} 100\%. \quad (17.25)$$

For example, if 10 kWh is pumped into the storage system during charging, but only 8 kWh can be retrieved during discharging, the round trip efficiency of the storage system is 80%. The round-trip efficiency of batteries can be broken down into two efficiencies: first, the *voltaic efficiency*, which is the ratio of the average discharging voltage to the average charging voltage,

$$\eta_V = \frac{V_{\text{discharge}}}{V_{\text{charge}}} 100\%. \quad (17.26)$$

This efficiency covers the fact that the charging voltage is always a little above the rated voltage in order to drive the reverse chemical (charging) reaction in the battery.

Secondly, we have the *coulombic efficiency* (or Faraday efficiency), which is defined as the ratio of the total charge got out of the battery to the total charge put into the battery over a full charge cycle,

$$\eta_C = \frac{Q_{\text{discharge}}}{Q_{\text{charge}}} 100\%. \quad (17.27)$$

The *battery efficiency* then is defined as the product of these two efficiencies,

$$\eta_{\text{bat}} = \eta_V \cdot \eta_C = \frac{V_{\text{discharge}}}{V_{\text{charge}}} \frac{Q_{\text{discharge}}}{Q_{\text{charge}}} 100\%. \quad (17.28)$$

When comparing different storage devices, usually this round-trip efficiency is considered. It includes all the effects of the different chemical and electrical non-idealities occurring in the battery.

### State of charge and depth of discharge

At another important battery parameter is the *State of Charge* (SoC), which is defined as the percentage of the battery capacity available for discharge,

$$\text{SoC} = \frac{E_{\text{bat}}}{C_{\text{bat}} V}. \quad (17.29)$$

Thus, a 10 Ah rated battery that has been drained by 2 Ah is said to have a SoC of 80%. Also the *Depth of Discharge* (DoD) is an important parameter. It is defined as the percentage of the battery capacity that has been discharged,

$$\text{DoD} = \frac{C_{\text{bat}}V - E_{\text{bat}}}{C_{\text{bat}}V}. \quad (17.30)$$

For example, a 10 Ah battery that has been drained by 2 Ah has a DoD of 20%. The SoC and the DoD are complimentary to each other.

### Cycle lifetime

The *cycle lifetime* is a very important parameter. It is defined as the number of charging and discharging cycles after that the battery capacity drops below 80% of the nominal value. Usually, the cycle lifetime is specified by the battery manufacturer as an absolute number. However, stating the battery lifetime as a single number is a oversimplification because the different battery parameters discussed so far are not only related to each other but are also dependent on the temperature.

Figure 17.29 (a) shows the cycle lifetime as a function of the DoD for different temperatures. Clearly, colder operating temperatures mean longer cycle lifetimes. Furthermore, the cycle lifetime depends strongly on the

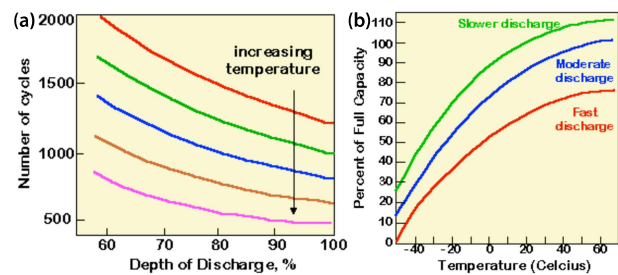


**Figure 17.29:** (a) Qualitative illustration of the cycle lifetime of a lead-acid battery in dependence of the DoD and temperature [100]. (b) Effect of the temperature on the battery capacity [100].

DoD. The smaller the DoD, the higher the cycle lifetime. Thus, that the battery will last longer if the average DoD can be reduced during the lifetime of the battery. Also, *battery overheating* should be strictly controlled. Overheating can because of overcharging and subsequent over-voltage of the lead acid battery. To prevent this, charge controllers are used that we address in the next section.

### Temperature effects

While the battery lifetime is increased at lower temperatures, one more effect must to be considered. The

temperature affects the battery capacity during regular use too. As seen from Fig. 17.29 (b), the lower the temperature, the lower the battery capacity. This is because, the chemicals in the battery are more active at higher temperatures, and the increased chemical activity leads to increased battery capacity. It is even possible to reach an above rated battery capacity at high temperatures. However, such high temperatures are severely detrimental to the battery health.

### Ageing

The major cause for ageing of the battery is *sulphation*. If the battery is insufficiently recharged after being discharged, sulphate crystals start to grow, which cannot be completely transformed back into lead or lead oxide. Thus the battery slowly loses its active material mass and hence its discharge capacity. *Corrosion* of the lead grid at the electrode is another common ageing mechanism. Corrosion leads to increased grid resistance due to high positive potentials. Further, the electrolyte can *dry out*. At high charging voltages, gassing can occur, which results in the loss of water. Thus, demineralised water should be used to refill the battery from time to time.

### 17.4.3 Charge controllers

After having discussed different types of batteries and different battery characteristics, it is now time to discuss *charge controllers*. Charge controllers are used in PV systems that use batteries, which are stand-alone systems in most cases. As we have seen before, it is very important to charge and discharge batteries at the right voltage and current levels in order to ensure a long battery lifetime. A battery is an electrochemical device that requires a small over-potential to be charged. However, batteries have strict voltage limits, which are necessary for their optimal functioning. Further, the amount of current sent to the battery by the PV array and the current flowing through the battery while being discharged have to be within well-defined limits for proper functioning of the battery. We have seen before that lead acid batteries suffer from overcharge and over-discharge. On the other hand, the PV array responds dynamically to ambient conditions like irradiance, temperature and other factors like shading. Thus, directly coupling the battery to the PV array and the loads is detrimental to the battery lifetime.

Therefore a device is needed that controls the currents flowing between the battery, the PV array and the load and that ensures that the electrical parameters present at the battery are kept within the specifications given by the battery manufacturer. These tasks are done by a *charge controller*, that nowadays has several different

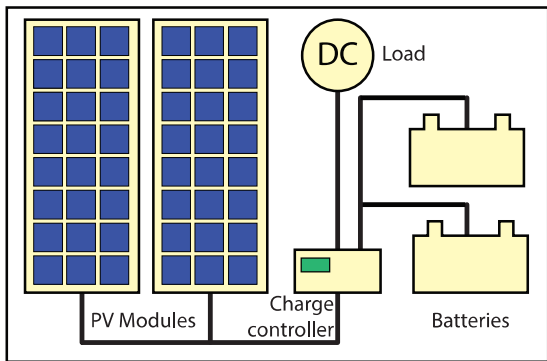


**Figure 17.30:** Illustrating the position of the *charge controller* in a generic PV system with batteries.

functionalities, which also depend on the manufacturer. We will discuss the most important functionalities. A schematic of its location in a PV system is shown in Fig. 17.30.

When the sun is shining at peak hours during summer, the generated PV power excesses the load. The excess energy is sent to the battery. When the battery is fully charged, and the PV array is still connected to the battery, the battery might overcharge, which can cause several problems like gas formation, capacity loss or overheating. Here, the charge controller plays a vital role by de-coupling the PV array from the battery. Similarly,

during severe winter days at low irradiance, the load exceeds the power generated by the PV array, such that the battery is heavily discharged. Over-discharging the battery has a detrimental effect on the cycle lifetime, as discussed above. The charge controller prevents the battery from being over-discharged by disconnecting the battery from the load.

For optimal performance, the battery voltage has to be within specified limits. The charge controller can help in maintaining an allowed voltage range in order to ensure a healthy operation. Further, the PV array will have its  $V_{mpp}$  at different levels, based on the temperature and irradiance conditions. Hence, the charge controller needs to perform appropriate voltage regulation to ensure the battery operates in the specified voltage range, while the PV array is operating at the MPP. Modern charge controllers often have an MPP tracker integrated.

As we have seen above, certain C-rates are used as battery specifications. The higher the charge/discharge rates, the lower the coulombic efficiency of the battery. The optimal charge rates, as specified by the manufacturer, can be reached by manipulating the current flowing into the battery. A charge controller that contains a proper current regulation is also able to control the C-rates. Finally, the charge controller can impose the limits on the maximal currents flowing into and from the battery.

If no *blocking diodes* are used, it is even possible that the battery can “load” the PV array, when the PV array is operating at a very low voltage. This means that the battery will impose a forward bias on the PV modules and make them consume the battery power, which leads to heating up the solar cells. Traditionally, blocking diodes are used at the PV panel or string level to prevent this *back discharge* of the battery through the PV array. However, this function is also easily integrated in the charge controller.

We distinguish between *series* and *shunt* controllers, as illustrated in 17.31. In a series controller, overcharging is prevented by disconnecting the PV array until a particular voltage drop is detected, at which point the array is connected to the battery again. On the other hand, in a parallel or shunt controller, overcharging is prevented by short-circuiting the PV array. This means that the PV modules work under short circuit mode, and that no current flows into the battery. These topologies also ensure over-discharge protection using power switches for the load connection, which are appropriately controlled by the algorithms implemented into the charge controller algorithm. As charge controllers are a necessary component of stand-alone PV systems, they should have a very high efficiency.

As we have seen above, temperature plays a crucial role in the functioning of the battery. Not only does temperature affect the lifespan of the battery, but it also

changes its electrical parameters significantly. Thus, modern charge controllers have a temperature sensor included, which allows the charge controller to adjust the electrical parameters of the battery, like the operating voltage, to the temperature. The charge controller thus keeps the operating range of the battery within the optimal range of voltages. The charge controller is usually kept in close proximity to the battery, such that the operating temperature of the battery is close to that of the charge controller. However, when the battery is heavily loaded, the battery might heat up, leading to differences between the temperature expected by the charge controller and the actual temperature of the battery. Therefore, high end charge controllers also take temperature effects due to high currents into account.

## 17.5 Cables

The overall performance of PV systems also is strongly dependent on the correct choice of the cables. We therefore will discuss how to choose suitable cables. But we start our discussion with *color conventions*.

PV systems usually contain DC and AC parts. For correctly installing a PV system, it is important to know the color conventions. For *DC cables*,

- red is used for connecting the +contacts of the different system components with each other while

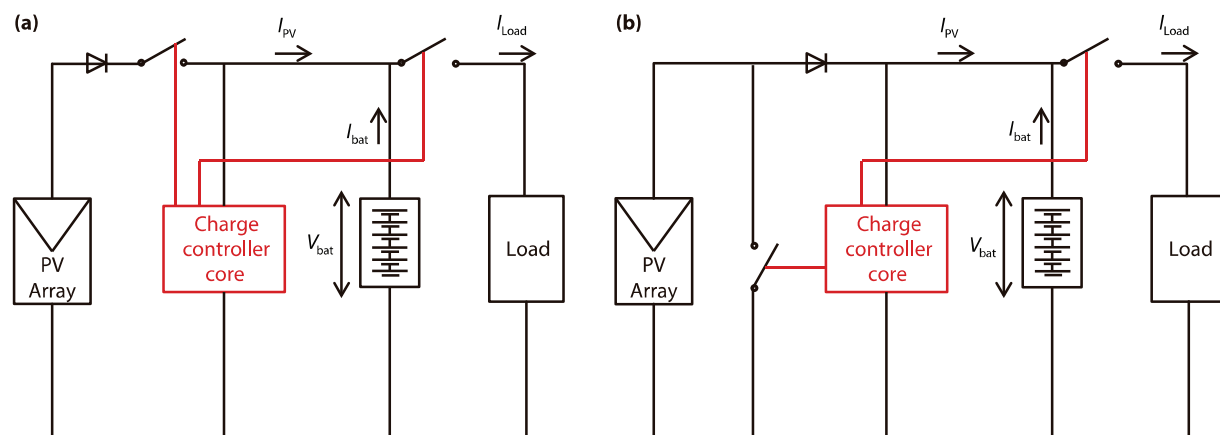


**Figure 17.31:** Basic wiring scheme of (a) a series and (b) a shunt charge controller.

- **black** is used for interconnecting the *--contacts*.

For AC wiring, different colour conventions are used around the world.

- For example, in the European Union, **blue** is used for **neutral**, **green-yellow** is used for the **protective earth** and **brown** (or another color) is used for the **phase**.
- In the United States and Canada, **silver** is used for **neutral**, **green-yellow**, **green** or a **bare** conductor is used for the **protective earth** and **black** (or another color) is used for the **phase**.
- In India and Pakistan, **black** is used for **neutral**, **green** is used for the **protective earth** and **blue**, **red**, or **yellow** is used for the **phase**.

Therefore it is very important to check the standards of the country in that the PV system is going to be installed.

The cables have to be chosen such that *resistive losses* are minimal. For estimating these losses, we look at a very simple system that is illustrated in Fig. 17.32. The system consists of a power source and a load with resistance  $R_L$ . Also the cables have a resistance  $R_{\text{cable}}$ , which also is sketched. The power loss at the cables is given

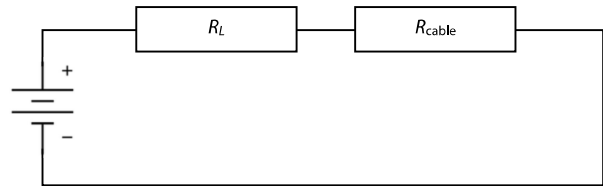


**Figure 17.32:** Illustrating a circuit with a load  $R_L$  and cable resistance  $R_{\text{cable}}$ . The connections drawn in between the components are lossless.

as

$$P_{\text{cable}} = I \cdot \Delta V_{\text{cable}}, \quad (17.31)$$

where  $\Delta V_{\text{cable}}$  is the voltage drop across the cable, which is given as

$$\Delta V_{\text{cable}} = V \frac{R_{\text{cable}}}{R_L + R_{\text{cable}}}. \quad (17.32)$$

Using

$$V = I(R_L + R_{\text{cable}}) \quad (17.33)$$

we find

$$P_{\text{cable}} = I^2 R_{\text{cable}}. \quad (17.34)$$

Hence, as the current doubles, four times as much heat will be dissipated at the cables. It now is obvious why modern modules have connected all cells in series.

Let us now calculate the resistance of a cable with length  $\ell$  and cross section  $A$ . It is clear, that if  $\ell$  is doubled, also  $R_{\text{cable}}$  doubles. In contrast, if  $A$  doubles,  $R_{\text{cable}}$  decreases to half. The resistance thus is given by

$$R_{\text{cable}} = \rho \frac{\ell}{A} = \frac{1}{\sigma} \frac{\ell}{A}, \quad (17.35)$$

where  $\rho$  is the *specific resistance* or *resistivity* and  $\sigma$  is the *specific conductance* or *conductivity*. If both,  $\ell$  and  $A$  are given in metres, their units are  $[\rho] = \Omega \cdot \text{m}$  and  $[\sigma] = \text{S/m}$ , where S denotes the unit for conductivity, which is *Siemens*.

For electrical cables it is convenient to have  $\ell$  in metres and  $A$  in  $\text{mm}^2$ . When using this convention, we find the following units for  $\rho$  and  $\sigma$ :

$$\begin{aligned} 1 \Omega \cdot \text{m} &= 1 \Omega \frac{\text{m}^2}{\text{m}} = 1 \Omega \frac{10^6 \text{mm}^2}{\text{m}} = 10^6 \Omega \frac{\text{mm}^2}{\text{m}}, \\ 1 \frac{\text{S}}{\text{m}} &= 1 \text{S} \frac{\text{m}}{\text{m}^2} = 1 \Omega \frac{\text{m}}{10^6 \text{mm}^2} = 10^{-6} \Omega \frac{\text{m}}{\text{mm}^2}. \end{aligned}$$

The most widely used metals used for electrical cables are *copper* and *aluminium*. Their resistances and con-

ductivities are

$$\rho_{\text{Cu}} = 1.68 \cdot 10^{-8} \Omega \cdot \text{m} = 1.68 \cdot 10^{-2} \Omega \frac{\text{mm}^2}{\text{m}},$$

$$\sigma_{\text{Cu}} = 5.96 \cdot 10^7 \frac{\text{S}}{\text{m}} = 59.6 \text{S} \frac{\text{m}}{\text{mm}^2},$$

$$\rho_{\text{Al}} = 2.82 \cdot 10^{-8} \Omega \cdot \text{m} = 2.82 \cdot 10^{-2} \Omega \frac{\text{mm}^2}{\text{m}},$$

$$\sigma_{\text{Al}} = 3.55 \cdot 10^7 \frac{\text{S}}{\text{m}} = 35.5 \text{S} \frac{\text{m}}{\text{mm}^2}.$$

Usual thicknesses for cables are  $0.75 \text{ mm}^2$ ,  $1.5 \text{ mm}^2$ ,  $2.5 \text{ mm}^2$ ,  $4 \text{ mm}^2$ ,  $6 \text{ mm}^2$ ,  $10 \text{ mm}^2$ ,  $16 \text{ mm}^2$ ,  $25 \text{ mm}^2$ ,  $35 \text{ mm}^2$ , *et cetera*. Since DC circuits are driven at lower voltages than AC currents, the currents are higher, requiring thicker cables.



# 18

## PV System Design

In the previous chapters we discussed how to estimate the irradiance on a PV module in dependence of the position on Earth, date and time (Chapter 16). Further we introduced and discussed all the different components of PV Systems in Chapter 17.

In this chapter, we will put the things together and use them such that we can design complete PV systems. Of course, PV system designs can be made with different levels of complexity. For a first approximation the STC performance of the PV modules and the performance of the other components (like the inverter) at STC conditions and the number of *Equivalent Sun Hours* (ESH) at the location of the PV system are sufficient. The notion of ESH will be discussed below. In a more detailed approach, performance changes of the modules and

the other components due to changing irradiance and weather conditions are taken into account. Since these performance changes can be quite high, they can alter the optimal system design considerably.

There are two main paradigms for designing PV systems. First, the system can be designed such that the generated power and the loads, *i.e.* the consumed power, match. A second way to design a PV system is to base the design on economics. We must distinguish between *grid-connected* and *off-grid* systems. As we will see, grid-connected systems have very different demands than off-grid systems.

This chapter is organised as follows: First, as an example, we will discuss a design of a simple off-grid

system in Section 18.1. After that we will take a more detailed look on *load profiles* in Section 18.2. In Section 18.3 and on how weather and irradiance conditions affect the performance of PV modules and BOS components, mainly inverters. Finally, in Sections 18.4 and 18.5 we learn how to design grid-connected and off-grid systems, respectively.

## 18.1 A simple approach for designing off-grid systems

In this section, we will design a simple off-grid system, as depicted in Fig. 18.1. The design presented here is based on very simple assumptions and does not take any weather-dependent performance changes into account. Nonetheless, we will see the major steps that are necessary for designing a system. Such a simple design can be performed in a six step plan:

1. Determine the total load current and operational time
2. Add system losses
3. Determine the solar irradiation in daily equivalent sun hours (ESH)
4. Determine total solar array current requirements

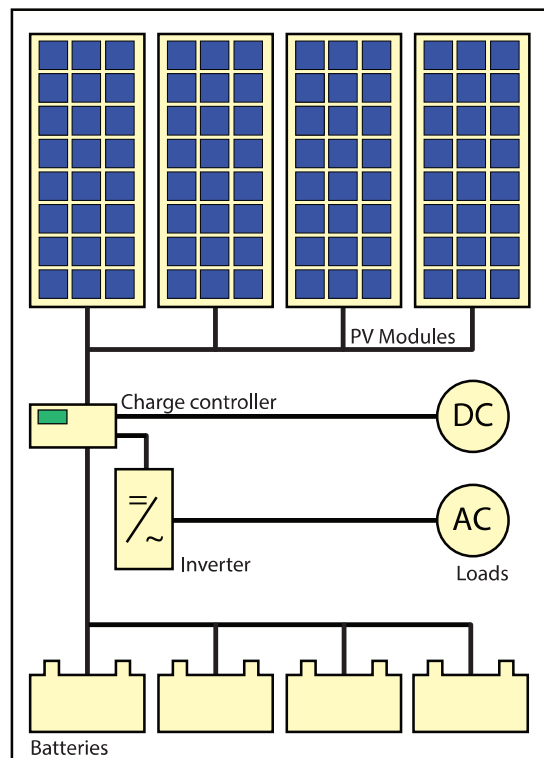


**Figure 18.1:** Illustrating a simple off-grid PV system with AC and DC loads (see also Fig. 15.1 b).

5. Determine optimum module arrangement for solar array
6. Determine battery size for recommended reserve time

### 1. Determine the total load current and operational time

Before starting determining the current requirements of loads of a PV system one has to decide the nominal operational voltage of the PV system. Usual nominal voltages are 12 V or 24 V. When knowing the voltage, the next step is to express the daily energy requirements of loads in terms of current and average operational time expressed in Ampere-hours [Ah]. In case of DC loads the daily energy [Wh] requirement is calculated by multiplying the power rating [W] of an individual appliance with the average daily operational time [h]. Dividing the Wh by the nominal PV system operational voltage, the required Ah of the appliance is obtained.

#### Example

A 12 V PV system has two DC appliances A and B requiring 15 and 20 W respectively. The average operational time per day is 6 hours for device A and 3 hours for device B. The daily en-

ergy requirements of the devices expressed in Ah are calculated as follows:

$$\text{Device A: } 15 \text{ W} \cdot 6 \text{ h} = 90 \text{ Wh}$$

$$\text{Device B: } 20 \text{ W} \cdot 3 \text{ h} = 60 \text{ Wh}$$

$$\text{Total: } 90 \text{ Wh} + 60 \text{ Wh} = 150 \text{ Wh}$$

$$150 \text{ Wh} / 12 \text{ V} = 12.5 \text{ Ah}$$

In case of AC loads the energy use has to be expressed as a DC energy requirement since PV modules generate DC electricity. The DC equivalent of the energy use of an AC load is determined by dividing the AC load energy use by the efficiency of the inverter, which typically can be assumed to be 85%. By dividing the DC energy requirement by the nominal PV system voltage the Ah is determined.

#### Example

An AC computer (device C) and TV set (device D) are connected to the PV system. The computer, which has rated power 40 W, runs 2 hours per day and the TV set with rated power 60 W is 3 hours per day in operation. The daily energy requirements of the devices expressed in DC Ah are calculated as follows:

*Device C:*  $40 \text{ W} \cdot 2 \text{ h} = 80 \text{ Wh}$

*Device D:*  $60 \text{ W} \cdot 3 \text{ h} = 180 \text{ Wh}$

*Total:*  $80 \text{ Wh} + 180 \text{ Wh} = 260 \text{ Wh}$

*DC requirement:*  $260 \text{ Wh} / 0.85 = 306 \text{ Wh}$

$306 \text{ Wh} / 12 \text{ V} = 25.5 \text{ Ah}$

## 2. Add system losses

Some components of the PV system, such as charge regulators and batteries require energy to perform their functions. We denote the use of energy by the system components as system energy losses. Therefore, the total energy requirements of loads, which were determined in step 1, are increased with 20 to 30% in order to compensate for the system losses.

### Example

The total DC requirements of loads plus the system losses (20%) are determined as follows:

$$(12.5 \text{ Ah} + 25.5 \text{ Ah}) \cdot 1.2 = 45.6 \text{ Ah}$$

## 3. Determine the solar irradiation in daily equivalent sun hours (EHS)

How much energy a PV module delivers depends on several factors, such as local weather conditions, seasonal changes, and installation of modules. PV modules should be installed under the optimal *tilt-angle* in order to achieve best year-round performance. It is also important to know whether a PV system is expected to be used all-year round or only during a certain period of a year. The power output during winter is much less than the yearly average and in the summer months the power output will be above the average.

In the PV community, 1 equivalent sun means a solar irradiance of  $1000 \text{ W/m}^2$ . This value corresponds to the standard, at which the performance of solar cells and modules is determined. The rated parameters of modules (see for example Table 17.1) are determined at solar irradiance of 1 sun.

When solar irradiation data are available for a particular location than the equivalent sun hours can be determined. For example, in the Netherlands the average annual solar irradiation is  $1000 \text{ kWh/m}^2$ . According to the AM1.5 spectrum, 1 sun delivers  $1000 \text{ W/m}^2 = 1 \text{ kW/m}^2$ . Hence, the Dutch average annual solar irradiation can be expressed as

$$\frac{1000 \text{ kWh} \cdot \text{m}^{-2}}{1 \text{ kW} \cdot \text{m}^{-2}} = 1000 \text{ h}$$

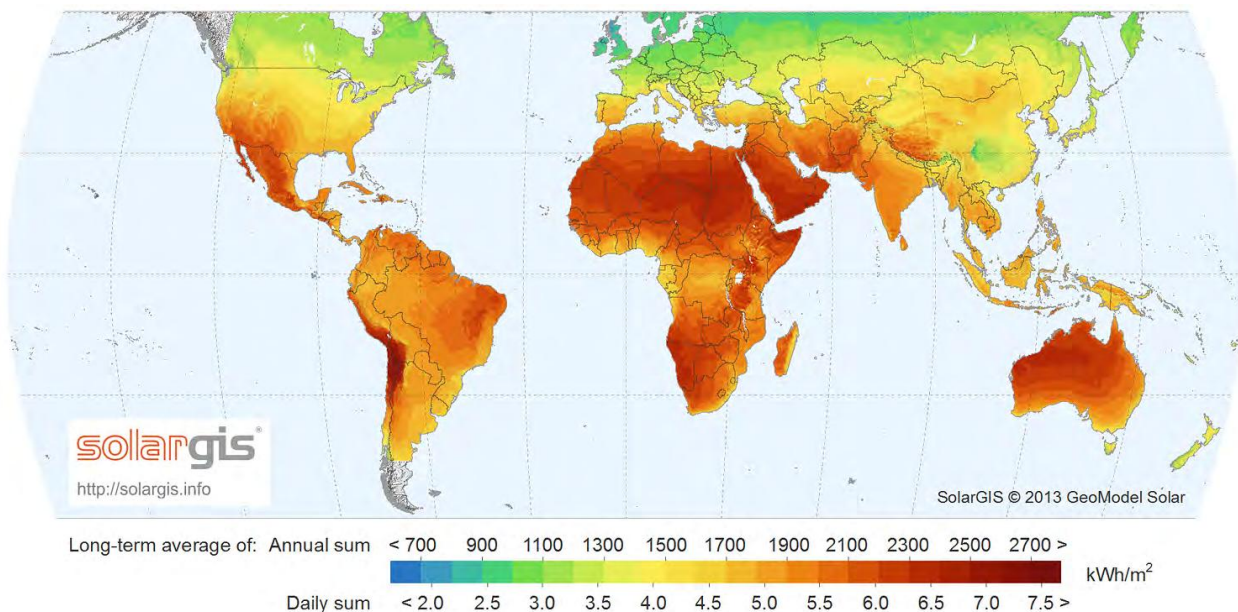


**Figure 18.2:** The average global horizontal insolation of the World given in kWh/year and PSH/day [101]. Note that this map only shows latitudes in between 60° N and 60° S.

i.e. 1000 equivalent sun hours, which corresponds to 2.8 h per day. Figures 18.2 and 18.3 show the *global horizontal irradiation* given in units of daily equivalent sun hours (ESH) and in kWh/year. Note that these figures show horizontal values, meaning that a PV module would get this irradiance if it would be flat. For a tilted module, the annual irradiance can be considerably higher, as we have seen in Chapter 16.

#### 4. Determine total solar array current requirements

The current that has to be generated by the solar array is determined by dividing the total DC energy requirement of the PV system including loads and system losses (calculated in step 2 and expressed in Ah) by the daily equivalent sun hours (determined in step 3).

##### Example

*The total DC requirements of loads plus the system losses are 45.6 Ah. The daily EHS for the Netherlands is about 3 hours. The required total current generated by the solar array is  $45.6 \text{ Ah} / 3 \text{ h} = 15.2 \text{ A}$ .*

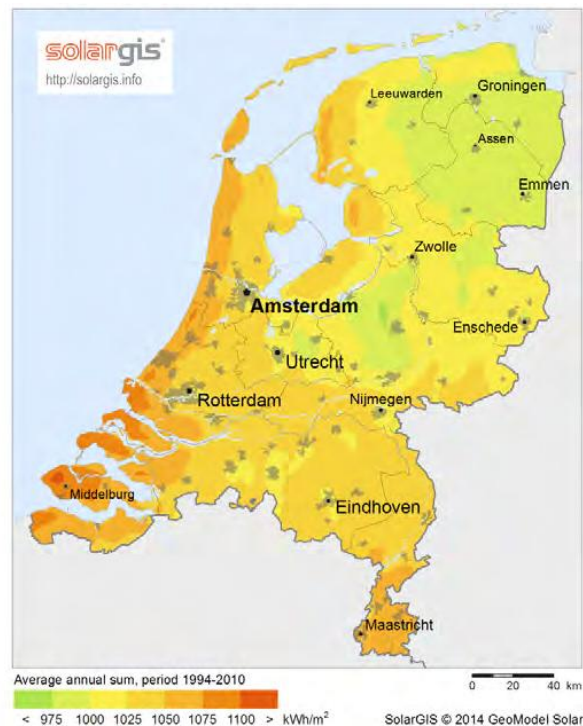


**Figure 18.3:** The average global horizontal insolation of the Netherlands given in kWh/year and PSH/day [101].

## 5. Determine optimum module arrangement for solar array

Usually, PV manufacturers produce modules in a whole series of different output powers. In the optimum arrangement of modules the required total solar array current (as determined in step 4) is obtained with the minimum number of modules. Modules can be either connected in series or in parallel to form an array. When modules are connected in series, the nominal voltage of the PV system is increased, while the parallel connection of modules results in a higher current.

The required number of modules in parallel is calculated by dividing the total current required from the solar array (determined in step 4) by the current generated by module at peak power (rated current in the specification sheet). The number of modules in series is determined by dividing the nominal PV system voltage with the nominal module voltage (in the specification sheet under configuration). The total number of modules is the product of the number of modules required in parallel and the number required in series.

### Example

The required total current generated by the solar array is 15.2 A. We have Shell SM50-H modules available. The specification of these modules is given in Table 17.1. The rated

current of a module is 3.15 A. The number of modules in parallel is  $15.2 \text{ A} / 3.15 \text{ A} = 4.8 < 5$  modules. The nominal voltage of the PV system is 12V and the nominal module voltage is 12 V. The required number of modules in series thus is  $12 \text{ V} / 12 \text{ V} = 1$  module. Therefore, the total number of modules in the array is  $5 \cdot 1 = 5$  modules.

## 6. Determine battery size for recommended reserve time

Batteries are a major component of stand-alone PV systems. The batteries provide load operation at night or in combination with the PV modules during periods of limited sunlight. For a safe operation of the PV system one has to anticipate periods with cloudy weather and plan a reserve energy capacity stored in the batteries. This reserve capacity is referred to as *PV system autonomy*, which means the period of time that the system is not dependent on energy generated by PV modules. It is given in days. The system autonomy depends on the type of loads. For critical loads such as telecommunications components the autonomy can be 10 days and more, for residential use it is usually 5 days or less. The capacity [Ah] of the batteries is calculated by multiplying the daily total DC energy requirement of the PV system including loads and system losses (calculated in step 2 and expressed in Ah) by the number of days of recommended reserve time. In order to prolong

**Table 18.1:** Worksheet for designing a simple off-grid PV system based on rough assumptions.

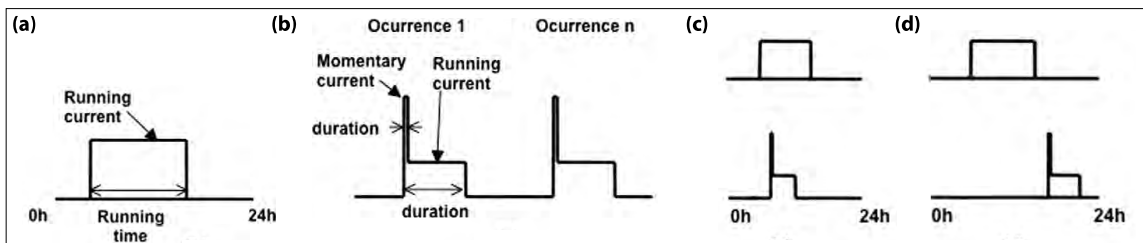
<b>Daily DC loads requirements</b>			
DC load	W ×	h =	Wh
<b>Total DC loads energy use:</b>			

<b>Daily AC loads requirements</b>			
DC load	W ×	h =	Wh
<b>Total AC loads energy use:</b>			
<b>/0.85 = DC energy requirement</b>			

<b>1</b>	Daily DC energy use (DC loads)	
<b>1</b>	Daily DC energy use (AC loads)	+
<b>1</b>	Daily DC energy use (all loads)	=
	PV system nominal voltage	/
	Daily Ah requirements (all loads)	=
<b>2</b>	Add PV system losses	×
	Daily Ah requirements (system)	=
<b>3</b>	Design EHS	/
<b>4</b>	Total solar array current	=
<b>5</b>	<b>Select module type</b>	
	Module rated current	/
	Number of modules in parallel	=
	PV system nominal voltage	/
	Modules nominal voltage	/
	Number of modules in series	=
	Number of modules in parallel	×
	Total number of modules	=
<b>6</b>	<b>Determine battery capacity</b>	
	Daily Ah requirements (system)	
	Recommended reserve time	×
	Usable battery capacity	/
	Minimum battery capacity	=



**Figure 18.4:** Illustrating different load profiles.

the life of the battery it is recommended to operate the battery using only 80% of its capacity. Therefore, the minimal capacity of the batteries is determined by dividing the required capacity by a factor of 0.8.

#### Example

The total DC requirements of loads plus the system losses are 45.6 Ah. The recommended reserve time capacity for the installation side in the Netherlands is 5 days. Battery capacity required by the system is  $45.6 \text{ Ah} \cdot 5 = 228 \text{ Ah}$ . The minimal battery capacity for a safe operation therefore is  $228 \text{ Ah}/0.8 = 285 \text{ Ah}$ .

Designing a simple PV system as described in this section can be carried out using a worksheet as in Table 18.1, where the PV system design rules are summarised.

## 18.2 Load profiles

Now we take a look at the load profile. Figure 18.4 illustrates different shapes that loads can have. (a) A simple load draws a constant amount of power for a certain time. (b) However, the consumed power does not need to be constant but can also show peaks that correspond to switching electrical appliances on or off. A household of course has several different loads that (c) can be switched on at the same time (coincident) or (d) at different times (non-coincident).

Analysing load profiles can be performed with increasing complexity and hence accuracy. The simplest method is to determine the loads on a 24-hour basis. To do this, an arbitrary day can be taken and the electricity consumption can be monitored. However, several loads do not fit in such a scheme. Several examples for

this already were treated in Section 18.1. For example, washing machines and dishwashers do not fit in a 24-hour scheme because typically they are only used several times in a week. Additionally, several loads are seasonal in nature, for example, air conditioning or heating, in case this is performed with a heat pump. Therefore it is advisable to look at load profiles for a whole year.

The total energy consumed in a year is given by

$$E_L^Y = \int_{\text{year}} P_L(t) dt. \quad (18.1)$$

It is expressed in kWh/year.

### 18.3 Meteorological effects

Standard Test Conditions (STC) of Photovoltaic (PV) modules are generally not representative of the real working conditions of a solar module. For example, high levels of incident irradiation, may cause the temperature of a module to rise many degrees above the STC temperature of 25°C, therefore lowering the module performances. For example, in the in a climate such as the one of the Netherlands, real operating conditions for PV systems correspond to relatively low levels of irradiance combined with a cold and windy weather. In order to effectively estimate real time energy production

from a given set of ambient parameters, it is essential to develop an accurate thermal model of the solar module, which evaluates the effects of the major meteorological parameters on the final temperature of a solar module.

In this section, we will develop an accurate thermal model for estimating the PV module working temperature as a function of meteorological parameters will be developed. The model is based on a detailed energy balance between the module itself and the surrounding environment. Both the installed configuration of the array together with external parameters such as direct incident solar irradiance on the panels, wind speed and cloud cover will be taken into account. From the calculated equilibrium temperature, the overall efficiency of the PV array will be calculated by separately assessing the temperature and irradiance effect on the efficiency at STC.

#### 18.3.1 Simplified thermal model for a photovoltaic array

The temperature strongly influences the performances of a PV module [102]. While the level of incident irradiation can be easily determined by measuring it with a pyranometer, the temperature reached inside the cell is much harder evaluate. In order to give an estimate of the average operating temperature of the module, manufacturers provide, together with rated per-

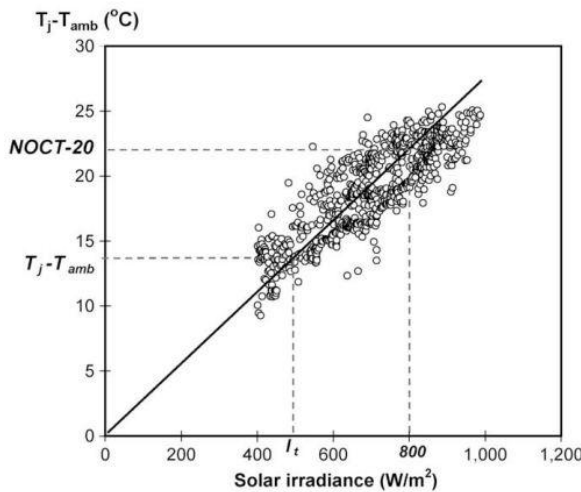


**Figure 18.5:** Rise in temperature above the ambient level with respect of increasing solar irradiance [103].

performances at STC, also the so called *Nominal Operating Cell Temperature* (NOCT). This value corresponds to the performances of a cell under an irradiance level of  $800 \text{ W/m}^2$ , ambient temperature of  $20^\circ\text{C}$  and an external wind speed of  $1 \text{ m/s}$  [102].

Simplified steady state models use a linear relationship between the solar irradiance  $G_M$  and the differ-

ence between the module temperature and the ambient temperature ( $T_M - T_a$ ), where the NOCT is used as a reference point, [103]

$$T_M = T_a + \frac{T_{NOCT} - 20^\circ}{800} G_M. \quad (18.2)$$

Equation (18.2) is however too simplistic and thus leads to significant errors in the modules temperature evaluations. The reason is that it does not take environmental conditions such as wind speed and mounting configuration of the array into account [103].

In order to take into mounting configuration of the module into account, the Installed Nominal Operating Conditions Temperature (INOCT) has been defined [104]. This value is described as the cell temperature of an installed array at NOCT conditions. Its value can therefore be obtained from the NOCT and the mounting configuration. The evaluation of how the INOCT varies with the module mounting configuration has been experimentally determined by measuring the NOCT at various mounting heights. The results can be found in literature and are here summarised in the Table 18.2.

Evaluating the influence of external meteorological parameters on the the module temperature is more complex and has been approached by developing a detailed thermal energy balance between the module and the surroundings. Here, the module is assumed to be a

**Table 18.2:** Derivation of the INOCT from the NOCT for various mounting configurations [104].

Rack Mount	INOCT = NOCT - 3°C
Direct Mount	INOCT = NOCT + 18°C
Standoff	INOCT = NOCT + X

where X is given by

W (inch)	X (°C)
1	11
3	2
6	- 1

single uniform mass at temperature  $T_M$ . The three types of heat transfer between the module itself with the surroundings are *conduction*, *convection* and *radiation*. The contributions considered in the model are:

- Heat received from the Sun in the form of insolation  $\varphi G_M$ , where  $\varphi$  is the absorptivity of the module.
- Convective heat exchange with surrounding air from the front and rear side of the module

$$h_c(T_M - T_a),$$

where  $h_c$  denotes the overall convective heat transfer coefficient of the module.

- Radiative heat exchange between the upper mod-

ule surface and the sky

$$\epsilon_{\text{top}} \sigma (T_M^4 - T_{\text{sky}}^4),$$

where  $\epsilon_{\text{top}} = 0.84$  is the emissivity of the module front glass and  $\sigma$  is the Stefan-Boltzmann constant as defined in Eq. (5.20). and between the rear surface and the ground

$$\epsilon_{\text{back}} \sigma (T_M^4 - T_{\text{gr.}}^4),$$

where the emissivity of the back is assumed to be  $\epsilon_{\text{back}} = 0.89$ .

- Conductive heat transfer between the module and the mounting structure. We neglect this contribution due to the small area of the contact points [105].

By separately considering each of the above mentioned contributions, we write down the balance for the heat transfer, [104]

$$mc \frac{dT_M}{dt} = \varphi G_M - h_c(T_M - T_a) - \epsilon_{\text{back}} \sigma (T_M^4 - T_{\text{gr.}}^4) - \epsilon_{\text{top}} \sigma (T_M^4 - T_{\text{sky}}^4). \quad (18.3)$$

Before providing a solution for this differential equation, it is appropriate to remark the fact that we are considering the entire module as a uniform piece at a

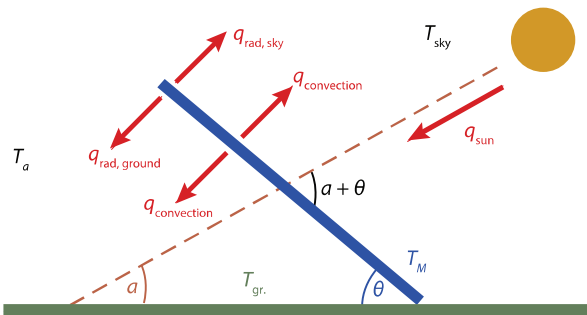


**Figure 18.6:** Representation of heat exchange between a tilted module surface and the surroundings.

temperature  $T_M$ . However, this is not entirely realistic since modules are made of various layers of different materials surrounding the actual solar cells. It is the purpose of this section to evaluate the temperature of the inner cell, which is the place where absorption of solar radiation effectively place. This temperature will be to some extent higher than the surface module temperature  $T_M$  due to the heat produced in the cell due to light absorption. The approximation of considering the temperature uniform throughout the module layers however is justified because of the relatively low thickness of the active cell together with the low heat capacity of the cell material compared to the other layers [105]. This results into a very low thermal resistance of

the cell to heat flow and therefore justifies the uniform temperature approximation.

In addition to this, a steady state approach will here be considered, meaning that the module temperature will not change over time for each of the 10-minute time steps. In reality, the temperature follows an exponential decay lagging behind variations in irradiation level. It is defined as *Time Constant* of a module, which is ‘the time it takes for the module to reach 63% of the total change in temperature resulting from a step change in irradiance’ [105]. Time constants for PV modules are generally of the order of approximately 7 minutes. For time steps greater than the Time Constant, as it is in our case, the module can be approximated as being in a steady state condition. In light of this assumption, the term on the left hand side of Eq. (18.3) vanishes.

It is now possible to proceed with the solution of the thermal energy balance equation. The formula can be linearised by noticing that

$$(a^4 - b^4) = (a^2 + b^2)(a + b)(a - b). \quad (18.4)$$

Since

$$(T_M^2 + T_{\text{sky}}^2)(T_M + T_{\text{sky}})$$

changes less than 5% for a 10°C variation in  $T_M$ , we can consider this term to be constant when  $T_M$  varies [104]. Therefore the energy balance can be simplified

becoming linear with respect to  $T_M$ . By defining

$$h_{r, \text{sky}} = \epsilon_{\text{top}} \sigma (T_M^2 + T_{\text{sky}}^2) (T_M + T_{\text{sky}}), \quad (18.5a)$$

$$h_{r, \text{gr.}} = \epsilon_{\text{back}} \sigma (T_M^2 + T_{\text{gr.}}^2) (T_M + T_{\text{gr.}}), \quad (18.5b)$$

we can rewrite Eq. (18.3) and find

$$\begin{aligned} \varphi G_M - h_c (T_M - T_a) - h_{r, \text{sky}} (T_M - T_{\text{sky}}) \\ - h_{r, \text{gr.}} (T_M - T_{\text{gr.}}) = 0. \end{aligned} \quad (18.6)$$

By rearranging the terms, the formula can be explicitly expressed as a function of  $T_M$ ,

$$T_M = \frac{\varphi G + h_c T_a + h_{r, \text{sky}} T_{\text{sky}} + h_{r, \text{gr.}} T_{\text{gr.}}}{h_c + h_{r, \text{sky}} + h_{r, \text{gr.}}} \quad (18.7)$$

However, since  $h_{r, \text{gr.}}$  and  $h_{r, \text{sky}}$  are also function of the module temperature, the equation needs to be solved iteratively: an initial module temperature is assigned and by  $h_{r, \text{gr.}}$  and  $h_{r, \text{sky}}$  are updated each iterations. A nearly exact solution can be obtained after 5 iterations.

Before solving iteratively Eq. (18.7) there are still many unknown variables that need to be determined, which we will do in the following sections.

### 18.3.2 Calculating the convective transfer coefficients

Convection is a form of energy transfer from one place to another caused by the movement of a fluid. Convective heat transfer can be either *free* or *forced* depending on the cause of the fluid motion.

In free convection, heat transfer is caused by temperature differences which affect the density of the fluid itself. Air starts circulating due to difference in buoyancy between hot (less dense) fluid and cold (denser) fluid. A circular motion is therefore initiated with rising hot fluid and sinking cold fluid. Free convection only takes place in a gravitational field [106].

Forced convection, on the other hand, is caused by a fluid flow due to external forces which therefore enhance the convective heat exchange. The heat transfer depends very much on whether the induced flow over a solid surface is laminar or turbulent. In the case of turbulent flow, an increased heat transfer is expected with respect to the laminar situation. This fact is due to an increased heat transport across the main direction of the flow. On the contrary, in laminar flow regime, only conduction is responsible for transport in the cross direction. For this reason, forced convection is always studied separately in the laminar and turbulent regime [106]. The overall convection transfer is made of the two relative contribution for free and forced compon-

ents. Mixed convective coefficient can be obtained by taking the cube root of the cubes of the forced and convective coefficients according to the equation [102]

$$h_{\text{mixed}}^3 = h_{\text{forced}}^3 + h_{\text{free}}^3. \quad (18.8)$$

Since the convective heat transfer coefficients will be different on the top and rear surface of the module, determining the total heat transfer coefficient has to be decoupled between the top  $h_c^T$  and rear  $h_c^B$  surfaces. The overall heat transfer will eventually be determined by the sum of the two components.

### Convective heat transfer on the top surface

Convective heat transfer has to be distinguished in free and forced components. For the forced component we further have to distinguish between laminar and turbulent flow. We obtain for the laminar and turbulent convective heat transfer coefficients

$$h_{\text{forced}}^{\text{lam.}} = \frac{0.86 \text{Re}^{-0.5}}{\text{Pr}^{0.67}} \rho c_{\text{air}} w, \quad (18.9a)$$

$$h_{\text{forced}}^{\text{turb.}} = \frac{0.028 \text{Re}^{-0.2}}{\text{Pr}^{0.4}} \rho c_{\text{air}} w. \quad (18.9b)$$

$\text{Re}$  is the *Reynolds number* that expresses the ratio of of the inertial forces to viscous forces,

$$\text{Re} = \frac{w D_h}{\nu}, \quad (18.10)$$

where  $w$  is the *wind speed* at the height of the PV array,  $D_h$  is the *hydraulic diameter* of the module, which is used as relevant length scale, and  $\nu$  is the *kinematic viscosity* of air.  $\text{Pr}$  is the *Prandtl number* which is the ratio of the momentum diffusivity to the thermal diffusivity. It is considered to be 0.71 for air. Finally,  $\rho$  and  $c_{\text{air}}$  are the density and heat capacity of air, respectively. The hydraulic diameter of a rectangle of length  $L$  and width  $W$ , and thus of the PV module, is given as

$$D_h = \frac{2LW}{L+W}. \quad (18.11)$$

Figure 18.7 shows the variation of the forced heat transfer coefficient at various wind speeds. We notice an overall increase in the heat transfer with increasing wind speeds due to the increased force transfer component. There are two different regions in the graph which represent the laminar and turbulent regimes, respectively. The laminar flow extends till around 3 m/s and is characterised by a lower convective heat exchange compared to the turbulent regime.

In a good approximation,  $h_{\text{forced}}$  and  $w$  are proportional

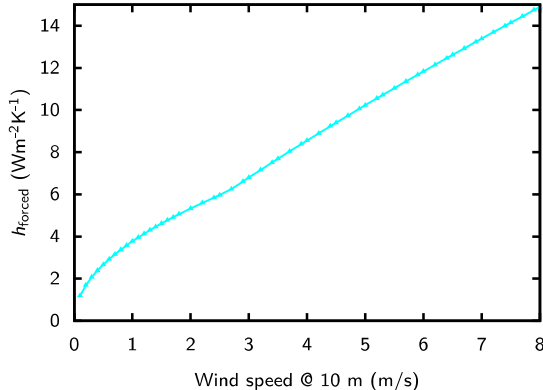


**Figure 18.7:** Forced convective heat transfer coefficient with increasing wind speeds

to each other and we may write

$$h_{\text{forced}}^{\text{lam.}} \simeq w^{0.5}, \quad (18.12\text{a})$$

$$h_{\text{forced}}^{\text{turb.}} \simeq w^{0.8}. \quad (18.12\text{b})$$

To determine the free heat transfer coefficient we only need to utilise the dimensionless *Nusselt number*  $\text{Nu}$ , which expresses the ratio between the convective and conductive heat transfer [104]

$$\text{Nu} = \frac{h_{\text{free}} D_h}{k} = 0.21(\text{Gr} \cdot \text{Pr})^{0.32}, \quad (18.13)$$

where  $k$  is the heat conductivity of air and  $\text{Gr}$  is the *Grashoff number* that is the ratio between the buoyancy and viscous forces,

$$\text{Gr} = \frac{g\beta(T - T_a)D_h^3}{\nu^2}. \quad (18.14)$$

Here,  $g$  is the *acceleration due to gravity on Earth* and  $\beta$  is the volumetric thermal expansion coefficient of air, which can be approximated to be  $\beta = 1/T$ .

With the value of both free and forced coefficient we can calculate the total mixed heat convective mass transfer coefficient using Eq. (18.8).

$$h_{\text{mixed}} = h_c^T = \sqrt[3]{h_{\text{forced}}^3 + h_{\text{free}}^3}. \quad (18.15)$$

### Convective heat transfer coefficient on the rear surface of the module.

Convection on the back side of the module will be lower than on the top because of the mounting structure and the relative vicinity to the ground. For example, a rack mount configuration, which is approximately installed at 1 m height, will achieve a larger heat exchange rate than a standoff mounted array that is mounted 20 cm above the ground. We model the effect of the different mounting configurations by scaling the convection coefficient obtained for the top of the module. We determine the scaling factor by performing an energy balance at the INOCT conditions [104],

$$\begin{aligned} \varphi G_M - h_c^T(T_{\text{INOCT}} - T_a) - h_{r,\text{sky}}(T_{\text{INOCT}} - T_{\text{sky}}) = \\ h_c^B(T_{\text{INOCT}} - T_a) + h_{r,\text{gr.}}(T_{\text{INOCT}} - T_{\text{gr.}}) \end{aligned} \quad (18.16)$$

We define  $R$  as the ratio of the actual to the ideal heat loss from the back side,

$$R = \frac{h_c^B(T_{\text{INOCT}} - T_a) + \epsilon_{\text{back}}\sigma(T_{\text{INOCT}}^4 - T_{\text{gr.}}^4)}{h_c^T(T_{\text{INOCT}} - T_a) + \epsilon_{\text{top}}\sigma(T_{\text{INOCT}}^4 - T_{\text{sky}}^4)}. \quad (18.17)$$

Substituting this into Eq. (18.16) at INOCT conditions yields

$$R = \frac{\varphi G_M - h_c^T(T_{\text{INOCT}} - T_a) - \epsilon_{\text{top}}\sigma(T_{\text{INOCT}}^4 - T_{\text{sky}}^4)}{h_c^T(T_{\text{INOCT}} - T_a) + \epsilon_{\text{top}}\sigma(T_{\text{INOCT}}^4 - T_{\text{sky}}^4)}. \quad (18.18)$$

The back side convection is therefore given by

$$h_c^B = R \cdot h_c^T. \quad (18.19)$$

We therefore find the overall convective heat transfer coefficient to be

$$h_c = h_c^T + h_c^B. \quad (18.20)$$

### 18.3.3 Other parameters

#### Sky temperature evaluation

The sky temperature can be expressed as a function of the measured ambient temperature, humidity, cloud cover and cloud elevation [104]. On a cloudy day, usually when the cloud cover is above 6 okta<sup>1</sup>, the sky temperature will approach the ambient temperature,  $T_{\text{sky}} = T_a$  [105]. However, on a clear day the sky temperature can drop below  $T_a$  and can be estimated by

$$T_{\text{sky}} = 0.0552 \cdot T_a^{3/2}. \quad (18.21)$$

#### Wind speed at module height evaluation

Since the anemometer used for the evaluation of the wind speed is at a higher height than the module array,

<sup>1</sup>Okta is a measure for the cloud cover, where 0 is clear sky and 8 is a completely cloudy sky.

the real wind speed experienced by the module will be scaled down with

$$w = w_r \left( \frac{y_M}{y_r} \right)^{\frac{1}{5}}, \quad (18.22)$$

where  $y_M$  and  $y_r$  denote the module and anemometer heights, respectively [104].

The elevation factor of 1/5 is determined by the landscape surrounding the installation, which is supposed to be open country.

### Absorptivity and emissivity of the module

In the thermal model developed, absorptivity is defined as the fraction of the incident radiation that is converted into thermal energy in the module. This value is linked to the reflectivity  $R$  and efficiency of the module by the equation [104]

$$\varphi = (1 - R)(1 - \eta). \quad (18.23)$$

Typical value for reflectivity of solar modules are 0.1 [104]. As far as the emissivity is concerned, a value of 0.84 has been used for the front glass surface and 0.89 for the back surface [107].

Now that all the unknown variables have been determined it is possible to the make iterations to calculate the

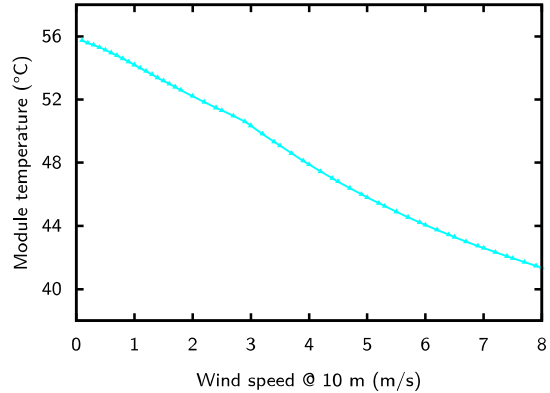


**Figure 18.8:** Influence of the wind speed on the temperature of a solar module at a fixed radiation of  $1000 \text{ W/m}^2$  and ambient temperature of  $25^\circ\text{C}$  on a clear day.

final temperature of the module as a function of the level of irradiance, wind speed and ambient temperature.

### 18.3.4 Evaluation of the thermal model

In the previous section, all the variables that are required to solve the thermal model have been derived. Therefore, the thermal model now can be solved via it-

eration.

Figure 18.8 below shows the effect of the wind speed on the module temperature at a fixed level of irradiance ( $1000 \text{ W/m}^2$ ) and an ambient temperature of  $25^\circ\text{C}$  on a clear day. It is obvious that the module temperature is significantly above the value of  $25^\circ\text{C}$  for all wind-speeds. Thus, STC are not representative for real operating cell conditions. Two different regions are visible in the graph corresponding to laminar and turbulent flow, respectively.

In Fig. 18.9 the thermal model and the NOCT model presented in Eq. (18.2) are compared to each other in dependence of the incident radiation for  $1 \text{ m/s}$  wind speed. We see that for  $1000 \text{ W/m}^2$  the NOCT model predicts a module temperature of  $54.3^\circ\text{C}$  regardless of the wind speed, which is much above the values obtained with the thermal model. The contribution of free convective and radiative heat exchange lower the module temperature with respect to the NOCT model. The difference between the two models is more pronounced at low levels of radiation, but for irradiances higher than  $1000 \text{ W/m}^2$  the two curves start diverging again. This can be understood when we consider that the NOCT model has been developed as a linearisation of the temperature/irradiation dependency around the NOCT conditions [103]. The accuracy of the model therefore decreases with the increasing distance from the NOCT.

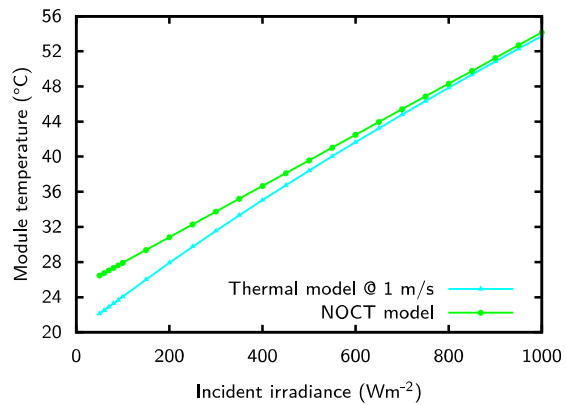


**Figure 18.9:** The module temperature calculated with the NOCT and the thermal model in dependence of the incident irradiance for  $1 \text{ m/s}$  wind speed.

### 18.3.5 Effect of temperature on the solar cell performance

The effect of a module temperature deviating from the 25°C of STC is expressed by the temperature coefficients that given on the data sheet provided by solar manufacturers. When knowing the temperature coefficient of a certain parameter, its value at a certain temperature  $T_M$  can be estimated with

$$V_{oc}(T_M, G_{STC}) = V_{oc} + \frac{\partial V_{oc}}{\partial T}(\text{STC})(T_M - T_{STC}), \quad (18.24)$$

$$I_{sc}(T_M, G_{STC}) = I_{sc} + \frac{\partial I_{sc}}{\partial T}(\text{STC})(T_M - T_{STC}), \quad (18.25)$$

$$P_{mpp}(T_M, G_{STC}) = P_{mpp} + \frac{\partial P_{mpp}}{\partial T}(\text{STC})(T_M - T_{STC}), \quad (18.26)$$

$$\eta(T_M, G_{STC}) = \frac{P_{mpp}(T_M, G_{STC})}{G_{STC}}. \quad (18.27)$$

If the efficiency temperature coefficient  $\partial\eta/\partial T$  is not given in the datasheet, it can be obtained by rearranging

$$\eta(T_M, G_{STC}) = \eta(\text{STC}) + \frac{\partial\eta}{\partial T}(\text{STC})(T_M - 25^\circ\text{C}). \quad (18.28)$$

An increase in the solar cell temperature will shift the  $I$ - $V$  curve as shown in Fig. 18.10. The slight increase

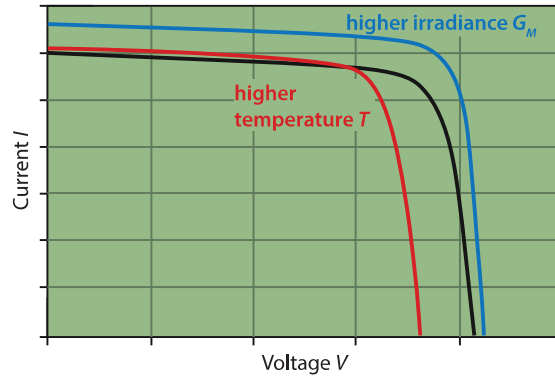


**Figure 18.10:** Effect of a temperature increase on the  $I$ - $V$  solar cell characteristic.

in the short circuit current at higher temperatures is completely outweighed by the decrease in open circuit voltage. The overall effect is of a general linear decrease in the maximum achievable power and therefore a decrease in the system efficiency and fill factor. This effect is due to an increase of the intrinsic carrier concentration at higher temperatures which in turns leads to an increase of the reverse saturation current  $I_0$ , which represents a measure of the *leakage* of carriers across the solar cell junctions, as we have seen in Chapter 8. The exponential dependence of  $I_0$  from the temperature is the main cause of the linear reduction of  $V_{oc}$  with the temperature,

$$V_{oc} = \frac{kT}{e} \ln \left( \frac{I_{sc}}{I_0} \right). \quad (18.29)$$

On the other hand, the slight increase in the generated current is due to a moderate increase in the photo-generated current resulting from an increased number of thermally generated carriers. The overall reduction of power at high temperature shows that cold and sunny climates are the best environment where to place a solar system.

### 18.3.6 Effect of light intensity on the solar cell performance

Intuitively, performances of a solar cell decrease considerably with decreasing light intensity incident on the module with respect to STC. The evaluation of the extent of this reduction is however less straightforward than for the case of the temperature since solar manufacturer often do not explicitly provide a reduction factor of the efficiency at every light intensity level.

By definition the efficiency is given by

$$\eta = \frac{I_{sc} V_{oc} FF}{G_M} \quad (18.30)$$

The maximum variation of the FF for light intensity between 1 and 1000 W/m<sup>2</sup> is about 2% for CdTe, 5% for a-Si:H, 22% for poly-crystalline silicon, and 23% for mono-crystalline silicon [108].

The short circuit current of a solar cell is directly proportional to the incoming radiation,

$$I_{sc} \simeq \lambda G_M, \quad (18.31)$$

where  $\lambda$  is simply a constant of proportionality. By expressing  $V_{oc}$  as in Eq. (18.29), the efficiency can be written as

$$\eta \simeq FF \lambda \frac{kT}{e} (\ln G_M + \ln \lambda - \ln I_0). \quad (18.32)$$

By defining

$$a = \text{FF} \lambda \frac{kT}{e}, \quad (18.33a)$$

$$b = \text{FF} \lambda \frac{kT}{e} (\ln \lambda - \ln I_0), \quad (18.33b)$$

the efficiency can be finally written as

$$\eta(25^\circ\text{C}, G_M) = a \ln G_M + b \quad (18.34)$$

The values of the coefficients  $a$  and  $b$  are device specific parameters and are rarely given by the manufacturer. The overall trend of the efficiency is represented by a straight line on a logarithmic scale [108].

From this model the values of  $I_{sc}$ ,  $V_{oc}$  and the efficiency at a irradiance level  $G_M$  can be determined from the STC as follows

$$V_{oc}(25^\circ\text{C}, G_M) = V_{oc}(\text{STC}) \frac{\ln G_M}{\ln G_{\text{STC}}}, \quad (18.35)$$

$$I_{sc}(25^\circ\text{C}, G_M) = I_{sc}(\text{STC}) \frac{G_M}{G_{\text{STC}}}, \quad (18.36)$$

$$P_{MPP}(25^\circ\text{C}, G_M) = \text{FF} V_{oc}(25^\circ\text{C}, G_M) I_{sc}(25^\circ\text{C}, G_M), \quad (18.37)$$

$$\eta(25^\circ\text{C}, G_M) = \frac{P_{MPP}(25^\circ\text{C}, G_M)}{A_M G_M}, \quad (18.38)$$

where  $A_M$  is the module area.

### 18.3.7 Overall module performance

By combining the two effects of temperature and light intensity, the final efficiency of the module at every level of irradiance and temperature can be determined as [109]

$$\eta(T_M, G_M) = \eta(25^\circ\text{C}, G_M) [1 + \kappa(T_M - 25^\circ\text{C})], \quad (18.39)$$

where

$$\kappa = \frac{\partial \eta}{\partial T} \frac{1}{\eta(\text{STC})}. \quad (18.40)$$

Typical values for  $\kappa$  are  $-0.0025/\text{ }^\circ\text{C}$  for CdTe,  $-0.0030/\text{ }^\circ\text{C}$  for CIS, and  $-0.0035/\text{ }^\circ\text{C}$  for c-Si [109].

All the other parameters such as  $I_{sc}$ ,  $V_{oc}$ , and  $P_{mpp}$  can also be evaluated at every level of irradiance and module temperature by simply adapting Eq. (18.39) to the corresponding coefficients and parameters.

In Fig. 18.11 the difference between  $\eta(25^\circ\text{C}, G_M)$  and  $\eta(T_M, G_M)$ , which takes both irradiance  $G_M$  and module temperature  $T_M$  into account, is shown. The graph has been derived by keeping the wind speed constant at a value of 1 m/s and by determining  $T_M$  iterating the heat thermal model at each level of irradiance for a constant ambient temperature of  $25^\circ\text{C}$ . At low levels of irradiance no effects of the module temperature are observed. At higher level of incident light intensity the difference between the two curves becomes more pronounced. since only  $\eta_{mpp}(G_M, T_M)$  takes into account

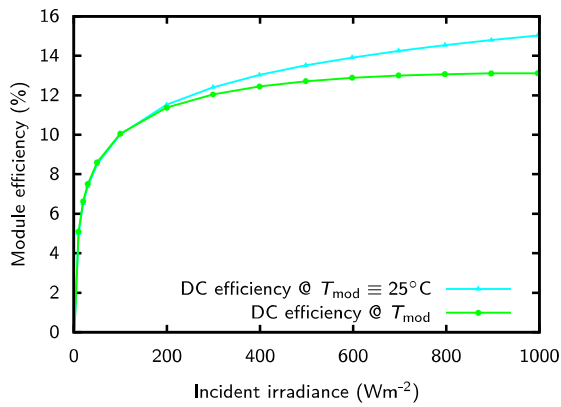


**Figure 18.11:** Comparison of  $\eta(25^{\circ}\text{C}, G_M)$  and  $\eta(T_M, G_M)$  in dependence of the light irradiance at a wind speed of 1 m/s and ambient temperature of  $T_a = 25^{\circ}\text{C}$  for a c-Si solar cell.

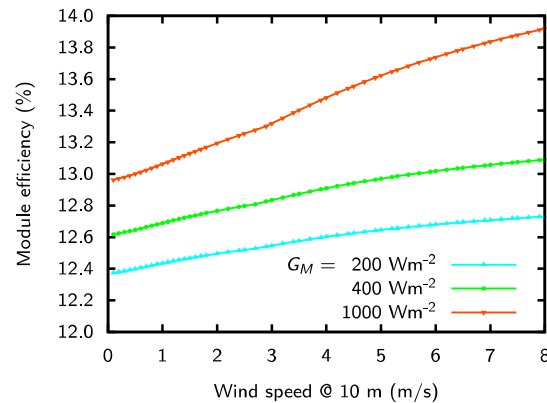


**Figure 18.12:** Overall efficiency of the module with increasing wind speed at various irradiance levels.

the marked reduction in efficiency resulting from the rising  $T_M$ .

Figure 18.12 shows the overall efficiency at various light intensities in dependence of the wind speed. Once more, the beneficial effect of turbulent motion in cooling the module is reflected by an increase of efficiency with the wind speed.

Finally, the power output of a module before the BOS is given by

$$P_{\text{DC}} = \eta(G_M, T_M) \cdot G_M \cdot A_M, \quad (18.41)$$

and the power output at STC is given by

$$P_{\text{STC}} = \eta(G_{\text{STC}}, 25^\circ\text{C}) \cdot G_{\text{STC}} \cdot A_M, \quad (18.42)$$

The *energy yield* of the DC side then is defined as

$$Y_{\text{DC}} = \frac{P_{\text{DC}}}{P_{\text{STC}}} \cdot 100\% = \frac{\eta(G_M, T_M) \cdot G_M}{\eta(G_{\text{STC}}, 25^\circ\text{C}) \cdot G_{\text{STC}}} \cdot 100\%. \quad (18.43)$$

## 18.4 Designing grid-connected PV-system

Now we can use all the things learned in this and the other chapters for actually designing a PV system. For designing the PV system we use the *energy balance* approach, meaning that we design the system such that the generated energy and the consumed energy during one year match. Of course, there are also other ways of designing systems for example based on economic arguments.

For the energy balance we first need to calculate the annual load, which already happened in section 18.2. The energy yield at the DC side is given by

$$E_{\text{DC}}^Y = A_{\text{tot}} \int_{\text{year}} G_M(t) \eta(t) dt, \quad (18.44)$$

where  $A_{\text{tot}}$  is the total module area. It is related to the area of one module  $A_M$  via

$$A_{\text{tot}} = N_T \cdot A_M, \quad (18.45)$$

where  $N_T$  is the number of modules. The energy balance now writes as

$$E_{\text{DC}}^Y = E_L^Y \cdot \text{SF}, \quad (18.46)$$

where SF is a *sizing factor* that usually is assumed to be 1.1. We therefore can calculate the required number of modules,

$$N_T = \left\lceil \frac{E_L^Y \cdot \text{SF}}{A_M \cdot \int_{\text{year}} G_M(t) \eta(t) dt} \right\rceil, \quad (18.47)$$

where  $\lceil x \rceil$  denotes the ceiling function, *i.e.* the lowest integer that is greater or equal than  $x$ .

Now it is important to decide how many modules are to be connected in *series* ( $N_S$ ) and in *parallel* ( $N_P$ ). Of course,

$$N_T = N_S \cdot N_P. \quad (18.48)$$

Such a PV array hence consists of  $P$  strings of  $S$  modules each. The  $N_T$  determined in Eq. (18.47) not necessarily needs to be an even number. For example, if  $N_T = 11$ , you might want to choose for  $N_T = 12$  panels, because you can install them as  $S \times P = 12 \times 1, 6 \times 2, 4 \times 3, 3 \times 4, 2 \times 6$  or  $1 \times 12$  strings. In principle, it is

preferable to connect as many modules as possible in series since then the currents on the DC side and hence the cable losses stay low. Further, thinner cables can be chosen. However, many modern inverters can connect two or even more individual strings, which can be important if the installation contains two or more areas with different shading, for example on two different sides of a roof. Further, it can be chosen to connect different strings to different inverters as well, such that the system uses several string inverters.  $N_S$  and hence the voltage at the inverter is also restricted by the chosen inverter type — or, if seen the other way round, the inverter has to be chosen such that its operating voltage fits well to the string voltage.

In a conservative assumption, the power on the DC side at STC now is given as

$$P_{DC}^{STC} = N_T \times P_{MPP}^{STC}. \quad (18.49)$$

The inverter must be chosen such that its maximal power  $P_{DC, max}^{inv}$  is above the maximal PV output,

$$P_{DC, max}^{inv} > P_{DC}^{STC}. \quad (18.50)$$

Further, the nominal DC power of the inverter should be approximately equal to the PV power,

$$P_{DC_0} \approx P_{DC}^{STC}. \quad (18.51)$$

Usually, for  $P_{DC_0} < 5 \text{ kWp}$ , *single-phase* inverters are used while for  $P_{DC_0} > 5 \text{ kWp}$  *three-phase* inverters are advised.

Also the inverter efficiency is dependent on the input power and voltage. A model discussing the inverter efficiency is presented below.

### 18.4.1 Inverter efficiency

As we already discussed in Chapter 17, modern *inverters* fulfil two major functions: First, *maximum power point tracking* (MPPT), and secondly, the actual inverter function, *i.e.* converting the incoming direct current (DC) to alternating current (AC) that can be fed into the electricity grid.

In order not to waste electricity produced by the PV array, an inverter should always work as close as possible at its maximum achievable efficiency. However, the inverter efficiency of an inverter strongly depends on the DC input voltage as well as the total DC input power as well as on the DC input voltage of the system. The inverter efficiency  $\eta_{inv}$  with respect to the input DC power at various DC voltage level is usually given at the data sheet, at least for some values. Often, only the *peak efficiency* is given as a single value.

#### Weighted Efficiencies

A more reliable way of expressing the inverter efficiency in a single number is to use *weighted efficiencies*,

which combine the inverter efficiencies over a wide range of solar resource regimes [110]. Two different weighted efficiencies are commonly used. First, the *European Efficiency*, which represents a low-insolation climate such as in central Europe, and the *California Energy Commission* (CEC) efficiency, which represents the PV system performance in high-insolation regions such as in the southwest of the United States [110]. They are given by

$$\eta_{\text{Euro}} = 0.03 \eta_{5\%} + 0.06 \eta_{10\%} + 0.13 \eta_{20\%} + 0.10 \eta_{30\%} + 0.48 \eta_{50\%} + 0.20 \eta_{100\%}, \quad (18.52\text{a})$$

$$\eta_{\text{CEC}} = 0.04 \eta_{10\%} + 0.05 \eta_{20\%} + 0.12 \eta_{30\%} + 0.21 \eta_{50\%} + 0.53 \eta_{75\%} + 0.05 \eta_{100\%}, \quad (18.52\text{b})$$

where  $\eta_{x\%}$  denotes the efficiency at  $x\%$  of nominal power of the inverter. Note that the CEC efficiency contains a 75% value that is not present in the European efficiency.

Even though the weighted efficiencies represents a more accurate approximation of the effective yearly working performance of the inverter compared to the mere peak efficiency, it still only is an approximation of the average performance of a system in the European climate.

If a better estimate of the *real time energy yield* of an extended PV system is needed, a more accurate representation of the instantaneous inverter performance at every

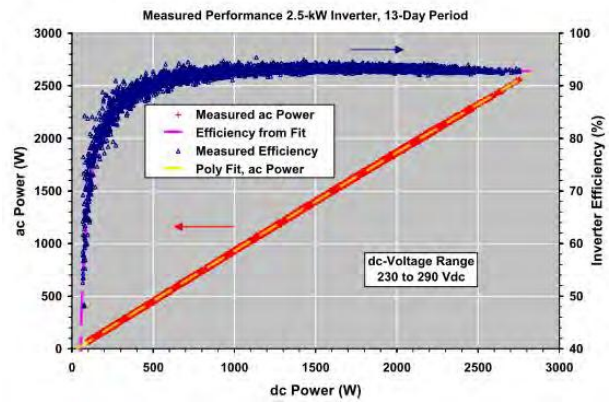


**Figure 18.13:** Field test results for a 2.5 kW Solecetria PVI2500 inverter recorded during a period of 13 days for system operation at Sandia Laboratories [111].

level of input power and voltage must be developed, for example the model discussed below.

### Sandia National Laboratories (SNL) model

Due to a lack of detailed data from inverters manufacturers, many research institutes around the world have published extended data, which are publicly available online. These data present efficiency curves for a large

range of inverters as a function of a several characteristic parameters. One database that can be used is the one provided by the Sandia National Laboratories [112].

Figure 18.13 shows an example of an inverter efficiency curve CITE. For the graph, field test measurements were taken during a period of 13 days with changing weather condition. While the relationship between the AC and DC power appears to be linear at first, a closer look to the graph reveals that this is not entirely the case, as shown in Fig. 18.14. The power consumption of the inverter itself together with the electrical characteristics of the switching modes and circuits at different power levels results in a degree of non linearity between AC and DC power at a given DC voltage level. Assuming that the inverter efficiency is a constant value throughout the whole DC power range is equivalent to assuming a linear relationship between DC and AC power, which has been shown not to be the case.

The dependency of the inverter efficiency on the DC input voltage is very complex phenomenon that still lacks a full physical explanation [113]. The differences between the different inverter types can partially be explained with different types of switches used. Figure 18.15 shows the voltage dependent inverter efficiency for different inverter types. These curves were determined with the Sandia model that is described in the next paragraph.

In the following, we will introduce a mathematical

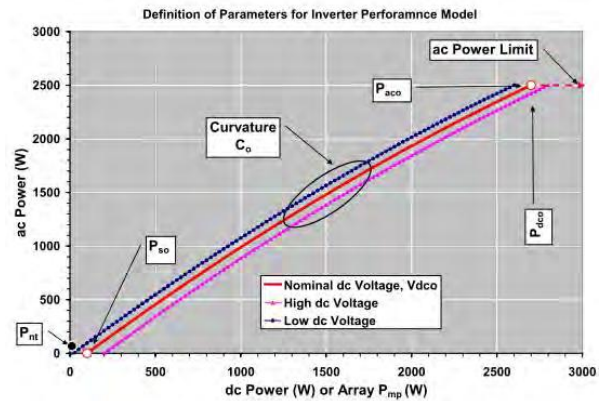


**Figure 18.14:** A closer look on to the relationship between AC output and DC input power for an inverter [111].

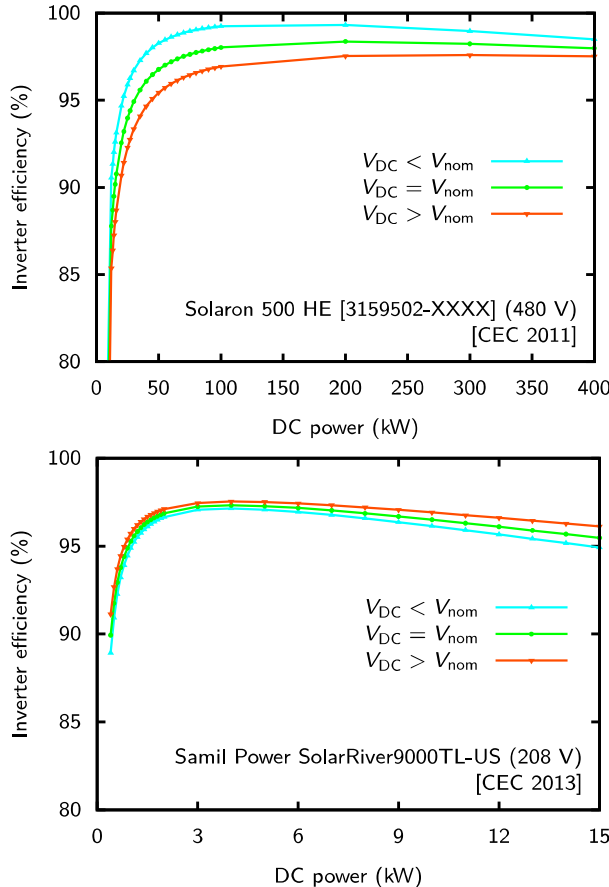


**Figure 18.15:** Variation in the inverter efficiency with DC input voltage for two different inverters.

model developed at Sandia Research Institute that has been chosen due to its accuracy of both the effect of DC input power and voltage on the AC power output. In this model the relationship between  $P_{AC}$  and  $P_{DC}$  is given by [111]

$$P_{AC} = \left[ \frac{P_{AC_0}}{A - B} - C(A - B) \right] \cdot (P_{DC} - B) - C(P_{DC} - B)^2, \quad (18.53)$$

where the coefficients  $A$ ,  $B$ , and  $C$  are given by

$$A = P_{DC_0} [1 + C_1 (V_{DC} - V_{DC_0})], \quad (18.54a)$$

$$B = P_{S_0} [1 + C_2 (V_{DC} - V_{DC_0})], \quad (18.54b)$$

$$C = C_0 [1 + C_3 (V_{DC} - V_{DC_0})]. \quad (18.54c)$$

Several of the parameters are depicted in Fig. 18.14. The parameters are [111]:

$P_{AC}$ : AC-power output from inverter based on input power and voltage, (W).

$P_{DC}$ : DC-power input to inverter, typically assumed to be equal to the PV array maximum power, (W).

$V_{DC}$ : DC-voltage input, typically assumed to be equal to the PV array maximum power voltage, (V).

$P_{AC_0}$ : Maximum AC-power “rating” for inverter at reference or nominal operating condition, assumed to be an upper limit value, (W).

$P_{DC_0}$ : DC-power level at which the ac-power rating is achieved at the reference operating condition, (W).

$V_{DC_0}$ : DC-voltage level at which the ac-power rating is achieved at the reference operating condition, (V).

$P_{S_0}$ : DC-power required to start the inversion process, or self-consumption by inverter, strongly influences inverter efficiency at low power levels, (W).

$C_0$ : Parameter defining the curvature (parabolic) of the relationship between AC-power and DC-power at the reference operating condition, default value of zero gives a linear relationship, (1/W).

$C_i$ : Empirical coefficient allowing  $P_{DC_0}$  to vary linearly with DC-voltage input, default value is zero, ( $i = 1, 2, 3, 1/V$ ).

This model takes the following losses into account [113]:

- Self consumption of the inverter. This value corresponds to the DC power required to start the inversion process.
- Losses proportional to the output power due to fixed voltage drops in semiconductors and switching losses.
- Ohmic losses

The accuracy of the model depends on the data available for determining the performance parameters. An initial estimate can be performed using the little information provided by the manufacturer. Using all the re-

quired parameters will provide a model with an error of approximately 0.1% between the modeled and measured inverter efficiency [113].

All the parameters required for handling Eq. (18.53) are given in the Sandia laboratory database where a full list of a wide range of inverters with nominal powers from 200 W up to 1 MW are covered [112]. This model therefore uses the instantaneous value of  $P_{DC}$  and  $V_{DC}$  produced by the entire PV array to evaluate the AC power output and inverter efficiency.

### Maximum Power Point Tracker and additional losses

The efficiency of the MPPT has not been included explicitly in the Sandia performance model. This is because the efficiency of most inverters ranges between 98% and nearly 100% at every level of input power and the voltage provided is within the accepted minimum and maximum window for the MPPT to function correctly. A decrease of 1% in the system performance has therefore been used to take the MPPT losses into account.

An additional decrease of 3% in the system performance can be considered to cover losses caused by mismatch between modules (-1.5%), ohmic cable losses (-0.5%) and soiling (-1%) [109], if the cable losses are not determined via the method described in section 17.5.

### 18.4.2 Performance Analysis

Now we will put all things together that we discussed earlier in this section. The *instantaneous power output* on the AC side can be described with

$$P_{AC}(t) = A_M G_M(t) \eta_M(t) \eta_{inverter}(t) \eta_{MPPT}(t) \eta_{other}. \quad (18.55)$$

The system efficiency then is given as

$$\eta_{system}(t) = \frac{P_{AC}(t)}{A_{tot} G_M(t)} \cdot 100\%, \quad (18.56)$$

which leads us to the *instantaneous AC-side yield* (also known as *performance ratio*),

$$Y_{AC}(t) = \frac{P_{AC}(t)}{P_{STC}} \cdot 100\%. \quad (18.57)$$

Then, the *yearly energy yield at the AC side* can be calculated with

$$E_{AC}^Y = \int_{\text{year}} P_{AC}(t) dt; \quad (18.58)$$

it is given in Wh/year. Another important parameter is the *annual efficiency* of the system

$$\eta_{system}^Y = \frac{E_{AC}^Y}{E_{i,sys}^Y} \cdot 100\%, \quad (18.59)$$

where  $E_{i,sys}^Y$  is the solar energy incident on the PV system throughout the year. It can be calculated with

$$E_{i,sys}^Y = A_{tot} \int_{\text{year}} G_M(t) dt. \quad (18.60)$$

The last parameter we look at is the *yearly electricity yield*

$$Y_E = \frac{E_{AC}^Y}{N_S N_P \cdot P_{STC}}, \quad (18.61)$$

which is given by Wh/(year kWp).

At the end of the design phase it is important to check whether the system really fulfils the requirements. If the yearly energy yield exceeds the annual load, the system is well designed. Otherwise, another iteration has to be done in order to scale up the system. However, as stated earlier, for a grid-connected system it also can be a choice not to require the whole load to be covered by PV electricity.

## 18.5 Designing off-grid PV systems

In this last section of this chapter on PV system design we take a closer look on the design of off-grid PV systems (also called stand-alone systems). Choosing a good design is more critical for off-grid systems than for grid-connected systems. The reason for this is that

off-grid systems cannot fall back on the electricity grid, which increases the requirements on the reliability of the off-grid system.

A major component of off-grid systems is the *storage component*, which can store energy in times when the PV modules generate more electricity than required and it can deliver energy to the electric appliances when the electricity generated by the PV modules is not sufficient. A major design parameter for off-grid systems is the required number of autonomous days, *i.e.* the number of days a fully charged storage must be able to deliver energy to the system until discharged.

The sizing of both the PV array and the storage component, usually a *battery bank*, is interconnected. Here, two parameters arise: first,  $E_{\text{fail}}$ , which is the energy required by the electric load that cannot be delivered by the PV system, for example if the batteries are emptied after several cloudy days. Secondly,  $E_{\text{dump}}$ , which is the energy produced by the PV array that neither is used for driving a load nor is stored in the battery, for example, if the batteries already are full after a number of sunny days. Now, we can define the *Loss of Load Probability*,

$$\text{LLP} = \frac{E_{\text{fail}}}{\int_{\text{year}} P_L(t) dt}. \quad (18.62)$$

Of course, the lower LLP, the more stable and reliable the PV system. Table 18.3 shows recommended LLPs for different applications.

**Table 18.3:** Recommended Loss of Load Probability (LLP) for some Applications

Application	Recommended LLP
Domestic illumination	$10^{-2}$
Appliances	$10^{-1}$
Telecommunications	$10^{-4}$

Figure 18.16 (a) shows a schematic of an off-grid system with all the required components, *i.e.* the PV array, a maximum power point tracker (MPPT), a charge controller (CC), a discharge controller (DC), a battery bank (BB), an inverter, and the load. The CC prevents the BB from being overcharged by the PV system, while the DC prevents the battery to be discharged below the minimal allowed SoC. In the simplest case, they (dis)connect the PV system and load from the battery by switches. For optimal charging, however, nowadays often CC with pulse-width modulation (PWM) are used. By far not all off-grid systems contain an MPPT, thus it is represented with a dashed line. However, if an MPPT is present it usually is delivered in one unit together with the CC. Usually, the DC and inverter are combined in one *battery inverter unit*. Especially at larger systems the inverter currents may become very large. For example, if a 2400 W load is present for a short time, this means 100 A on the DC side in a 24 V system. Therefore the battery inverter usually is directly connected to the BB with thick cables. In very small

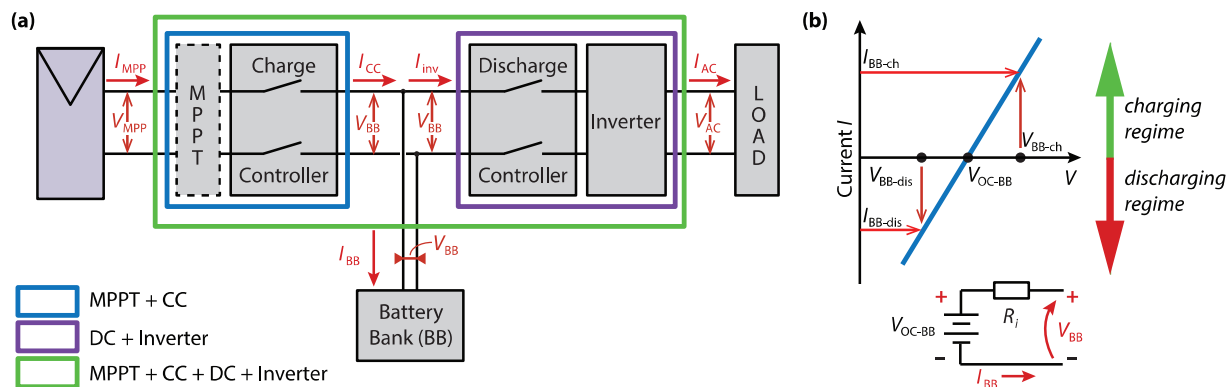


**Figure 18.16:** (a) PV topology of an off-grid system. (b) Simplified  $I$ - $V$  curve and schematic of the battery bank.

systems with maximal powers of several hundreds of Watt, the CC and DC may be combined in one unit.

### 18.5.1 A closer look at the battery

The battery bank is the workhorse of any off-grid system, because it is its stable power source. It is thus very important to understand how the battery bank will act in the PV system. Therefore, we will discuss it in more detail in this section.

When we want to understand how a battery works we have to consider *the net effect of all the forces that try to charge or discharge the battery*. In Fig. 18.16 (a) the most important currents and voltages that we need and the following discussion are depicted. In Fig. 18.16 (b) a schematic and an  $I$ - $V$  curve of an idealised battery bank is shown. As we can see, this battery bank is considered to consist of an voltage source with a total voltage  $V_{OC-BB}$  and an internal resistance  $R_i$ . In reality,  $V_{OC-BB}$  will not be constant, but a function of the state of charge, the ambient temperature, and others,

$$V_{OC-BB} = f(\text{SoC}, T, \dots). \quad (18.63)$$

In the following discussion, however, we will neglect this dependence and assume  $V_{OC-BB}$  to be constant. Because of  $R_i$ , the voltage  $V_{BB}$  will differ from  $V_{OC-BB}$  and also is dependent on the current  $I_{BB}$  flowing through

the battery, as seen by the equation

$$I_{BB} = \frac{1}{R_i} (V_{BB} - V_{OC-BB}). \quad (18.64)$$

Note that we use the convention, where  $I_{BB}$  is positive when the battery is charged and negative when it is discharged. Let us now derive an expression for the voltage of the battery bank ( $V_{BB}$ ) as a function of the other PV system parameters. We start with the power on the left and right-hand sides of the MPPT,

$$\eta_{MPP} I_{MPP} V_{MPP} = I_{CC} V_{BB} =: \beta, \quad (18.65)$$

and hence

$$I_{CC} = \frac{\eta_{MPP} I_{MPP} V_{MPP}}{V_{BB}} = \frac{\beta}{V_{BB}}. \quad (18.66)$$

Consequently,  $\beta = 0$  means that the PV system is not active, for example during night.

In a similar manner, we look at the power on the left and right hand side of the inverter:

$$P_L = I_{AC} V_{AC} = \eta_{inv} I_{inv} V_{BB} =: \eta_{Inv} \alpha, \quad (18.67)$$

and consequently

$$I_{inv} = \frac{P_L}{\eta_{inv} V_{BB}} = \frac{\alpha}{V_{BB}}. \quad (18.68)$$

Combining Eqs. (18.66) and (18.68), we find

$$I_{BB} = I_{CC} - I_{inv} = \frac{\beta - \alpha}{V_{BB}}. \quad (18.69)$$

Clearly,  $\alpha = 0$  indicates that no load is present.

Combining Eqs. (18.64) and (18.69), multiplying with  $R_i V_{BB}$  and rearranging leads to a quadratic equation,

$$V_{BB}^2 - V_{OC-BB} V_{BB} - R_i(\beta - \alpha) = 0. \quad (18.70)$$

with the solutions

$$V_{BB}^{\pm} = \frac{V_{OC-BB}}{2} \pm \sqrt{\left(\frac{V_{OC-BB}}{2}\right)^2 + R_i(\beta - \alpha)}. \quad (18.71)$$

The correct solution is the "+" solution as we can check with

$$V_{BB}^+(\beta - \alpha = 0) = V_{OC-BB}. \quad (18.72)$$

Hence, the final solution is

$$V_{BB} = \frac{V_{OC-BB}}{2} + \sqrt{\left(\frac{V_{OC-BB}}{2}\right)^2 + R_i(\beta - \alpha)}. \quad (18.73)$$

Let us now take a short look on this solution. If the battery is charged,  $I_{CC}$  is higher than  $I_{inv}$  and hence  $(\beta - \alpha)$  and  $I_{BB}$  are positive. From Eq. (18.73) it follows that in this case  $V_{BB}$  is higher than  $V_{OC-BB}$ . On the other hand, if the battery is discharged,  $I_{CC}$  is lower than  $I_{inv}$  and hence  $(\beta - \alpha)$  and  $I_{BB}$  are negative. Therefore,  $V_{BB}$  will be lower than  $V_{OC-BB}$ .

Note that only the net current  $I_{BB} = I_{CC}$  flows in or out of the battery. Therefore, only this current determines

**Table 18.4:** Recommended number of autonomous days  $d_A$  at several latitudes.

Latitude ( $^{\circ}$ )	Recommended $d_A$
0-30	5-6
20-50	10-12
50-60	15

the power loss in the battery,

$$P_{BB}(\text{loss}) = I_{BB}^2 R_i. \quad (18.74)$$

This power always is lost, irrespective of the sign of  $I_{BB}$ .

### 18.5.2 Designing a system with energy balance

Now we discuss how to design a PV system based on the principle of *energy balance*. For determining the adequate components, the analysis for the load side and the PV side is performed separately. Let us begin with the *load side*. We can determine the annual load  $E_L^Y$  as discussed in section 18.2 and Eq. (18.1),

$$E_L^Y = \int_{\text{year}} P_L(t) dt. \quad (18.75)$$

From that we can estimate the *average daily load* with

$$E_L^D = \frac{1}{365} E_L^Y. \quad (18.76)$$

Next, we have to choose an adequate number of days of autonomy  $d_A$ . Some values given in table 18.4. Now, we can calculate the required energy of the battery bank,

$$E_{BB} = d_A \frac{E_L^D \cdot SF_{bat}}{DoD_{max}}, \quad (18.77)$$

where  $SF_{bat}$  is the sizing factor of the battery, which is similar to the sizing factor for the PV array already defined in section 18.4.  $DoD_{max}$  is the maximally allowed depth of discharge of the batteries. The rated energy of the chosen batteries is

$$E_{bat} = V_{OC\text{-}bat} C_{bat}, \quad (18.78)$$

where  $C_{bat}$  is the battery capacity (unit Ampere-hours). Hence, the required number of batteries is

$$N_{bat} = \left\lceil \frac{E_{BB}}{E_{bat}} \right\rceil. \quad (18.79)$$

Similarly as for grid-connected systems we now need to choose a suitable inverter. Therefore we must consider the maximal load power  $P_L^{\max}$ . This we can do, for example, by looking at the appliance with the maximal power consumption, or by adding up the power of all

appliances. It may be more beneficial to choose a system design, such that not all appliances can be used at the same time. The final decision of course is up to the designer of the system. Similar as for grid-connected systems, the inverter must fulfil several requirements: First, its maximally allowed power output must exceed the maximal power required by the appliances,

$$P_{DC,\max}^{\text{inv}} > P_L^{\max}. \quad (18.80)$$

Secondly, the nominal power of the inverter should be approximately equal to the maximal load power,

$$P_{DC,0} \approx P_L^{\max}. \quad (18.81)$$

Thirdly, the nominal inverter input voltage should be approximately equal to the nominal voltage of the battery back,

$$V_{DC,\text{inv}} \approx V_{OC\text{-}BB}. \quad (18.82)$$

For a more detailed analysis of the inverter performance the Sandia model can be used that was discussed in section 18.4.

Typical voltages for the battery bank are 12 V, 24 V, 48 V or 96 V. It can be adjusted by the number of batteries that are connected in series,

$$N_{bat}^S = \frac{V_{OC\text{-}BB}}{V_{OC\text{-}bat}}. \quad (18.83)$$

From that we also can determine the number of batteries that must be connected in parallel,

$$N_{\text{bat}}^P = \left\lceil \frac{N_{\text{bat}}}{N_{\text{bat}}^S} \right\rceil. \quad (18.84)$$

Now, after designing the load side is completed with choosing inverter and batteries, we look at the PV side of the system. Sizing the PV array is very similar to the procedure used for grid-connected systems in section 18.4. The energy balance can be written down as. The energy balance now writes as

$$E_{\text{DC}}^Y = E_L^Y \cdot \text{SF}, \quad (18.85)$$

where SF is a *sizing factor* that usually is assumed to be 1.1. We therefore can calculate the required number of modules,

$$N_T = \left\lceil \frac{E_L^Y \cdot \text{SF}}{A_M \cdot \int_{\text{year}} G_M(t) \eta(t) dt} \right\rceil. \quad (18.86)$$

For minimising losses, the MPP voltage of the PV array and the nominal voltages of the inverter and the battery pack should be approximately equal, since otherwise the losses of the DC-DC converter that is included in the MPPT-CC unit will be higher. The number of PV modules that are connected in series in the PV array is given by

$$N_S = \left\lceil \frac{V_{\text{OC-BB}}}{\bar{V}_{\text{mod-MPP}}} \right\rceil, \quad (18.87)$$

where  $\bar{V}_{\text{MPP-mod}}$  denotes the annual average of the MPP voltage of the PV modules. Of course, the maximally allowed input voltage of the MPPT-CC unit must not be exceeded by the PV array,

$$V_{\text{MPP}} \geq N_S \cdot V_{\text{mod-MPP}}^{\max}. \quad (18.88)$$

The number of required parallel PV strings is given by

$$N_P = \left\lceil \frac{N_T}{N_S} \right\rceil. \quad (18.89)$$

### 18.5.3 Performance Analysis

Like for grid-connected systems, also for off-grid systems, a performance analysis should be done to evaluate the chosen design. For this analysis, it is useful to use an algorithm that can simulate the performance of the PV system throughout the year. Conceptually, this algorithm can look as follows

1. Set a starting state of charge (SoC) of the battery bank.
2. Then calculate the SoC of the battery throughout the year for time steps  $\Delta t$ ,
  - Depending on the actual load and PV array output, determine the battery current  $I_{\text{BB}}(t)$ .
  - Determine the actualised SoC.

Of course, the function of the charge controller, *i.e.* its switching behaviour, must be accurately mimicked by the algorithm.

3. Determine when the system cannot deliver the required load and hence  $E_{\text{fail}}$ .
4. Now, calculate the Loss of Load Probability of the system (LLP).
5. Finally, determine the yearly energy yield on the AC-side of the system,  $E_{\text{AC}}^Y$ .

Mathematically, the annual energy yield on the AC side can be expressed by

$$E_{\text{AC}}^Y = \int_{\text{year}} P_L(t) dt - E_{\text{fail}} + \Delta E_{\text{BB}}. \quad (18.90)$$

In contrast to the expression used for determining the AC yield for grid-connected systems in Eq. (18.58), this equation contains two additional components:  $E_{\text{fail}}$ , the energy that is required by the load but cannot be delivered and  $\Delta E_{\text{BB}}$  is the difference in energy stored in the battery bank between the beginning and end of the year,

$$\Delta E_{\text{BB}} = (\text{SoC}_{\text{end}} - \text{SoC}_{\text{beginning}}) C_{\text{bat}} V_{\text{BB}}. \quad (18.91)$$

If  $\Delta E_{\text{BB}} < 0$ , the system might not be sustainable. On the other hand, if it is  $> 0$ ,  $E_{\text{dump}}$  will increase in the following, if the average meteorological conditions are unchanged.

Because of  $E_{\text{fail}} > 0$ ,

$$E_{\text{AC}}^Y < \int_{\text{year}} P_L(t) dt. \quad (18.92)$$

As already stated earlier, the Loss of Load Probability is given by

$$\text{LLP} = \frac{E_{\text{fail}}}{\int_{\text{year}} P_L(t) dt}. \quad (18.93)$$

For evaluating the design, it is very important to look at LLP:

- LLP acceptable:
  - $E_{\text{dump}}$  low: The system design is OK.
  - $E_{\text{dump}}$  high: Resize the PV array.
- LLP not acceptable:
  - Increase the size of the PV array.
  - Increase the capacity of the battery bank.



# 19

## PV System Economics and Ecology

### 19.1 PV System Economy

We conclude our discussions on PV systems with looking on several important topics on the economics of PV systems. Note that the economics of PV can be discussed at several levels, such as the consumer level, the manufacturing level, the level of PV installers, and the technology level where PV is compared to other electricity generation technologies on the scale of the electricity grid.

We will start this discussion with the definition of the *payback time*, which in finance is defined as the amount of time required to recover the cost of an investment. It

can be calculated with

$$\text{payback time} = \frac{\text{initial investment}}{\text{annual return}}. \quad (19.1)$$

Translated to the consumer level, the payback time is the time it takes to recover the initial investment of the PV system as the system continuously reduces the electricity bill. Please note that the *financial* payback time is different from the *energy payback time* that we will discuss in Section 19.2 Let us look at an example:

#### Example

*Let us assume that family Smith have installed a PV system with a power of  $1 \text{ kW}_p$  on their rooftop. The initial investment*

*was €8000. Family Smith has an annual electricity bill of €2000. The installation of the PV system leads to an average annual reduction of the electricity bill of €800. As a part of their consumed electricity is provided by their PV system, the electricity bill is therefore constantly reduced. Hence, the average annual return on their PV system is €800. As a consequence, the Smith's have earned the final investment back after 5 years, the payback time hence is 5 years.*

The payback time is strongly influenced by the annual solar radiation on the PV system. As we have seen in Chapter 16, this is dependent on the orientation of the PV modules and on the location of the PV systems. In general we can say that the sunnier the location, the greater the PV yield and the shorter the payback time. Another factor that influences the payback time is the grid electricity costs: the higher these costs, the shorter the payback time. Finally, the payback time also is strongly dependent on the initial costs of the PV system.

In practice, often more factors must be taken into account than in the simple example above. This will increase the complexity of calculating the payback time. For instance, if we are considering a significant period of time, also the change of the value of money has to be taken into account, which is due to inflation. For example today €1000 will have a different *purchasing power* than in ten years time. Another factor that should be considered are policies regarding renewable energy.

For example, subsidies and feed-in tariffs can affect the initial investments and savings.

Let us briefly discuss the concept of *feed-in tariffs*. At the consumer level, the feed-in tariff is the price at which a consumer can sell renewable electricity to the electricity provider. We distinguish between two kinds of feed-in tariffs, gross and net. *Gross* feed-in tariffs are paid for all the electricity the panels produce, irrespective of the consumer's electricity consumption. In contrast, *net* feed-in tariffs promise a higher rate for the surplus electricity fed into the grid after domestic use of the consumers is subtracted. For implementing feed-in tariff schemes at consumer level, the facility of *net metering* is pivotal.

Another very important concept is the *Levelized Cost of Electricity* (LCoE), which is defined as the cost per kWh of electricity produced by a power generation facility. It is usually used to compare the lifetime costs of different electricity generation technologies. To be able to estimate the effective price per kWh, the concept of LCoE allocates the costs of an energy plant across its full lifecycle. It is somehow similar to averaging the upfront costs of production over a long period of time. Depending on the number of variables that are to be taken into account, calculating the LCoE can become very com-

plex. In a simple case the LCoE can be determined with

$$\text{LCoE} = \frac{\sum_{t=1}^n \frac{I_t + M_t + F_t}{(1+r)^t}}{\sum_{t=1}^n \frac{E_t}{(1+r)^t}}. \quad (19.2)$$

The sums expand across the whole lifetime of the system  $n$ , every year accounts for one summand.  $I_t$  are the investment expenditures in the year  $t$ ,  $M_t$  are the operational and maintenance expenditures in the year  $t$ , and  $F_t$  are the fuel expenditures in the year  $t$ . Of course, for PV  $F_t \equiv 0$ . Further,  $E_t$  is the electricity yield in the year  $t$ . Finally,  $r$  is the discount rate which is a factor used to discount future costs and translating them into the present value.

Figure 19.1 shows the LCoE for different methods of electricity generation. We see that the LCoE of wind energy is lowest, it is even below the LCoE of fossil fuel and nuclear based electricity. The LCoE of PV generated electricity is still slightly above that of the non-renewable technologies.

Depending on the location of a PC system and the initial investment required for the PV system, the LCoE for PV can vary a lot between different projects. Additionally, the discount rate  $r$  used for the calculation will strongly influence the LCoE.

For the electricity supplier, the LCoE is a valuable indicator of the cost competitiveness of a certain energy technology. It is also a good indicator for determining

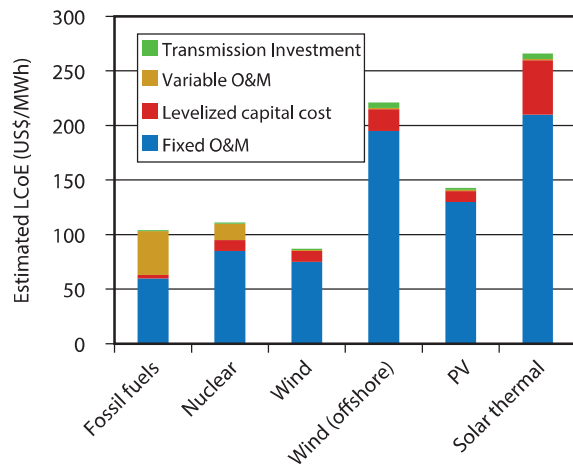


**Figure 19.1:** The levelised cost of electricity for different electricity generation technologies.

the electricity price: for making profit this price must be above the LCoE. Surely, the supplier cannot determine the electricity price independently, as it is strongly influenced by policy factors such as feed-in tariffs, subsidies and other incentives.

The final concept that we discuss is that of *grid parity*. For solar electricity this is the situation at which it can be generated at an LCoE that is equal to the electricity price from the conventional electric grid. Of course, if the PV electricity price is below the grid price, the situation becomes even better,

$$\text{LCOE}_{\text{PV}} \leq \text{LCoE}_{\text{conventional}}. \quad (19.3)$$

In principle, the concept of grid parity can be generalised to the other renewable technologies as well. However, there is one significant difference between PV and other renewable technologies such as wind and hydro electricity. Wind and hydro electricity installations usually only can be financed by companies but are no option for a single consumer. In contrast, PV can be scaled down to the level of a single module, such that a house owner can become an electricity producer with his small scalable PV installation on his roof. As a consequence, the consumer offering PV electricity to the grid now is effectively competing with the retail grid price, which conventionally includes other costs like transmission, distribution, and so on. As for the consumer these costs are no part of the PV electri-

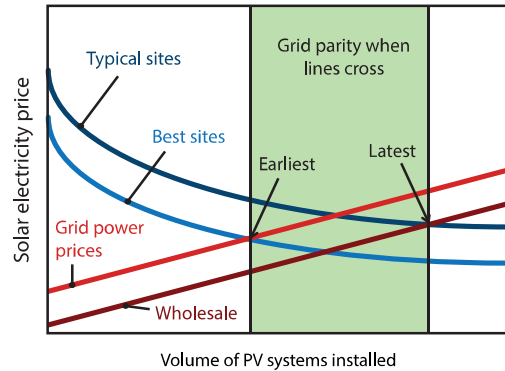


**Figure 19.2:** Grid parity for PV systems [114].

city price, PV grid parity for retail grid prices can be reached faster, as shown in Fig. 19.2.

The graph is showing the volume of installed PV systems versus the price of PV electricity. The installed volume can be directly correlated with time, as the past decade has seen the implemented PV volume rise tremendously. As capital costs decline with increasing volumes, the price of PV generated electricity is expected to decrease in the future. On the other hand, the price of fossil fuels is expected to rise because of increasing scarcity and cost linked to the right to emit CO<sub>2</sub> emissions into the atmosphere costs. These trends

will lead to increasing prices for electricity generated with combusting fossil fuels. Grid parity is reached when the prices of PV electricity and grid electricity are crossing. Naturally, with incentives and subsidies grid parity can be reached even faster, however grid parity reached with public financial support often is disregarded. Therefore it is said that true grid parity is reached when the PV electricity prices fall below the grid prices without any subsidies. Real grid parity for example already is reached in the sunny country of Spain.

To conclude, grid parity is a very useful concept to indicate the feasibility of a renewable energy technology. The closer a technology is to grid parity, the easier it can be integrated in the electricity mix. With the advancements in technology and the maturity of manufacturing processes, grid parity for solar is expected to be reached at many locations around the World in the next years.

## 19.2 PV System Ecology

Besides discussing the economics of PV systems, it also is very important to consider their ecological and environmental aspects. The main reason for that is that the aim of photovoltaics is to generate electricity without any considerable effect on the environment. It is there-

fore very important to check the ecological aspects of the different PV technologies. In this section we will discuss different concepts to quantify the environmental impact of PV systems.

The concept of the *carbon footprint* estimates the emissions of CO<sub>2</sub> caused by manufacturing the PV modules and compares them with the reduction of CO<sub>2</sub> emissions due to the electricity generated with PV instead of combusting fossile fuels. A more analytical approach is to look at the total energy required to produce either the PV modules or all the components of a PV system. As the different PV technologies vary considerably in the required production processes, the energy consumption for producing 1 kW<sub>p</sub> varies considerably between the different technologies. If a complete *life cycle assessment* (LCA) is performed, it is tried to trace the energy and carbon footprints of the PV panels throughout their lifetime. Therefore LCA also is known as *cradle-to-grave analysis*.

We now are going to introduce several indicators that are used to judge the different ecological aspects. The *Energy Yield Ratio* is defined as the ratio of the total energy yield of a PV module or system throughout its lifetime with all the energy that has to be invested in the PV system in that time. This invested energy not only contains the energy for producing the components, transporting them to the location and installing them but also the energy that is required to recycle the differ-

ent components at the end of their lifecycle.

As the energy required for producing a PV system depends strongly on the PV technology and also on the quality of the panels, the energy yield ratio for the different technologies varies a lot. While the energy yield ratio for PV modules can be as large as 10 to 15, PV systems usually have a lower ratio because of the energy invested in the components other than the modules.

A very important concept is the *Energy Payback Time*, which is defined as the total required energy investment over the lifetime divided by the average annual energy yield of the system,

$$\text{Energy Payback Time} = \frac{\text{totally invested energy}}{\text{average annual energy yield}}. \quad (19.4)$$

Note that the energy payback time is different from the economic payback time introduced in Section 19.1.

The energy payback time of typical PV systems is between 1 and 7 years and it also depends on location issues such as the orientation of the PV array as well as the solar irradiance throughout the year.

Figure 19.3 shows the specific energy required for producing PV modules with different technologies. As we can see, the differences between the technologies are large. The specific energy required for producing thin-film modules from materials such as amorphous silicon,

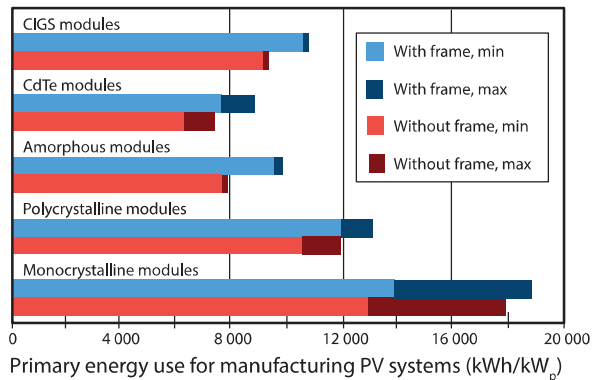


**Figure 19.3:** Specific energy used to produce PV modules of different technologies (Data from [115]).

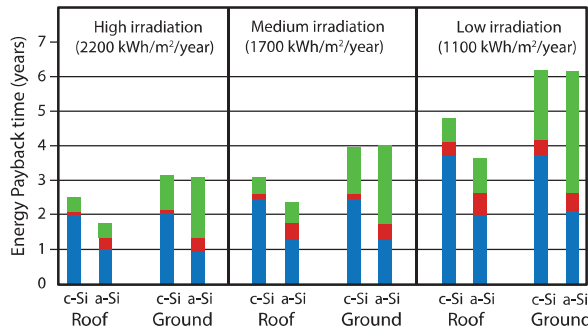


**Figure 19.4:** The energy payback time for the different components constituting PV systems (Data from [114]).

cadmium telluride and CIGS is significantly below that of modules made from polycrystalline and monocrystalline silicon, where the specific energy can reach values up to 12000-18000 kWh/kW<sub>p</sub>. Because of further improvements in the module efficiency and the manufacturing process we however may expect that that the specific energy follows a decreasing trend.

For a PV system it is more difficult to allocate the energy that was used for its production, as all the components constituting the balance of system have to be taken into account as well. For example, for components like batteries and inverters the technologies and manufacturing processes may vary a lot between the

different products available on the market. Nonetheless, studies were carried out that estimated the energy required by whole PV systems. Generally, as we can see in Fig. 19.4 it is found that the energy required for the BOS is significantly below that used for manufacturing the modules. In the figure, amorphous and crystalline silicon modules are compared. As expected, we see that the energy payback time in regions with high solar irradiance have significantly shorter energy payback times than regions with low irradiance. While a-Si:H based modules have a shorter energy payback time than c-Si based modules, the energy payback time for the module frame and the BOS of a-Si:H based systems can be significantly higher than that of c-Si based systems. This can be explained with the lower efficiency of a-Si:H that increases the required framing material per W<sub>p</sub>.

The irradiance strongly influences the energy payback time and varies between two years (high irradiance) and six years (low irradiance). Roof-mounted systems always have a shorter energy payback time than systems mounted on the ground, mainly because of the BOS that is more energy extensive for ground-mounted systems.

No matter which PV technology is chosen, the energy payback time always is far below the expected system lifetime, which usually is between 25 and 30 years. For the PV systems discussed in Fig. 19.4, the energy yield

ratio is between 4 and 10. Hence, the energy invested in the PV system is paid back several times throughout the life cycle of the PV system. The urban legend that PV modules require more energy to be produced than they will ever produce thus is not backed by any data. In contrast, the net energy produced is much larger than the energy required for PV production.

However, a lot of work still needs to be done and can be done. Some studies indicate that the energy required for producing PV modules can be reduced by up to 80%. Further, as the amount of installed PV systems becomes larger and larger, recycling of the components at the end of the lifecycle becomes very important. For example, the European Union introduced already several directives that induced recycling schemes for c-Si based PV modules.

The last environmental issue that we want to mention is pollution caused by the production of PV modules. As many sometimes toxic chemicals are required for producing PV modules, this can be a serious threat to the environment. Therefore it is very important to have strong legislation in order to prevent pollution of the surroundings of PV factories. Especially in countries with weak environmental legislation pollution can be a severe problem that affects the environment and people living in the surroundings negatively.